*Living Rev. Solar Phys.*, **9**, (2012), 2
http://www.livingreviews.org/lrsp-2012-2

LIVING REVIEWS
in solar physics

# Prominence Oscillations

Iñigo Arregui
Departament de Física, Universitat de les Illes Balears,
E-07122 Palma de Mallorca (Spain)
email: iarregui@iac.es

Ramón Oliver
Departament de Física, Universitat de les Illes Balears,
E-07122 Palma de Mallorca (Spain)
email: ramon.oliver@uib.es

José Luis Ballester
Departament de Física, Universitat de les Illes Balears,
E-07122 Palma de Mallorca (Spain)
email: joseluis.ballester@uib.es

Accepted on 10 February 2012
Published on 5 April 2012

**Abstract**

Prominences are intriguing, but poorly understood, magnetic structures of the solar corona. The dynamics of solar prominences has been the subject of a large number of studies, and of particular interest is the study of prominence oscillations. Ground- and space-based observations have confirmed the presence of oscillatory motions in prominences and they have been interpreted in terms of magnetohydrodynamic (MHD) waves. This interpretation opens the door to perform prominence seismology, whose main aim is to determine physical parameters in magnetic and plasma structures (prominences) that are difficult to measure by direct means. Here, we review the observational information gathered about prominence oscillations as well as the theoretical models developed to interpret small amplitude oscillations and their temporal and spatial attenuation. Finally, several prominence seismology applications are presented.

# Imprint / Terms of Use

*Living Reviews in Solar Physics* is a peer reviewed open access journal published by the Max Planck Institute for Solar System Research, Max-Planck-Str. 2, 37191 Katlenburg-Lindau, Germany. ISSN 1614-4961.



Because a *Living Reviews* article can evolve over time, we recommend to cite the article as follows:

Iñigo Arregui, Ramón Oliver and José Luis Ballester,
"Prominence Oscillations",
*Living Rev. Solar Phys.*, **9**, (2012), 2. [Online Article]: cited [<date>],
http://www.livingreviews.org/lrsp-2012-2

The date given as <date> then uniquely identifies the version of the article you are referring to.

# Article Revisions

*Living Reviews* supports two ways of keeping its articles up-to-date:

**Fast-track revision** A fast-track revision provides the author with the opportunity to add short notices of current research results, trends and developments, or important publications to the article. A fast-track revision is refereed by the responsible subject editor. If an article has undergone a fast-track revision, a summary of changes will be listed here.

**Major update** A major update will include substantial changes and additions and is subject to full external refereeing. It is published with a new publication number.

For detailed documentation of an article's evolution, please refer to the history document of the article's online version at http://www.livingreviews.org/lrsp-2012-2.

# Contents

# List of Tables

# 1 Prominences

Quiescent solar filaments are clouds of cool and dense plasma suspended against gravity by forces thought to be of magnetic origin. They form along the inversion polarity line in or between the weak remnants of active regions. Early observations already suggested that their fine structure is apparently composed by many horizontal and thin dark threads (de Jager, 1959; Kuperus and Tandberg-Hanssen, 1967). More recent high-resolution H$\alpha$ observations obtained with the Swedish Solar Telescope (SST) in La Palma (Lin *et al.*, 2005) and the Dutch Open Telescope (DOT) in La Palma (Heinzel and Anzer, 2006) have allowed to observe this fine structure with much greater detail (see Lin, 2010, for a review). The measured average width of resolved thin threads is about 0.3 arcsec ($\sim$ 210 km), while their length is between 5 and 40 arcsec ($\sim$ 3500 – 28,000 km). The fine threads of solar filaments seem to be partially filled with cold plasma (Lin *et al.*, 2005), typically two orders of magnitude denser and cooler than the surrounding corona, and it is generally assumed that they outline the magnetic flux tubes in which they reside (Engvold, 1998; Lin, 2005; Lin *et al.*, 2005; Okamoto *et al.*, 2007; Engvold, 2008; Martin *et al.*, 2008; Lin *et al.*, 2008). This idea is strongly supported by observations which suggest that threads are skewed with respect to the filament long axis in a similar way to what has been found for the magnetic field (Leroy, 1980; Bommier *et al.*, 1994; Bommier and Leroy, 1998). On the opposite, Heinzel and Anzer (2006) suggest that these dark horizontal filament structures are a projection effect. According to this view, many magnetic field dips of rather small vertical extension, but filled with cool plasma, are aligned in the vertical direction and the projection against the disk produces the impression of a horizontal thread.

Prominences are highly dynamic structures that display flows. These flows have been observed in H$\alpha$, UV, and EUV lines, and their study and characterization are of great interest for the understanding of prominence formation and stability, the mass supply, and the prominence magnetic field structure. In the H$\alpha$ line, and in quiescent limb prominences, a complex dynamics with vertical downflows and upflows (Berger *et al.*, 2008) as well as horizontal flows is often observed. The velocities are in the range between 2 and 35 km s$^{-1}$, while in EUV lines flow velocities seem to be slightly higher. When comparing these values one should be aware that these lines correspond to different temperatures, so probably the reported flow speeds correspond to different parts of the prominence. In active region prominences, flow velocities seem to be higher than in quiescent prominences, even reaching 200 km s$^{-1}$, and some of these high-speed flows are probably related with the prominence formation itself. In the case of filaments observed on the disk in the H$\alpha$ line, horizontal flows in the filament spine are often observed, while in barbs flows are vertical. The range of observed velocities of filament flows is between 5 and 20 km s$^{-1}$. A particular feature in these observations is the presence of counter-streaming flows, i.e., oppositely directed flows (Zirker *et al.*, 1998; Lin *et al.*, 2003). Because of the physical conditions of the filament plasma, all these flows seem to be field-aligned. For a thorough information about flows in prominences see Labrosse *et al.* (2010) and Mackay *et al.* (2010).

Solar prominences are subject to various types of oscillatory motions. Some of the first works on this subject were concerned with oscillations of large amplitude induced by disturbances coming from a nearby flare. Later, observations performed with ground-based telescopes pointed out that many quiescent prominences and filaments display small amplitude oscillations (Harvey, 1969). These oscillations have been commonly interpreted in terms of standing or propagating magneto-hydrodynamic (MHD) waves. Using this interpretation, a number of theoretical models have been set up in order to try to understand the prominence oscillatory behaviour. Such as we will point out in the following, the study of prominence oscillations can provide an alternative approach for probing their internal structure. The magnetic field structure and physical plasma properties are often hard to infer directly and wave properties directly depend on these physical conditions. Therefore, prominence seismology seeks to obtain information about prominence physical conditions from a

comparison between observations and theoretical models of oscillations.

This review is mainly devoted to small amplitude oscillations, although a brief section deals with large amplitude oscillations. The layout of the review is the following: large amplitude oscillations are succinctly summarized in Section 2; in Section 3, the observational background about small amplitude oscillations is reviewed; in Section 4, theoretical models of small amplitude oscillations based on linear ideal MHD waves in different configurations are described; next, in Section 5, the damping of prominence oscillations produced by different mechanisms is studied from a theoretical point of view; finally, in Section 6, prominence seismology using large and small amplitude oscillations is introduced.

## 2 Large Amplitude Oscillations

Oscillations with velocity amplitude greater than 20 km $s^{-1}$ have been observed in filaments. It was suggested that their exciter was a wave, caused by a flare, which disturbs the filament and induces damped oscillations. This hypothesis was confirmed by Moreton and Ramsey (1960), who used a refined photographic technique that permitted the observation of the propagating perturbation, with velocities in the range 500 – 1500 km $s^{-1}$. In some cases, during the course of the oscillations, the filament becomes visible in the H$\alpha$ image when the prominence is at rest, but when its line-of-sight velocity is sufficiently large, the emission from the material falls outside the bandpass of the filter and the prominence becomes invisible in H$\alpha$. This process is repeated periodically and for this reason this type of event is called a "winking filament". Ramsey and Smith (1965) and Hyder (1966) studied 11 winking filaments and derived oscillatory periods between 6 and 40 min, and damping times between 7 and 120 min. They reported that there seemed to be no correlation between the period and the filament dimensions, the distance to the perturbing flare or its size. In addition, a single filament perturbed by four flares during three consecutive days oscillated with essentially the same frequency and damping time in each event. As a consequence, it was suggested that prominences possess their own frequency of oscillation.

The oscillatory velocity of the winking filaments studied by Ramsey and Smith (1965, 1966) and Hyder (1966) is quite large compared with the relevant wave speeds in prominences (namely the sound and Alfvén speeds). For this reason, one usually refers to these events as large amplitude oscillations. Recently, and thanks to space- and ground-based instruments, new observations of large amplitude oscillations have been published. The exciters seem to be Moreton or EIT waves (Eto *et al.*, 2002; Okamoto *et al.*, 2004; Gilbert *et al.*, 2008) or nearby jets and subflares (Jing *et al.*, 2003, 2006; Vršnak *et al.*, 2007), while in other cases the oscillations are associated to the eruptive phase of a filament (Isobe and Tripathi, 2006; Isobe *et al.*, 2007; Pouget, 2007; Chen *et al.*, 2008) or are produced by the Alfvénic vortex shedding mechanism recently developed by Nakariakov *et al.* (2009). In this last case, oscillations could be a signature of the transition from a stable to an unstable situation. Although in most of the observed flare-induced filament oscillations the material undergoes vertical oscillations, Kleczek and Kuperus (1969) and Hershaw *et al.* (2011) have also reported horizontal oscillations. Moreover, periodic motions along the longitudinal filament axis have also been observed (Jing *et al.*, 2003, 2006; Vršnak *et al.*, 2007).

The most recent interpretation of observations of large amplitude oscillations in a prominence has been given by Hershaw *et al.* (2011), who studied this kind of oscillations in an arched prominence observed with SoHO/EIT on 30 July 2005. The perturbations were produced by two consecutive trains of coronal waves coming from two different flares in an active region located far away from the prominence site. Both oscillatory trains had periods of around 100 min and excited prominence oscillations that lasted for about 18 h. During the oscillations, the displacement of the prominence was horizontal with respect to the solar surface. In the case of the first wave train, induced by a more energetic flare than the second one, the displacement in all the considered prominence locations shows a clear time damped oscillatory behaviour (see Figure 1). The oscillatory period, the damping time, and the horizontal velocity at different heights along the two prominence legs were determined (see Table 1 in Hershaw *et al.*, 2011). The prominence oscillatory periods seem to depend on the height at which they were measured and, for each wave train, they show some differences depending on the leg in which they were measured. Focussing on the first wave train, which seems to trigger a clearly damped oscillation, the periods range between 86 and 101 min in one leg, and between 92 and 104 min in the other. Furthermore, the velocity amplitude also changes with height and reaches a maximum value of 50 km $s^{-1}$ in one leg and 33 km $s^{-1}$ in the other. This growth of the velocity amplitude with height, together with the fact that the oscillation seems to start in phase for both legs, led the authors to suggest that the oscillatory behaviour is caused by a global kink mode. The approximate analytical relationship between the damping time

and the period $\tau = (1.6 \pm 0.2)P^{0.9\pm0.1}$ was derived for the disturbance caused by the first wave train. This analytical fit suggests a linear dependence between the damping time and the period that could be compatible with resonant absorption as the damping mechanism (Ruderman and Roberts, 2002; Ofman and Aschwanden, 2002; Arregui *et al.*, 2008b). However, this interpretation must be taken with care since the use of scaling laws to discriminate between damping mechanisms is questionable, at least for resonant absorption (Arregui *et al.*, 2008a). Furthermore, some observational features such as differences in the periods measured in both legs, in the velocity amplitudes at both legs, etc., enabled the authors to suggest that the prominence could be composed by separate oscillating filamentary threads. In summary, from the reported observations it seems that one of the wave trains was able to induce large amplitude oscillations in the prominence while the effect of the second wave train was not so strong. The reason for these different behaviours could be attributed to the different energy carried by the wave trains or, in spite of the wave train periods being apparently similar, to a resonance effect between the wave train frequency and the natural oscillatory frequency of the prominence. Also, it is worth to remark that the reported observation was made in EUV while other observations of large amplitude oscillations have been made in H$\alpha$. The correspondence between oscillations observed in EUV and in H$\alpha$ remains to be ascertained. Probably, only simultaneous observations could cast light on this relationship.

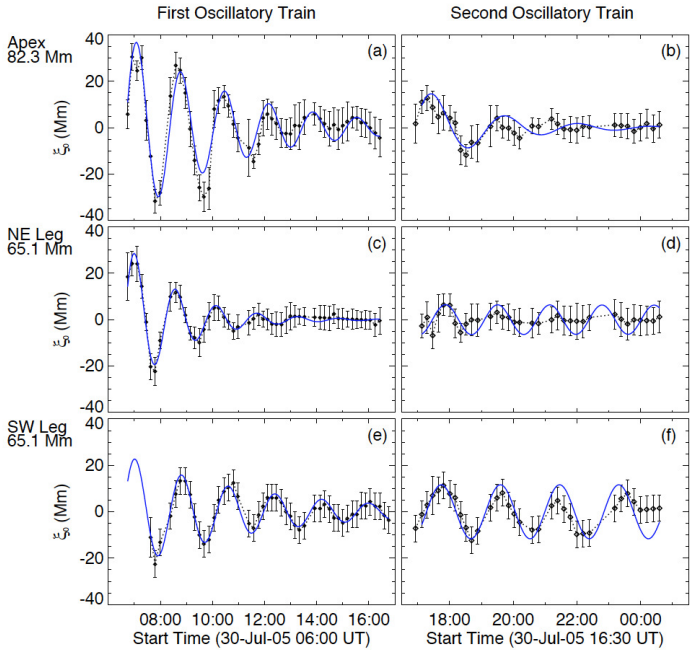


**Figure 1:** Displacement versus time produced by two wave trains impacting on a prominence: (a) and (b) in the prominence apex; (c) and (d) in the NE leg; (e) and (f) in the SW leg (from Hershaw *et al.*, 2011).

From the theoretical point of view, models that explain large amplitude filament oscillations are lacking. To explain the vertical motions, Anderson (1967) suggested that the disturbance coming from the flare propagates along the magnetic field and when it arrives to the filament, the material is pushed down. Hyder (1966) proposed a model which explains the vertical motions in terms of harmonically damped oscillations. The restoring force is provided by the magnetic tension, while the damping is due to coronal viscosity. Using this model, Hyder was able to calculate the strength of the vertical component of the magnetic field in the prominence. Later, Kleczek and Kuperus

(1969) proposed a similar model to explain the horizontal oscillations, although in this case the damping is provided by the emission of acoustic waves. On the other hand, Sakai *et al.* (1987) developed a model for the formation of a prominence in a current sheet. One of the features of this model is the presence of non-linear oscillations of the current sheet. Bakhareva *et al.* (1992) considered a partially ionized plasma and developed a dynamical model for a solar prominence in which non-linear oscillations are present. Chin *et al.* (2010) have considered possible oscillatory regimes of non-linear thermal over-stability which can occur in prominences. Finally, numerical simulations (Chen *et al.*, 2002) suggest that Moreton and EIT waves can be produced by CMEs. Then, the theoretical modelling of large amplitude oscillations excited by these events is a task that remains to be done. For a more extensive review about large amplitude prominence oscillations see Tripathi *et al.* (2009).

# 3 Small Amplitude Oscillations: Observational Aspects

Quiescent prominences are also subject to small amplitude oscillations, a type of periodic events characterized by one or more of these features:

1. Not related to flare activity.
2. Small velocity amplitude.
3. Only a restricted volume of the prominence displays periodic variations.

Regarding item 1, so far it has not been possible to identify the trigger of small amplitude oscillations. A popular conjecture about their excitation is that it lies in the periodic motions of magnetic fields caused by photospheric or chromospheric oscillations. The idea is that Alfvén waves ought to propagate upwards and that any prominence material threaded by the field should also be subject to periodic motions if there is enough energy available to overcome the inertia of the dense plasma (Harvey, 1969); this idea was later suggested by other authors too (e.g., Yi *et al.*, 1991). Harvey made order-of-magnitude calculations to show that the ratio of prominence to photospheric oscillatory energy is around or smaller than $10^{-4}$, which indicates that this excitation mechanism is feasible. On the other hand, Harvey also noted that a few prominences in his study appear to oscillate with periods nearly twice as large as those of the photospheric oscillation. This appears to contradict the above hypothesis about the initiator of small amplitude oscillations. Much longer and shorter periods than those present in Harvey's work have been detected afterwards (see Section 3.3), so probably this mechanism of energy transfer from the photosphere (or chromosphere), if correct, may not be the only one to cause these prominence oscillations. Mashnich *et al.* (2009a,b) studied the Doppler velocity field in some filaments and the underlying photosphere by means of simultaneous observations of the H$\beta$ line and the neighbouring photospheric Fe I line at 4863 Å. They detected a quasi-hourly oscillation in certain areas of the filaments and photosphere and found a good spatial correlation between them. They also reported that the parts of the photosphere displaying this oscillation are often observed below filament barbs. The spatial coincidence of this periodicity and the relation of filament barbs and the photosphere led these authors to suggest that the photosphere was the origin of these particular prominence oscillations. From an observation of a limb prominence with Hinode, Ning *et al.* (2009b) reported that the detected oscillatory behaviour only lasted about one period and that new oscillations appeared nearby simultaneously. These authors then concluded that the exciters or drivers of such oscillations are numerous and of small scale. The current understanding (see Section 4) is that periodic perturbations in prominences can be produced by an external impulsive agent that excites different eigenmodes of the structure or by a continuous agent, as may be the case with the 5-min photospheric and 3-min chromospheric oscillations whose influence could propagate along magnetic field lines and force motions of the prominence plasma. Recently, some evidence about the effect of the chromospheric 3-min oscillations on the corona has been found by Sych *et al.* (2009).

Regarding item 2, the detected Doppler velocity peak ranges from the noise level (down to 0.1 km s$^{-1}$ in some cases) to 2 – 3 km s$^{-1}$ (e.g., Harvey, 1969), although larger values have also been reported (e.g., Bashkirtsev and Mashnich, 1984; Molowny-Horas *et al.*, 1999; Ning *et al.*, 2009a). This maximum value has to be compared with the typical speeds of the prominence plasma (the sound and Alfvén speeds), which are larger than 10 km s$^{-1}$ for typical prominence conditions. The main purpose of studying prominence oscillations is to obtain insight into their physics via a seismological approach (see Section 6). Therefore, the information that observations should provide are the periods, wavelength, phase, and group velocity and damping time of these phenomena. In addition, observations should also determine whether these periodic variations are standing oscillations or propagating waves, whether they affect some prominence threads or larger

areas of a prominence, whether threads oscillate independently from their neighbours or which physical variables are disturbed and by which amount.

The solar origin of prominence oscillations remained controversial until the beginning of the 1990s. For example, Engvold (1981) failed to detect oscillatory motions in the velocity field of a limb prominence, although the observational setup used prevented him from reliably distinguishing velocity amplitudes below 2 km $s^{-1}$, the range in which many peak values are found. In addition, Malherbe *et al.* (1981, 1987) recognized no oscillatory pattern in time series of line-of-sight velocities obtained with the MSDP operating on the Meudon solar tower, although positive results were later achieved using the same instrument (Thompson and Schmieder, 1991). On the other hand, the lack of small amplitude, periodic variations in signals coming from solar prominences cannot be considered a proof against the existence of these kind of processes. Harvey (1969) noted that in a sample of 68 non-active region prominences, 31% of the objects presented no significant velocity change along the line-of-sight, 28% showed apparently random line-of-sight velocity variations, and 41% presented a definite oscillatory behaviour. Analogous results were obtained for a set of 45 active region prominences. There are several reasons that may lead to the absence of periodic variations in some prominences: the velocity amplitude or its projection along the line-of-sight may be too small to stand above the instrumental noise level; or the prominence material may actually not oscillate at the time the observations are performed; or the light emitted or absorbed by various plasma elements along the line-of-sight and having different oscillatory properties may result in a noisy signal.

## 3.1 Detection methods

The investigation of small amplitude prominence oscillations has most often been done by spectroscopical means, but also using images (e.g., Foullon *et al.*, 2004) or filtergrams, i.e., images taken in a given spectral line (e.g., Yi *et al.*, 1991; Yi and Engvold, 1991; Lin, 2005; Berger *et al.*, 2008; Ning *et al.*, 2009b,a). Regarding these studies using a two-dimensional field of view, in some of them the variations along selected straight paths have been analyzed (Berger *et al.*, 2008; Ning *et al.*, 2009b,a). This simplifies the study but also reduces the amount of oscillatory information that can be derived (see Figure 2).

Regarding spectroscopic observations, different setups have been used to gather the temporal variation of the spectral indicators and more complexity and refinement has been gained over the years. For example, in some initial studies an entrance hole was placed on a selected area of a prominence (Wiehr *et al.*, 1984). Another technique that provides information about a small region of a prominence is the so-called differential method (Kobanov, 1983; Bashkirtsev and Mashnich, 1984). A very widely used method in the investigation of small amplitude prominence oscillations is to place a spectrograph slit on a prominence (a few examples from a very long list are: Tsubaki and Takeuchi, 1986; Suematsu *et al.*, 1990; Balthasar *et al.*, 1993; Balthasar and Wiehr, 1994; Suetterlin *et al.*, 1997). Then, this yields a time series of spectra on each slit position (see, for example, Figure 4 of Tsubaki and Takeuchi 1986), from which the temporal variation of the spectral indicators (Doppler shift, line intensity, integrated line intensity, line width) can be derived. These time series can be later analyzed to obtain the period, wavelength, etc. of the oscillations (an example is shown in Figure 5 of Tsubaki and Takeuchi 1986). Slit observations have also been conducted from space, using SUMER on SoHO (Blanco *et al.*, 1999; Régnier *et al.*, 2001) and CDS on SoHO (Pouget *et al.*, 2006).

A spectroscopic observation using a slit yields restricted information on the spatial distribution of oscillations and, what is even worse, does not ensure that the same plasma elements are placed on the slit during the observing time. The first of these concerns also applies to the analysis of a two-dimensional data set in which only variations in one direction are considered. Observations using a two-dimensional field of view and with high spatial resolution have diminished these worries,

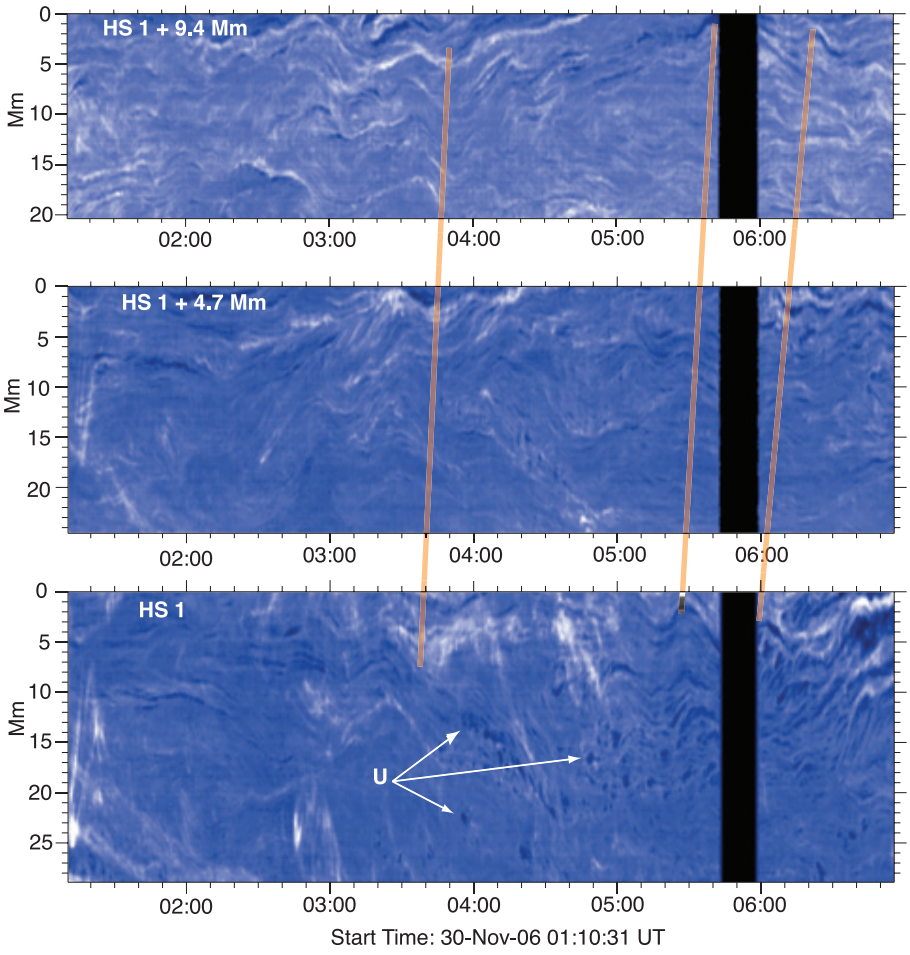


**Figure 2:** Time slices taken at three heights in a quiescent prominence. The bright sinusoidal patterns are caused by horizontal oscillations of the plasma with periods between 20 and 40 min. The orange lines denote oscillations with phases that approximately match. The slope of these lines implies an upward propagation speed of about 10 km $s^{-1}$ (projected on the plane of the sky) (from Berger *et al.*, 2008).

while allowing to study how prominence threads participate of the oscillatory motions. These observations have been conducted both with ground-based telescopes (Yi *et al.*, 1991; Yi and Engvold, 1991; Lin *et al.*, 2003; Lin, 2005; Lin *et al.*, 2005, 2007, 2009) and with space-based telescopes (Okamoto *et al.*, 2007). In addition, two-dimensional Dopplergrams have also been employed (Molowny-Horas *et al.*, 1999; Terradas *et al.*, 2002), although the spatial resolution of this particular observation is not good enough to appreciate the prominence thread structure.

Although most data used in the analysis of small amplitude prominence oscillations come from typical prominence lines, in some cases spectral lines or images formed at hotter temperatures have also been considered. Examples are the He I line at 584.33 Å, formed at 20,000 K (Régnier *et al.*, 2001; Pouget *et al.*, 2006); the Si IV and O IV lines at 1393.76 Å and around 1401 – 1405 Å, formed at transition region temperatures (Blanco *et al.*, 1999); and 195 Å images, with a formation temperature of 1.5 MK (Foullon *et al.*, 2004). Cool prominences or filaments can be identified in coronal lines since the line intensity is reduced by means of two different mechanisms: absorption and volume blocking (Anzer and Heinzel, 2005). In the first case, coronal radiation coming from behind the cool structure is partially absorbed, while in the second case the volume filled with cool plasma does not contribute to coronal emission and in this region the radiative output is reduced as compared with the surrounding corona. These two mechanisms give place to a brightness reduction of coronal lines and allows us to identify the volume occupied by cool and dark structures like prominences or filaments. Arguably, oscillations in the dense prominence affect their rarer neighbourhood, so a joint investigation of the dynamics of the two media has a very promising seismological potential.

## 3.2 Spectral indicators

The vast majority of spectroscopic reports of prominence oscillations are based on the analysis of the Doppler velocity. Some other spectral indicators (line intensity and line width) have also been used in the search for periodic variations in prominences and, sometimes, a periodic signal has been recognized in more than one of these indicators. Landman *et al.* (1977) observed periodic fluctuations in the integrated line intensity and line width with period around 22 min, but not in the Doppler shift. In addition, Yi *et al.* (1991) detected periods of 5 and 12 min in the power spectra of the line-of-sight velocity and the line intensity. Also, Suematsu *et al.* (1990) found signs of a $\sim 60$ min periodic variation in the Doppler velocity, line intensity, and line width. Nevertheless, the Doppler signal also displayed shorter period variations (with periods around 4 and 14 min) which were not present in the other two data sets. We here encounter a common feature of other investigations, namely that the temporal behaviour of various indicators corresponding to the same time series of spectra do not agree, either because they show different periods in their power spectra (as in Tsubaki *et al.*, 1987) or because one indicator presents a clear periodicity while the others do not (Wiehr *et al.*, 1984; Tsubaki and Takeuchi, 1986; Balthasar *et al.*, 1986; Tsubaki *et al.*, 1988; Suetterlin *et al.*, 1997). Only rarely have the oscillations been detected in several of these spectral indicators at the same time and with the same period, which constitutes a puzzling feature of prominence oscillations. This can be caused by insufficient instrumental sensitivity or by the effect different waves have on the plasma parameters (pressure, magnetic field, ...), which in turn may give rise to perturbations of one spectral indicator alone. In addition, Harvey (1969) failed to detect periodic perturbations in the line-of-sight component of the magnetic field in a set of prominences that displayed oscillations of the Doppler velocity. He attributed this to the fact that variations in this magnetic field component were below the observational limit.

Special mention must be made of the study performed by Balthasar and Wiehr (1994), who simultaneously observed the spectral lines He at 3888 Å, $H_8$ at 3889 Å and $Ca^+IR_3$ at 8498 Å. From this information they analyzed the temporal variations of the thermal and non-thermal line broadenings, the total $H_8$ line intensity, the He 3888 Å to $H_8$ emission ratio and the Doppler shift

of the three spectral lines. The power spectra of all these parameters yield a large number of power maxima, but only two of them (with periods of 29 and 78 min) are present in more than one indicator.

The interpretation of the results just summarized appears difficult. First, the theoretical models (see Section 4) can give the temporal behaviour of the plasma velocity, the density, and other physical parameters, in a prominence. The observations, however, yield information on quantities such as the line intensity or the line width. Hence, a clear identification of the spectral parameters with physical variables (density, pressure, temperature, magnetic field strength) is required before further progress can be achieved. Then, the presence of a certain period in more than one signal could be used to infer the properties of the MHD wave involved. Another useful source of information could be the detection of a given period in one signal but not in the others, such as reported in some works discussed above.

### 3.3 Detected periods

Early observational studies of small amplitude prominence oscillations revealed a wide range of characteristic periods, ranging from a few minutes (Harvey, 1969; Wiehr *et al.*, 1984; Tsubaki and Takeuchi, 1986; Balthasar *et al.*, 1986), to 15 – 25 min (Harvey, 1969; Landman *et al.*, 1977), to 40 – 90 min (Bashkirtsev *et al.*, 1983; Bashkirtsev and Mashnich, 1984; Wiehr *et al.*, 1984; Balthasar *et al.*, 1986). The apparent tendency of periods to group below 10 min or in the range 40 – 90 min led to the distinction between short- and long-period oscillations to refer to these two period ranges. Later, more reports of periods in the range 10 – 40 min were published (e.g., Yi *et al.*, 1991; Suetterlin *et al.*, 1997; Blanco *et al.*, 1999; Régnier *et al.*, 2001) and the intermediate-period class emerged. However, this classification (solely based on the period value) is far from complete: Balthasar *et al.* (1993) observed a prominence simultaneously with the GCT and VTT telescopes in Tenerife to remove doubts about the instrumental or atmospheric origin of prominence oscillations and obtained strong power in the Doppler shift from both telescopes with period around 30 s; hence, very short-period small amplitude oscillations also exist. Furthermore, a few works in which prominences have been observed from space during extended time intervals show that very long-period oscillations also exist: Pouget *et al.* (2006) detected periodicities of 5 – 6 h, while Foullon *et al.* (2004) and Foullon *et al.* (2009) have observed variations in EUV filaments with periods around 12 h, and 10 – 30 h, respectively. Although the classification in terms of short-period, long-period, etc. oscillations is still in use, it does not cast any light nor gives any help with regard to the nature, origin, or exciter of the oscillations.

In some occasions, a given prominence has been observed over a few consecutive days and the outcome is that the same period seems to be recovered (Bashkirtsev and Mashnich, 1984; Mashnich and Bashkirtsev, 1990; Suetterlin *et al.*, 1997). This seems to indicate that the overall properties of this prominence did not change much over this time interval. Similar studies have not been later carried out.

Some authors have tried to find correlations of the periods of small amplitude oscillations with other parameters. Harvey (1969) reported a correlation of the period with the unperturbed longitudinal magnetic field, such that long periods are associated with strong field strengths (Figure 3). This dependence is difficult to understand since, other parameters being equal (density, magnetic field line length, etc.), one expects just the inverse behaviour for fast MHD waves, and no dependence of the period on the magnetic field strength for slow MHD waves. Bashkirtsev and Mashnich (1993) claimed that the period of oscillation depends on solar latitude. Only periods above 40 min were included in this study and some 40 observations gathered along more than eight years were taken into account. The question then is whether this latitudinal dependence, if real, is related to the solar activity cycle or not. In a subsequent work by Mashnich and Bashkirtsev (1999) a similar latitudinal dependence was obtained for the quasi-hourly oscillations of the photosphere

and chromosphere. The implications of these findings are profound and further checks are essential before their reality is firmly demonstrated.

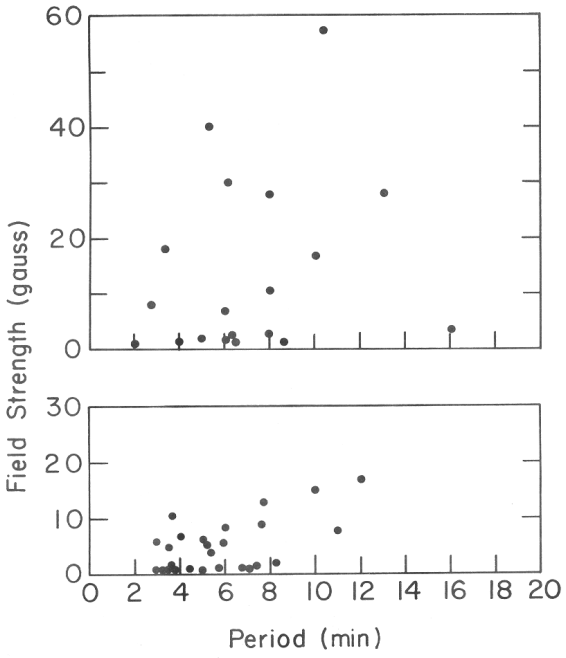


**Figure 3:** Period of prominence Doppler velocity oscillations as a function of the line-of-sight magnetic field strength. The top and bottom panels correspond to active region and non-active region prominences, respectively (from Harvey, 1969).

### 3.4 Spatial distribution of oscillations

It now appears well established that small amplitude, periodic changes in solar prominences do not normally affect the whole object at a time, but are of local nature instead, and that this conclusion is independent of the oscillatory period. Thus, variations with a given period are seldom reported to occur over the whole prominence (see Tsubaki and Takeuchi, 1986). One case in which a periodic signal is present in all slit positions was presented by Balthasar *et al.* (1988), who detected long-period oscillations over the whole height of three limb prominences by placing a vertical spectrograph slit on them. In contrast, it is usually found that only a few consecutive points along the slit present time variations with a definite period, while all other points lack any kind of periodicity (e.g., Tsubaki and Takeuchi, 1986; Suematsu *et al.*, 1990; Balthasar *et al.*, 1993; Balthasar and Wiehr, 1994; Suetterlin *et al.*, 1997; Molowny-Horas *et al.*, 1997).

The works mentioned in the previous paragraph use a spectrograph slit to detect oscillations; obviously, a two-dimensional data set is much more advantageous when it comes to ascertaining which part of a prominence is affected by oscillations. Terradas *et al.* (2002) reported on the propagation of waves over a large region (some 54,000 km by 40,000 km in size) in a limb prominence and high spatial resolution observations with Hinode/SOT (Berger *et al.*, 2008) also show oscillations that affect a small area of a prominence. See also the discussion in Section 3.6.4 of the work by Lin *et al.* (2007) that gives evidence of coherent Doppler shift oscillations over a rectangular area 3.4 arcsec $\times$ 10 arcsec in size.

Other observations with high spatial resolution have shown that individual threads or small groups of threads may oscillate independently from the rest of the prominence with their own periods (Thompson and Schmieder, 1991; Yi *et al.*, 1991). Figure 4 displays some of the results in Yi *et al.* (1991). It is clear that threads 1, 4, 13, and 14 oscillate in phase with their own period, which ranges from 9 to 14 min. In addition, Tsubaki *et al.* (1988) obtained successively two time series of spectra by placing the spectrograph slit first at a height of 30,000 km above the solar limb and next 40,000 km above the limb. A group of vertical threads detached from the prominence main body displayed 10.7-min periodic variations at both heights, which was a first indication that threads can oscillate collectively. After these preliminary studies, much attention has been given to the detection of thread oscillations (Lin *et al.*, 2003; Lin, 2005; Lin *et al.*, 2005, 2007, 2009; Okamoto *et al.*, 2007; Ning *et al.*, 2009b,a). Apart from reporting on thread oscillations, these works have also provided detailed information about wave features such as the period, wavelength, and phase speed. Because of the importance of these quantities in the seismology of prominences, these works are discussed in more detail in Section 3.6.4.

There is also some evidence that velocity oscillations are more easily detected at the edges of prominences or where the material seems fainter, while they sometimes look harder to detect at the prominence main body (Tsubaki and Takeuchi, 1986; Tsubaki *et al.*, 1988; Suematsu *et al.*, 1990; Thompson and Schmieder, 1991; Terradas *et al.*, 2002). This result has occasionally been interpreted as the consequence of integrating the velocity signals coming from various moving elements along the line-of-sight. This explanation, however, would imply the presence of broader spectral lines at the positions showing periodic variations, which is not observed, so other explanations are also possible (Suematsu *et al.*, 1990). Mashnich *et al.* (2009a,b) gave evidence that different parts of filaments may support different periodicities: short-period variations (with periods shorter than 10 min) had coherence scales shorter than 10 arcsec and were detected near the edges of filaments placed close to the Sun's central meridian. These oscillations, hence, were characterized preferentially by vertical plasma displacements. On the other hand, variations with period around 1 h occured in different positions of the filament and the size of the oscillating area was not larger than 15 – 20 arcsec. In addition, these oscillations had an amplitude that increased by an order of magnitude or more in filaments far from the solar center compared to those near the center of the Sun's disk. Then, these oscillations showed a mainly horizontal velocity.

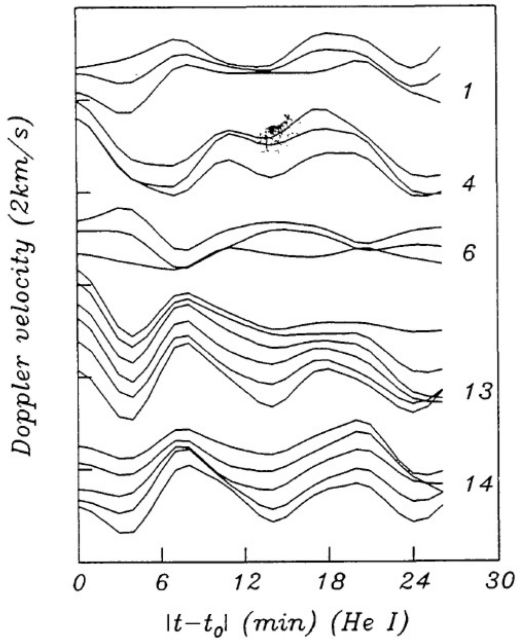


**Figure 4:** Temporal variation of the Doppler velocity along threads of a solar filament. Numbers on the right label the various threads. For each thread, the curves correspond to the Doppler velocity measured at different points along the thread (from Yi *et al.*, 1991).

More information about the spatial distribution of prominence oscillations comes from Ning *et al.* (2009b), who detected transverse oscillations of 13 threads in a quiescent prominence observed with Hinode/SOT. These authors found that prominence threads in the upper part of the prominence oscillate independently, whereas oscillations in the lower part of the prominence do not follow this pattern. Furthermore, the oscillatory periods were short (between 210 to 525 s), with the dominant one appearing at 5 min (more information is given in Section 3.6.4). In a subsequent work, Ning *et al.* (2009a) used the same data set to analyze the motions of two spines in the same quiescent prominence. The spine is synonymous with the horizontal fine structure along the filament axis and is the highest part of the prominence. In the observations of Ning *et al.* (2009a), the spines showed drifting motions that were removed by the subtraction of a linear trend, which allowed the authors to uncover the existence of oscillations with a very similar period (around 98 min) in both structures. Further insight into the behaviour of the spines comes from a fit of a function $A[0]\sin(2\pi t/A[1] + A[2])\exp(A[3]t)$ to the detrended data. Here $A[0]$ is the oscillatory amplitude, $A[1]$ the period, $A[2]$ the oscillatory phase, and $-1/A[3]$ the damping time. The detrended signals and the function fits are displayed in Figure 5, which includes the fitted parameters, that give the following information: from the oscillatory amplitude, the peak velocities of the spines are 1 and 5 km s$^{-1}$. The periods are almost identical (96.5 and 98.5 min) and the phase difference is 149°, which means that the spines oscillated almost in anti-phase. These results about the period and phase were taken by Ning *et al.* (2009a) as an indication of a collective behaviour of the two structures. These authors considered an analogy with the transverse MHD oscillations of two cylinders (a problem studied by Luna *et al.*, 2008, and discussed in Section 4.4) and concluded that a coupling of kink-like modes can give the observed behaviour. In particular, the $A_x$ mode of the system has motions resembling the anti-phase oscillatory behaviour found by Ning *et al.* (2009a).

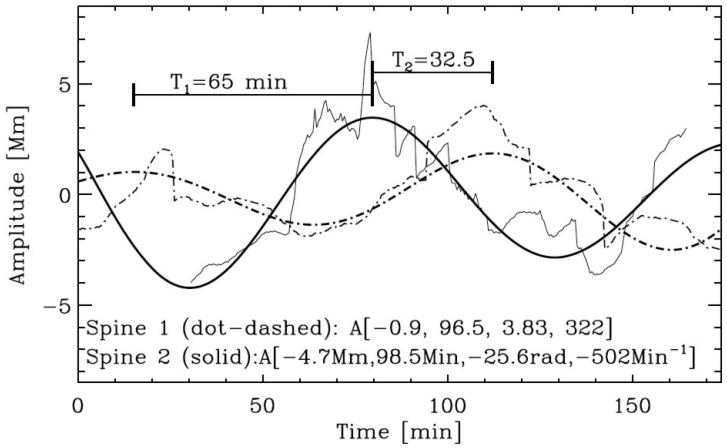


**Figure 5:** Displacement of two spines of a quiescent prominence (thin lines) and best fits using the function $A[0]\sin(2\pi t/A[1] + A[2])\exp(A[3]t)$ (thick lines). The fitted values of the parameters $A[0]$ to $A[3]$ are written at the bottom of the figure. Note that the values of $A[3]$ displayed in the figure cannot be correct since they give a very strong amplification/damping that totally disagrees with the almost undamped behaviour of the thick lines (from Ning *et al.*, 2009a).

## 3.5 Wave damping and oscillation lifetime

A visual inspection of the data sometimes reveals the existence of outstanding periodic variations and use of the FFT, or even better the periodogram (which yields an increased frequency resolution), is only necessary to derive a precise value of the period. In such cases it usually turns out that the oscillatory amplitude tends to decrease in time in such a way that the periodicity totally disappears after a few periods (e.g., Landman *et al.*, 1977; Tsubaki and Takeuchi, 1986; Wiehr *et al.*, 1989; Molowny-Horas *et al.*, 1999; Terradas *et al.*, 2002; Lin, 2005; Berger *et al.*, 2008; Ning *et al.*, 2009b,a), just as found in large amplitude oscillations. This is then interpreted as a sign of wave damping, although the specific mechanism has not been commonly agreed on (see Section 5 for a summary of theoretical results on this topic).

Reliable values of the damping time, $\tau$, have been derived by Molowny-Horas *et al.* (1999) after fitting the function $v_0\cos(\omega t+\phi)\exp(-t/\tau)$ to Doppler velocity time series recorded simultaneously in different positions of a polar crown prominence (Figure 6). The values of $\tau$ thus obtained are usually between 1 and 4 times the corresponding period, in agreement with previous observational reports. In addition, there is one particular case for which the line-of-sight velocity grows in time, but no interpretation of this result is given by these authors.

Terradas *et al.* (2002) performed a deeper investigation of the data of Molowny-Horas *et al.* (1999). After fitting the same sinusoidal function to all points in the two-dimensional field of view, Terradas *et al.* (2002) generated two-dimensional maps of various oscillatory parameters, such as the period, damping time and velocity amplitude (Figure 7). Terradas *et al.* (2002) stressed that there is a region near the prominence edge (54,000 km by 40,000 km in size) in which the correlation coefficient of the fit is rather large and in which the period and damping time are very uniform. The mentioned region is around position $x = 80$, $y = 50$ of Figure 7. In Section 3.6.3 we discuss other aspects of this work, which is unique since it is one of a few in which coherent wave behaviour has been found in a large area of a prominence and the only one in which the wave parameters in a two-dimensional prominence area have been computed.

Very often the presence of a periodic signal in the data is not obvious under a visual scrutiny and the FFT or periodogram simply provide the period of such signal, but not its duration.

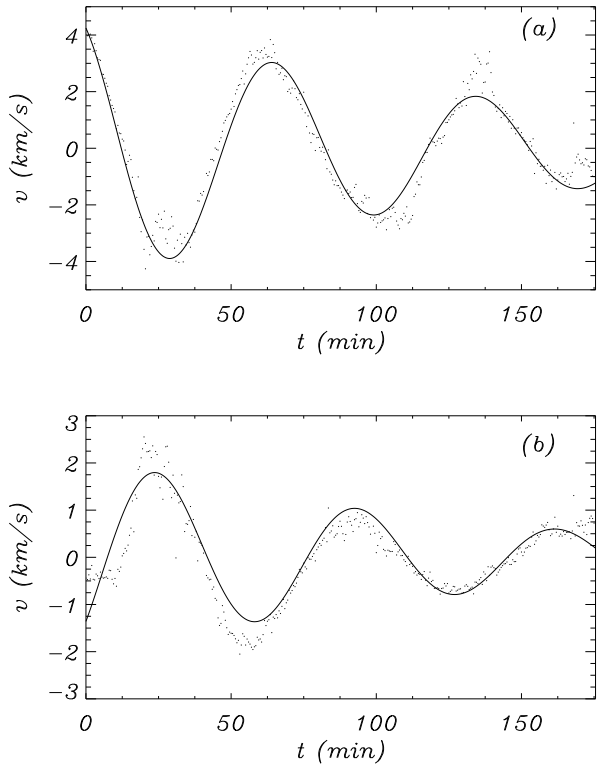


**Figure 6:** Observed Doppler velocity (dots) and fitted function (continuous line) versus time at two different positions in a quiescent prominence. The period is 70 min in both positions and the damping time is 140 and 101 min, respectively. The function fitted to the observational data is of the form $v_0 \cos(\omega t + \phi) \exp(-t/\tau)$ (adapted from Molowny-Horas *et al.*, 1999).

Dividing the time series into shorter intervals and calculating the Fourier spectrum of each of them allows to narrow down the epoch of occurrence of the oscillation. Wiehr *et al.* (1984) followed this procedure and determined that a 3-min oscillation found in a 2-h Doppler velocity record only existed in the last 40 min of the sample. The wavelet technique, however, is much better suited for the calculation of lifetimes since it can be used to precisely determine the beginning and end of the time interval in which a periodicity, previously detected in the Fourier spectrum, takes place. This approach was used by Molowny-Horas *et al.* (1997), who obtained a period around 7.5 min in 16 consecutive points, spanning a distance of 7300 km, along the spectrograph slit. The time/frequency diagram of the corresponding 16 time signals indicates that the periodic perturbation is not present for the whole duration of the data and that it only operates for about 12 min (Figure 8). Molowny-Horas *et al.* (1998) performed a similar study by placing the slit on a filament, rather than on a limb prominence, with comparable results. Two oscillations with periods around 2.7 and 12.5 min were present at consecutive points covering some 2000 and 3300 km, respectively. From the wavelet analysis, the lifetimes of these two perturbations are of the order of 10 and 20 min, respectively. These results provide convincing evidence of the train-like character of some prominence oscillations. Further details of the work by Molowny-Horas *et al.* (1997) are provided in Section 3.6.2.

Oscillations of prominence threads also display fast attenuation. For example, Lin (2005)

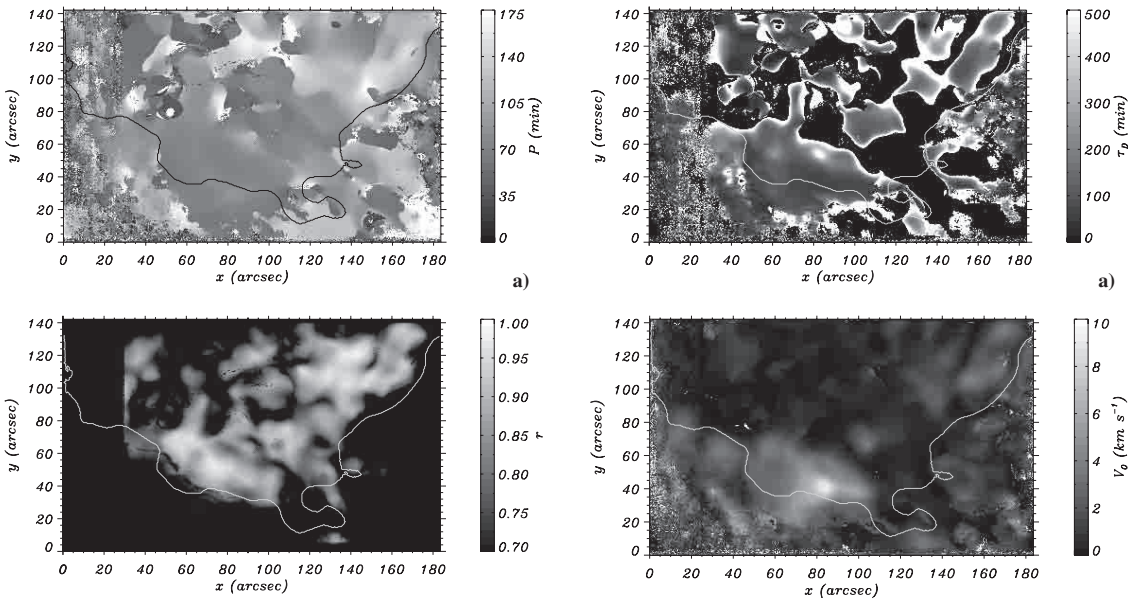


**Figure 7:** Results of fitting the function of Figure 6 to the Doppler velocity in the whole two-dimensional field of view. The spatial distribution of the fitted period and damping time is shown in the top panels, while that of the correlation coefficient and fitted amplitude is displayed in the bottom panels. The continuous white line (black in the top left panel) represents the approximate position of the prominence edge. The photosphere is slightly outside the image top (from Terradas *et al.*, 2002).

detected several periodicities over large areas of a filament, with maximum power at periods of 26, 42, and 78 min. Pronounced Doppler velocity oscillations with 26 min period could only be observed for 2 – 3 periods, after which they became strongly damped.

## 3.6 Wavelength, phase speed, and group velocity

To derive the wavelength ($\lambda$) and phase speed ($c_{\rm p}$) of oscillations, time signals at different locations on the prominence must be acquired. The signature of a propagating wave is a linear variation of the oscillatory phase with distance. Hence, when several neighbouring points are found to oscillate with the same frequency, one can compute the Fourier phase of the signal at each of the points and check whether it varies linearly with distance. If it does, this gives place to a wave propagation interpretation and the wavelength can be calculated. This approach has been followed by Thompson and Schmieder (1991), Molowny-Horas *et al.* (1997) (about which more details are given in Section 3.6.2), and Terradas *et al.* (2002) (see Section 3.6.3). On the other hand, Lin (2005) and Lin *et al.* (2007) (see Section 3.6.4) detected wave propagation along threads by studying Doppler velocity variations at fixed times. They observed a sinusoidal variation of the Doppler shift with distance along the thread, which allowed them to compute the wavelength. Moreover, the phase velocity of the oscillations can be derived from the inclination of the coherent features in the Doppler velocity time-slice diagrams. Other authors have followed less strict methods to calculate these wave parameters.

It must be mentioned that observations of wave propagation in slender waveguides or plane wave propagation in a uniform medium do not provide the actual value of the wavelength ($\lambda$), but its projection on the plane of the sky, which is shorter than $\lambda$. And if a slit or some points along a straight line are used, then the computed wavelength is the projection of $\lambda$ on the slit or the line.

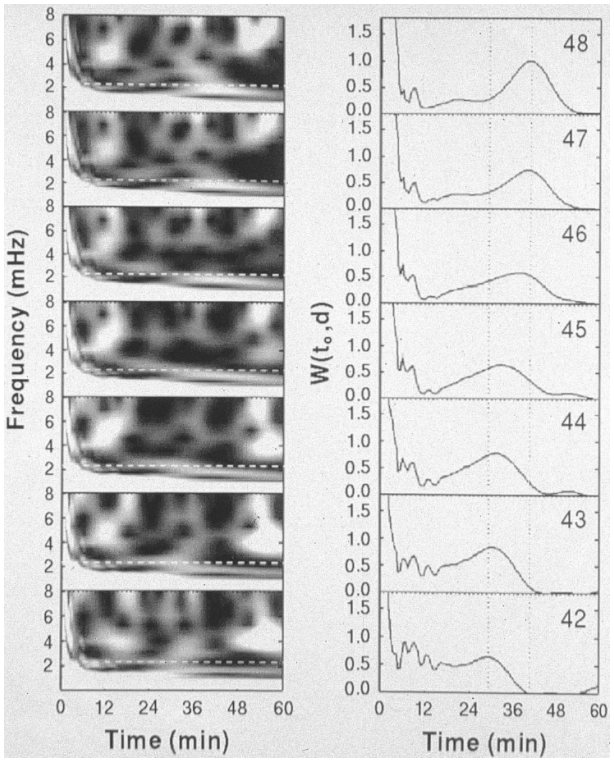


**Figure 8:** *Left:* Time-frequency diagrams of the Doppler velocity at several aligned, equispaced points in a quiescent prominence. White/black correspond to large/small wavelet power. *Right:* Time variation of wavelet power from the diagrams on the left column for a period of 7.5 min (i.e., frequency around 2.2 mHz). The presence of power peaks suggests a finite duration of the perturbation, while the linear displacement of these peaks at the seven positions from $t = 28$ min to $t = 42$ min is an indication of a disturbance travelling with a group velocity $v_g \geq 4.4$ km s$^{-1}$ (from Molowny-Horas *et al.*, 1997).

The observationally measured period and wavelength can in turn be used to calculate the phase speed, but since the observational wavelength is a lower limit to $\lambda$, this observational phase speed is also a lower limit to $c_{\rm p}$ (Oliver and Ballester, 2002). Hence, even if it is not explicitly mentioned, the values of $\lambda$ and $c_{\rm p}$ quoted here are observationally derived lower bounds to the actual values.

The results presented in this section are grouped in four parts, the first three of them in increasing order of complexity of the data analysis; the fourth one is devoted to thread oscillations. The reported wavelength values cover a range from less than 3000 km (for waves propagating along some threads) to 75,000 km (for waves propagating in a large area of a quiescent prominence). These numbers must be taken into account in the theoretical study of these events.

### 3.6.1 Simple analyses

Malville and Schindler (1981) observed a loop prominence some 90 min before the onset of a nearby flare and detected periodic changes with a wavelength along the loop of 37,000 km. This value, together with the period of 75 min, results in a phase speed of about 8 km s$^{-1}$.

Subsequent reports, which we now describe, are based on sheet-like prominences. Thompson and Schmieder (1991) detected periodic variations with periods between 3.5 and 4.5 min in a filament thread. They then computed the Fourier phase of the points along the thread and, after confirming its linearity from a phase versus distance plot, the value $\lambda \simeq 50,000$ km was derived, from which the phase speed is $c_{\rm p} \simeq 150-200$ km s$^{-1}$. In other works (e.g., Tsubaki and Takeuchi, 1986; Tsubaki *et al.*, 1987, 1988; Suematsu *et al.*, 1990) the signal in some consecutive locations along the slit has been found to be in phase. Although this seems to indicate that the wavelength of oscillations is much larger than the distance between the first and last of those points, this may not be necessarily true and a proper determination of the wavelength requires computing the Fourier phase corresponding to the oscillatory period.

Blanco *et al.* (1999) detected 15 – 20 min periodic variations corresponding to a pulse travelling with a speed of 170 km s$^{-1}$. Such a large phase velocity is hard to reconcile with the typical speeds in a prominence, but it must be taken into account that this result has been obtained using Si IV and O IV lines, which are formed at transition region temperatures. Still, Blanco *et al.* (1999) mention that the sound speed in the prominence-corona transition region must be considerably faster than 170 km s$^{-1}$, which leads them to conclude that the detected wave is of fast or Alfvénic character. Assuming a density of $10^{10}$ cm$^{-3}$, a magnetic field of 8 G is derived.

Foullon *et al.* (2004) analyzed the intensity on a set of points along the main axis of a filament in 195 Å images. A time-space plot shows a clear oscillatory pattern at one end of the filament (around position 25 in Figure 9a). The oscillatory phase, displayed in Figure 9b, presents oscillatory fronts that are well correlated along the filament, meaning that the oscillations of neighbouring points along the filament are almost in phase. This is true in particular for positions around 25, although in positions around 5 and 10 the phase presents a linear trend in neighbouring points, which can be interpreted as wave propagation along the filament axis. Lower bounds to the wavelength and phase speed in this area could be determined as explained above. It is remarkable that the most pronounced periodic intensity variations, those around position 25, were detected during 6 days, which suggests that they suffered very little damping or were excited continuously during this time span.

Berger *et al.* (2008) used high-resolution observations of limb prominences made by SOT on Hinode and detected oscillations that do not affect the whole prominence body. They considered three horizontal time slices at heights separated by 4.7 Mm and detected the presence of coherent oscillations in the three slices (Figure 2). A phase matching of the sinusoidal profiles of these oscillations results in a vertical propagation speed (i.e., phase speed) around 10 km s$^{-1}$. Again this value comes from a projection on the plane of the sky and is therefore a lower bound of the real value.

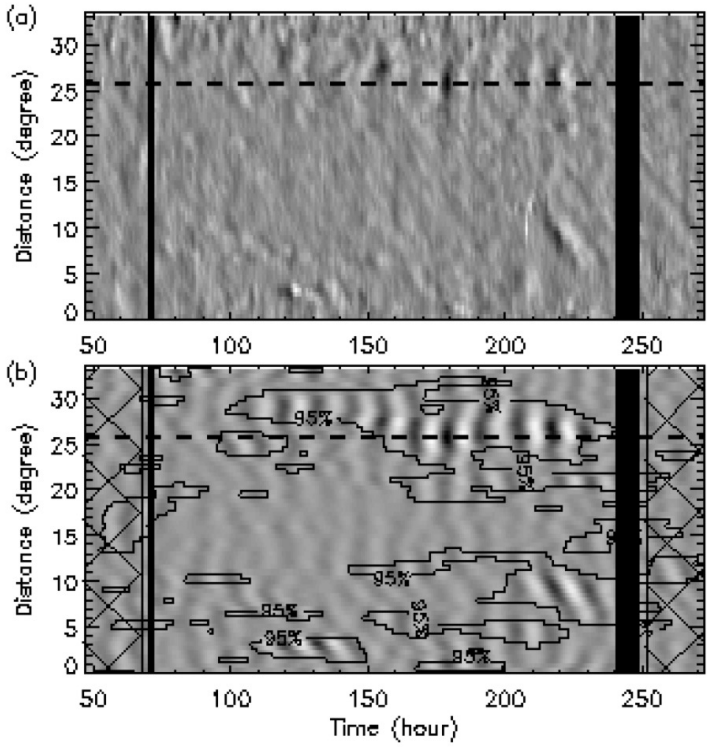


**Figure 9:** (a) Time-space diagram of the 195 Å image intensity along the main axis of a filament. The vertical black stripes are caused by the lack of observational data. (b) Spatial distribution of the Fourier phase (gray coloured contours) (from Foullon *et al.*, 2004).

### 3.6.2 An elaborate one-dimensional analysis

Molowny-Horas *et al.* (1997) took into account the projection effects in their analysis of the Doppler velocity along the spectrograph slit. They detected periodic velocity variations with period of 7.5 min some 7300 km along the slit and found that the Fourier phase of the velocity at this period changes linearly with distance (Figure 10). The value $\lambda \geq 20,000$ km was derived. The corresponding phase speed is $c_{\rm p} \geq 44$ km s$^{-1}$.

To obtain the group velocity of this event, Molowny-Horas *et al.* (1997) performed a wavelet analysis of the same set of data, which revealed the presence of a train of 7.5-min waves in the slit locations (Figure 8). Moreover, the time of occurrence of the train of waves increases linearly along the slit, which agrees with the assumption of a propagating disturbance. The velocity of propagation along the slit can then be computed and the value $v_{\|} \simeq 4.4$ km s$^{-1}$ is obtained. Taking into account that $v_{\|}$ is the projection of the group velocity, $v_{\rm g}$, on the slit, one concludes that the above value provides a lower limit for the group velocity, so $v_{\rm g} \geq 4.4$ km s$^{-1}$.

### 3.6.3 A two-dimensional analysis

This section is devoted to review the work by Terradas *et al.* (2002), that stands out among all other works in which wave properties have been determined since in this one a fully two-dimensional analysis is carried out. Figure 11 shows a time series of H$\beta$ filtergrams of the prominence studied by Terradas *et al.* (2002). The corresponding time series of the Doppler signal is presented in

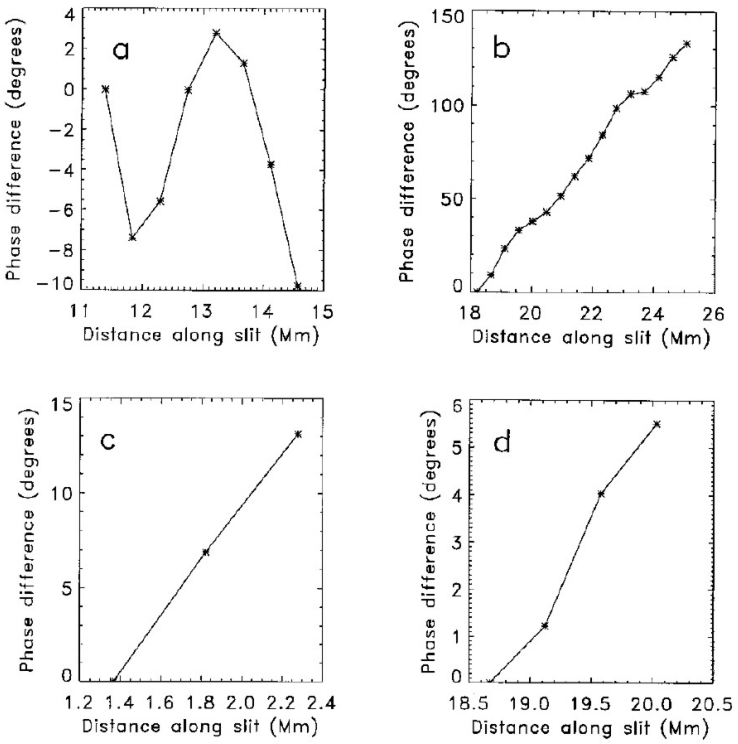


**Figure 10:** Relative Fourier phase as a function of position along the slit for several sets of consecutive points with similar oscillatory period: (a) 10.0 min, (b) 7.5 min, (c) 12.0 min, and (d) 4.0 min. The variation of the phase in (a) is not linear and so this oscillatory feature is not interpreted as a true signal. Regarding (c) and (d), the phase varies linearly with position, but the number of points involved is too small to make a firm conclusion. Finally, the phase in (b) displays a very robust linear dependence with distance, so this is interpreted as a signature of wave propagation (from Molowny-Horas *et al.*, 1997).

Figure 12.

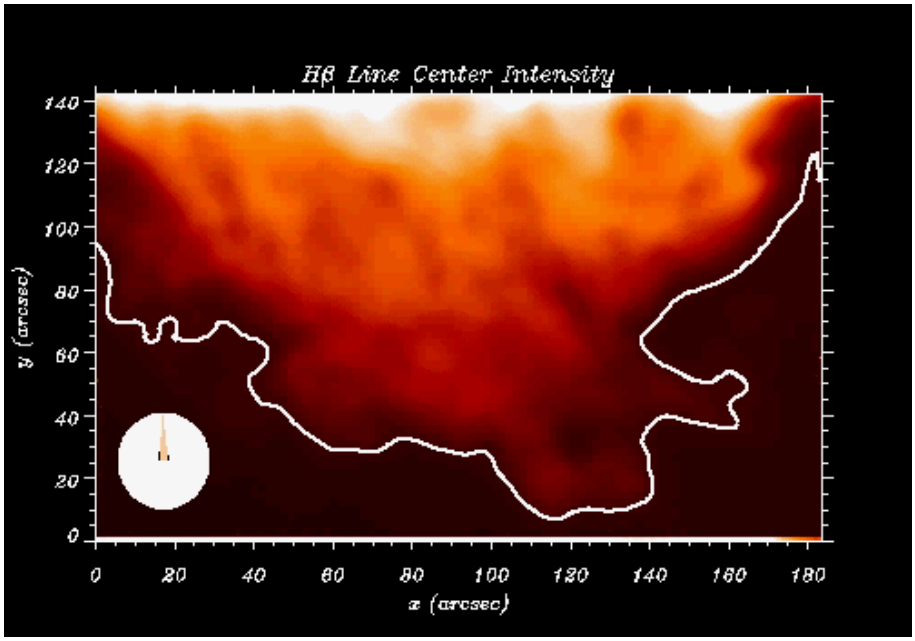


**Figure 11:** Still from a movie showing H$\beta$ line center images of a quiescent prominence observed with the VTT of Sacramento Peak Observatory. Images have been coaligned and a persistent drift towards the left has been suppressed. The thick white line displays the prominence edge and the solar photosphere is at the top (from Terradas *et al.*, 2002). (To watch the movie, please go to the online version of this review article at http://www.livingreviews.org/lrsp-2012-2.)

The data used by Molowny-Horas *et al.* (1999) were re-analysed by Terradas *et al.* (2002) and clear evidence for propagating and standing waves was uncovered. These authors started from the Doppler velocity, which in many areas of the two-dimensional field of view can be very well fitted by a damped sinusoid (Figures 6 and 7). The subsequent analysis was performed in a rectangle (black box in Figure 13) that includes an area in which the correlation coefficient of the fit is large. The period of the oscillations in this rectangle is quite uniform and with a value around 75 min. First, Terradas *et al.* (2002) conducted an analysis of the phase along two straight lines inside the rectangle. Along the continuous line in Figure 13, it is found that waves emanate from a point and propagate away from it (Figure 14). It is clear both from the raw and the fitted signals in Figure 14 that the slope of wave propagation to the left is larger than that to the right. To derive the wavelength, Terradas *et al.* (2002) plotted the Fourier phase associated to the most relevant period in the Fourier spectrum (i.e., the one with 75 min period) along the selected path (right panel of Figure 14). There is an almost linear decrease of the phase between positions 5 and 30, a linear increase between positions 50 and 62 and a region of roughly constant phase in between. The first two patterns correspond to propagation to the left and right along the path, such as was pointed out from the first two panels of Figure 14, while the third pattern is caused by standing wave motions. The slope of a straight line fitted to the Fourier phase in each of the regions with wave propagation gives the wavelength of oscillation (projected on the selected path) which is around 75,000 km and 70,000 km for propagation to the left and right, respectively. The corresponding phase velocities are around 17 km s$^{-1}$ and 15 km s$^{-1}$.

Another interesting feature of this data set can be discerned by considering the dashed path in Figure 13. A representation of the Doppler velocity versus position and time (Figure 15)

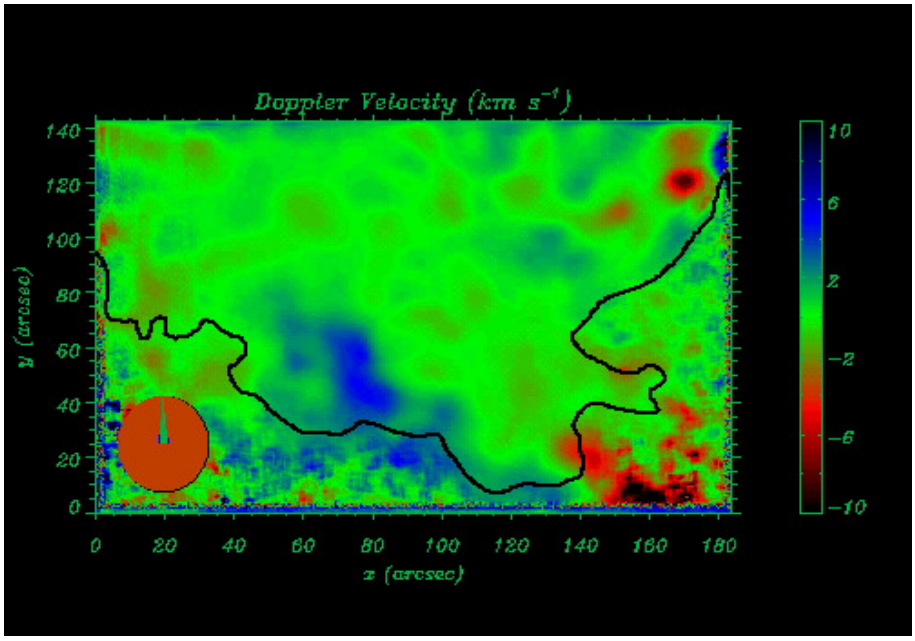


**Figure 12:** Still from a movie showing Temporal evolution of the Doppler velocity in all points of the field of view of Figure 11 (from Terradas *et al.*, 2002). (To watch the movie, please go to the online version of this review article at http://www.livingreviews.org/lrsp-2012-2.)

shows that, at least for the first half of the observational time, positive and negative velocities seem to alternate in phase separated by a region, around position 25, with nearly zero amplitude. This pattern suggests that rather than a propagating feature, the signal in this area behaves like a standing wave with two regions completely out of phase. The Fourier phase (right panel of Figure 15) is practically constant in a small region around position 10 and in a larger region for positions greater than 30, which indicates that there is no signal propagation in these locations. The phase difference between positions 10 and 50 is close to $\pi$, which, together with the fact that between these points the amplitude takes low values, is in close agreement with the standing wave picture and so a tentative identification of nodes and antinodes is possible. The estimated distance between the two antinodes visible in the left panel of Figure 15 is around 22,000 km. This implies that the (projected) wavelength of the standing wave is about 44,000 km and the corresponding phase speed is 10 km s$^{-1}$. These values are about half those obtained for propagation along the other selected path and are a consequence of the anisotropic propagation of the perturbation.

In addition to the identification of standing and propagating wave features in the prominence, Terradas *et al.* (2002) went on to perform an investigation of the two-dimensional distribution of the wavelength and phase speed. They started by plotting the Fourier phase for the most relevant period in the Fourier spectrum at each point (Figure 16), which shows that a deep global minimum is found around the central position of the plot. This particular phase structure is an indication that motions have their origin at the position of the minimum and propagate, although in an anisotropic way, from this point. Terradas *et al.* (2002) gave a much more clear interpretation of the two-dimensional phase by plotting the wavevector field (Figure 17), computed as the gradient of the Fourier phase. The arrows in this figure indicate the direction of wave propagation, their length being proportional to the modulus of the wavenumber, $k$. The projection of the phase velocity on the plane of the sky (computed from $c_{\rm p} = \omega/k$) is also displayed in Figure 17. The analysis of the wavevector field shown in this figure clearly indicates that motions seem to be generated

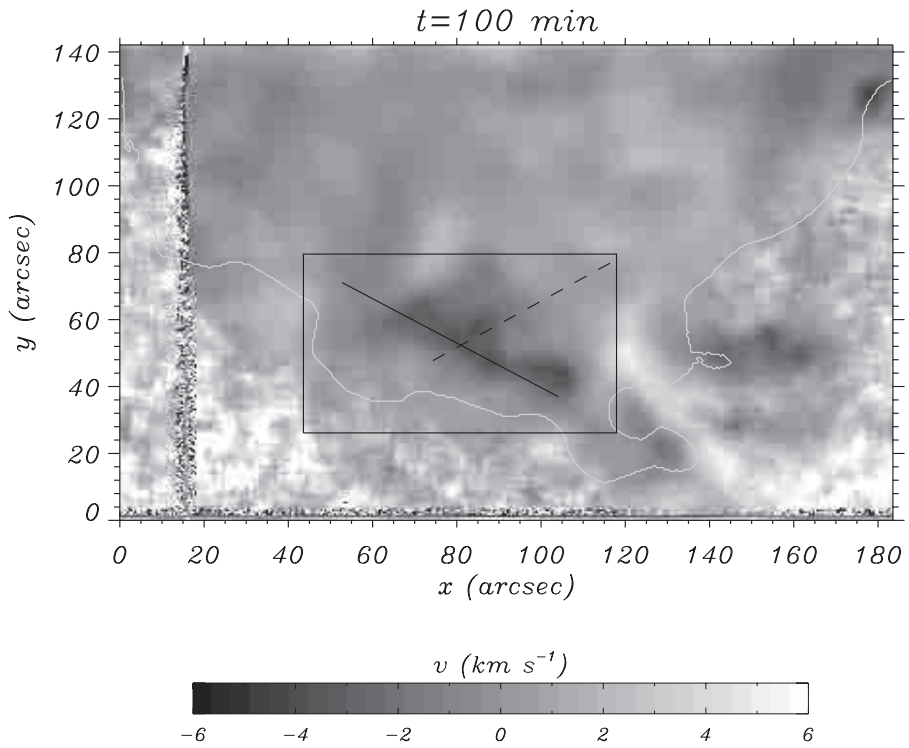


**Figure 13:** Two-dimensional Doppler velocity distribution at a given time in a quiescent prominence. The signal in the black rectangle can be fitted by a damped sinusoid with a high correlation coefficient (see Figure 7). Two paths (straight continuous and dashed lines) were selected. The continuous white line represents the approximate position of the prominence edge. The photosphere is slightly outside the image top (from Terradas *et al.*, 2002).

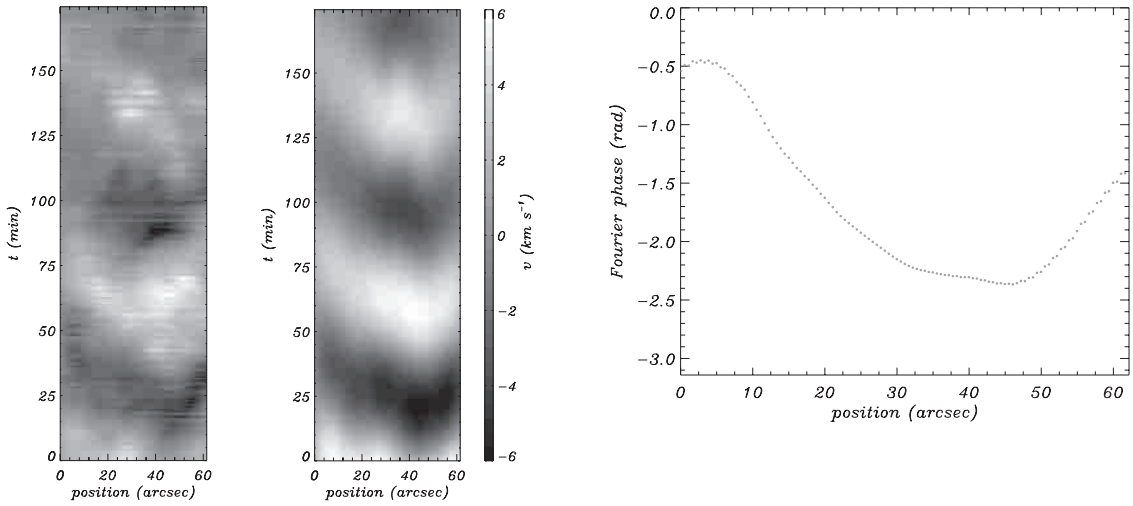


**Figure 14:** Doppler velocity versus position and time along the solid path in Figure 13. *Left:* raw Doppler signal; *middle:* fitted exponentially damped sinusoid; *right:* Fourier phase associated to the 75 min periodicity (from Terradas *et al.*, 2002).

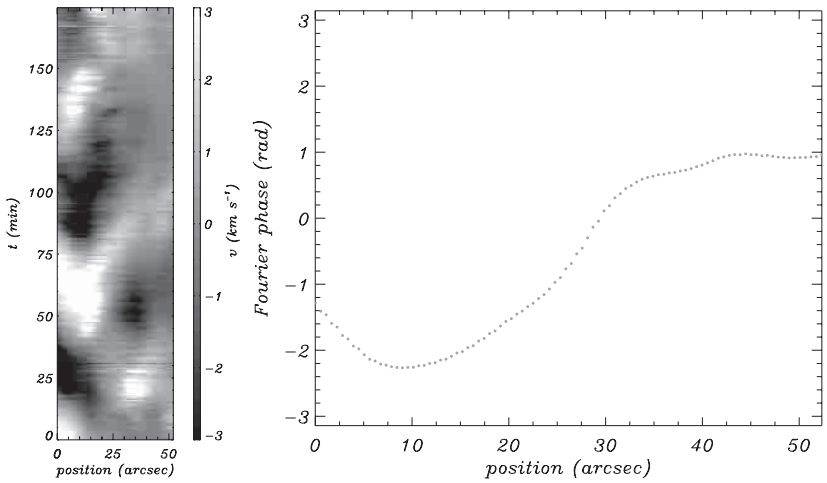


**Figure 15:** Doppler velocity versus position and time along the dashed path in Figure 13. *Left:* raw Doppler signal; *right:* Fourier phase associated to the 75 min periodicity (from Terradas *et al.*, 2002).

in a narrow strip close to positions $x = 35-50$ and $y = 20-30$ and spread out from this region. It is remarkable that the direction of the propagating waves from the source region is essentially parallel to or towards the prominence edge, revealing the anisotropic character of the observed wave propagation. The values of the phase velocity in Figure 17 are also quite different for both directions, being greater for the direction parallel to the edge, with $c_{\rm p} \sim 20$ km s$^{-1}$, than for the direction perpendicular to the edge, with $c_{\rm p} \sim 10$ km s$^{-1}$. This is an indication of the possible existence of some wave guiding phenomenon, which shows a preferential direction of propagation. Note the good agreement between the values of the phase velocity in the directions parallel and perpendicular to the edge and those derived from the analysis of the two selected paths based on Figures 14 and 15.

### 3.6.4 Thread oscillations

Yi *et al.* (1991) and Yi and Engvold (1991) used two-dimensional spectral scans and investigated the presence of periodic variations of the Doppler shift and central intensity of the He I 10,830 Å line in two filaments. Yi *et al.* (1991) performed a first examination of the data and found oscillations with well-defined periods along particular threads in each prominence. For this reason, Yi and Engvold (1991) plotted the Doppler velocity versus position for different times in a given thread, so that a periodic spatial structure would directly yield a measure of the wavelength. Instead of this pattern, an almost linear variation of the velocity along the thread was found and consequently a value of $\lambda$ much larger than the length of the threads, some 20,000 km in the two cases considered, was reported. Given that the periods are between 9 and 22 min, the corresponding phase speed is $c_{\rm p} \gg 15$ km s$^{-1}$. This result suggests that the thread is oscillating in the fundamental kink mode (whose wavelength is of the order of the length of the supporting magnetic tube, that is, around 100,000 – 200,000 km; see Section 4.4.1), rather than being disturbed by a travelling wave. Let us mention that, in general, this analysis may be misleading since the velocity signal does not generally consist of the detected periodic component only, but it is made of this component mixed with other velocity variations. If the periodic component is weak, then the method used by Yi and Engvold (1991) may fail because the signature of the propagating wave is masked by the rest of the signal.

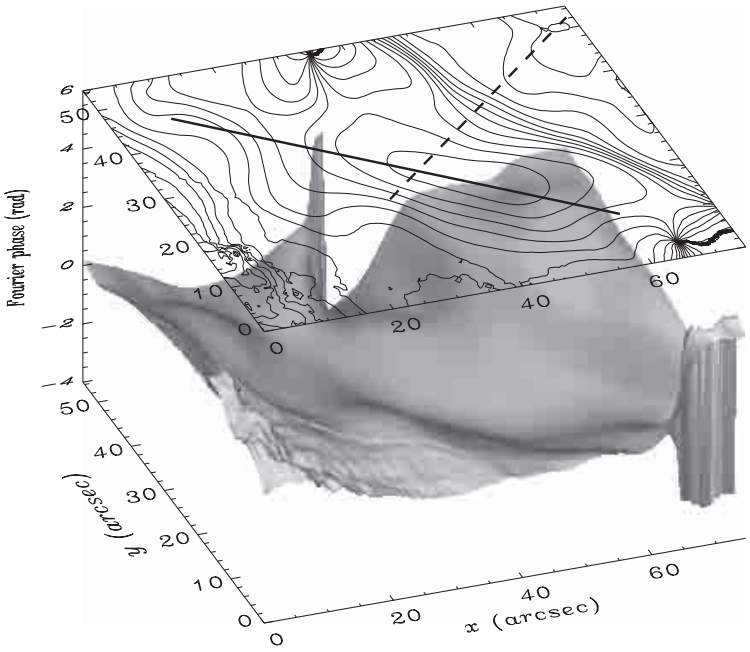


**Figure 16:** Fourier phase associated to a period around 75 min (that is, the one corresponding to the largest peak in the Fourier spectrum) for the rectangular region selected in Figure 13, both as a contour and as a surface plot. The selected paths are also displayed with continuous and dashed straight lines. Note that cuts of the Fourier phase along these two paths give rise to the Fourier phase displayed in Figures 14 and 15 (from Terradas *et al.*, 2002).

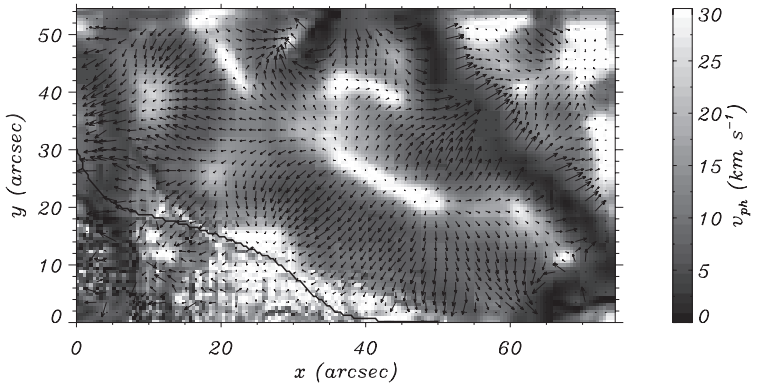


**Figure 17:** Arrows represent the wavevector field computed from the gradient of the Fourier phase displayed in Figure 16, where the length of the arrows is proportional to the modulus of the wavevector. The phase velocity is shown with the help of different levels of grey and black and white colors (from Terradas *et al.*, 2002).

In the analysis of the Doppler velocity in two threads (denoted as T1 and T2) belonging to the same filament, Lin (2005) found a clear oscillatory pattern in time-slice diagrams along the two thin structures. She determined the following wave properties for thread T1: $c_{\rm p} = 60$ km s$^{-1}$, $\lambda = 22$, 12, 15 arcsec, and $P$ in the range 2.5 – 5 min (the 4.4 min period being particularly pronounced). For thread T2, the wave properties are: $c_{\rm p} = 91$ km s$^{-1}$, $\lambda = 38$, 23, 18 arcsec, and $P$ in the range 2.5 – 5 min (the 5-min period being particularly pronounced).

The previous study by Lin (2005) is followed by a much more profound one in which the two-dimensional motions and Doppler shifts of 328 features (or absorbing "blobs") of different threads are examined (see also Lin *et al.*, 2003). Forty nine of these features are observed to flow along the filament axis with speeds of 5 – 20 km s$^{-1}$ while oscillating in the line-of-sight at the same time with periods of 4 – 20 min (see Figure 18). To simplify the examination of oscillations, Lin (2005) computed average Doppler signals along each thread and found that groups of adjacent threads oscillate in phase with the same period. This has two consequences: first, since the periodicity is outstanding in the averaged signal for each thread, the wavelength of oscillations is larger than the length of the thread. Again the interpretation of this result is that the threads oscillate in their fundamental kink mode. Second, in this data set threads have a tendency to vibrate collectively, in groups, rather than independently.

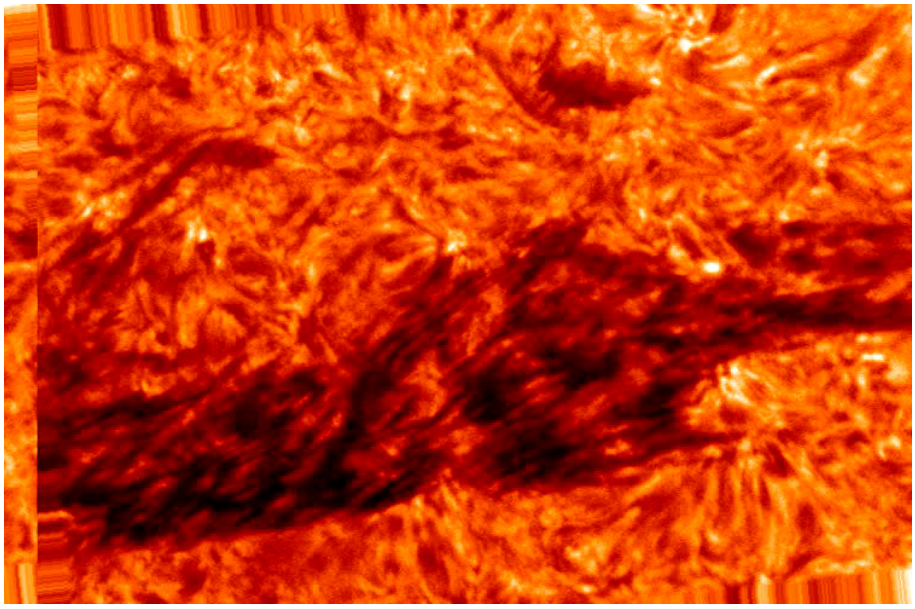

**Figure 18:** Still from a movie showing H$\alpha$ line center images of a quiescent filament observed with the Swedish Solar Telescope in La Palma. The small-scale structures display the characteristic filament counter-streaming motions and undergo simultaneous transverse oscillations, detected as periodic Doppler variations (from Lin *et al.*, 2003). (To watch the movie, please go to the online version of this review article at http://www.livingreviews.org/lrsp-2012-2.)

Horizontally flowing threads that undergo simultaneous transverse oscillations have not only been detected by Lin *et al.* (2003) and Lin (2005), but also by Okamoto *et al.* (2007) using SOT on Hinode. A Ca II H line movie shows continuous horizontal thread motions along an active region prominence (cf. Figure 19). This movie also shows that the threads suffer apparently synchronous vertical oscillatory motions. An example of this phenomenon is shown in Figure 20. Six threads displaying the same behaviour were studied and periods in the range 135 – 250 s were measured. The thread flow velocities range from 15 to 46 km s$^{-1}$ and the vertical oscillation amplitudes

range from 408 to 1771 km. These values are, of course, minimum estimates. A particularly interesting feature of these oscillations is that points along each thread oscillate transversally with the same phase. To reach this conclusion, a given thread is selected and several cuts along its length are considered. A representation of the signal as a function of time reveals that oscillations are synchronous along the entire length of the thread (Figure 21). Once more this points to the kink mode as the responsible for the oscillations, as first pointed out by Van Doorsselaere *et al.* (2008a).

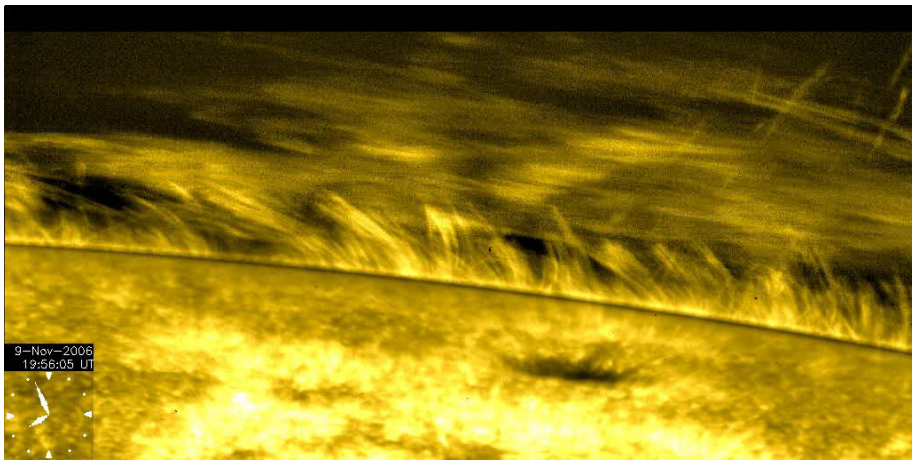


**Figure 19:** Still from a movie showing Ca II H line images taken with Hinode/SOT that shows ubiquitous continuous horizontal motions along the prominence threads at the top right of the image. These threads also oscillate up and down as they flow (from Okamoto *et al.*, 2007). (To watch the movie, please go to the online version of this review article at http://www.livingreviews.org/lrsp-2012-2.)

H$\alpha$ observations conducted with the Swedish 1-m Solar Telescope by Lin *et al.* (2007) allowed to detect waves propagating in some selected threads. Figure 22 serves to illustrate the data analysis procedure for one thread. Here the line intensity shows no coherent behaviour (Figure 22a), while the line-of-sight velocity presents some inclined features caused by waves propagating along the thread; two such features are labelled 1 and 2 in Figure 22b. Figure 22c is another way of presenting Figure 22b and is useful to illustrate more clearly the wavy character of the line-of-sight velocities along an individual thread. Two shorter time sequencies of Doppler velocity are extracted from Figure 22c and shown in Figures 22d and e. It is clear that oscillations are of small amplitude since the Doppler shift has an amplitude of $1-2$ km s$^{-1}$. The power spectra of two of the curves in Figure 22c (shown in Figures 22f and g) yield wavelengths of the oscillatory pattern of, respectively, 3.8 arcsec and 4.7 arcsec. The phase velocity of the oscillations can be derived from the inclination of the features appearing in the Doppler time-slice diagrams of Figure 22b. The phase velocities thus obtained correspond to, respectively, 8.8 and 10.2 km s$^{-1}$. Lin *et al.* (2007) found similar evidence of travelling waves in eight different threads. The mean phase velocity and period (obviously affected by the projection effect) are 12 km s$^{-1}$ and 4.3 min. Periods between 3 and 9 min were found; longer period oscillations could not be detected in the data set used in this work because of its limited duration (18 min).

To test the coherence of oscillations over a larger area, covering several threads, Lin *et al.* (2007) averaged the line-of-sight velocity in a 3.4 arcsec $\times$ 10 arcsec rectangle containing closely packed threads. The averaged Doppler signal (left panel of their Figure 4) displays a very clear oscillation. In addition, the power spectrum of this signal has a significant power peak at 3.6 min. Thus, the conclusion is that neighboring threads tended to oscillate coherently in this rectangular area, possibly because they were separated by very short distances. This signal averaging could be

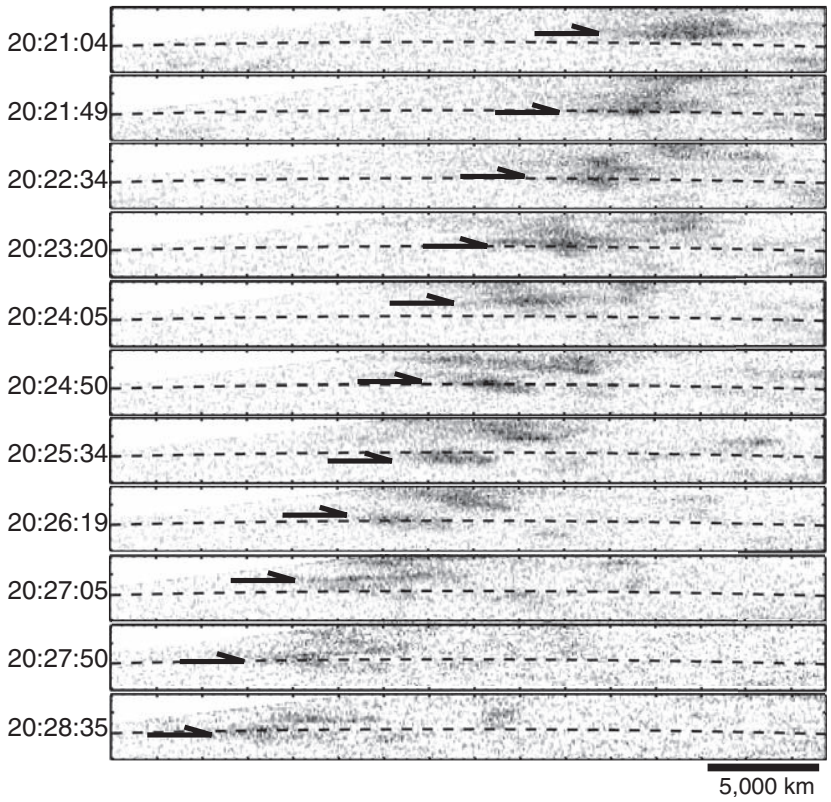


**Figure 20:** Close-up view of a flowing thread displaying transverse oscillations. The measured flow speed is 39 km $s^{-1}$, the amplitude of vertical oscillations is 900 km and the period is 174 s (from Okamoto *et al.*, 2007).

analogous to acquiring data with poor seeing, such as in Terradas *et al.* (2002) (see Section 3.6.3).

Using data from the Swedish 1-m Solar Telescope in La Palma, Lin *et al.* (2009) performed a novel analysis of thread oscillations by combining simultaneous recordings of motions along the line-of-sight and in the plane of the sky, which provides information about the orientation of the oscillatory velocity vector. From the measurements of swaying motions in the plane of the sky, several threads in this work presented travelling disturbances whose main features were characterized (period, phase velocity, and oscillatory amplitude). These parameters were obtained following the procedure of Figure 22. Moreover, two of the previous threads also showed Doppler velocity oscillations with a period similar to that of the swaying motions, so that the threads had a displacement that was neither in the plane of the sky nor along the line-of-sight. By combining the observed oscillations in the two orthogonal directions, Lin *et al.* (2009) derived the full velocity vectors. They suggested that thread oscillations were probably polarized in a fixed plane that may attain various orientations relative to the local reference system (for example, horizontal, vertical, or inclined). Swaying motions are most clearly observed when a thread sways in the plane of the sky, while Doppler signals are strongest for oscillations along the line of sight. In the case of the two analyzed threads, a combination of the observed velocity components yielded an orientation of the velocity vectors of 42° and 59° with respect to the plane of the sky. Once the heliocentric position of the filament was taken into account, these angles transformed into oscillatory motions which were reasonably close to the vertical direction. Lin *et al.* (2009) alerted that this conclusion is only based on two cases and that it is not possible to draw any general conclusion about the orientation

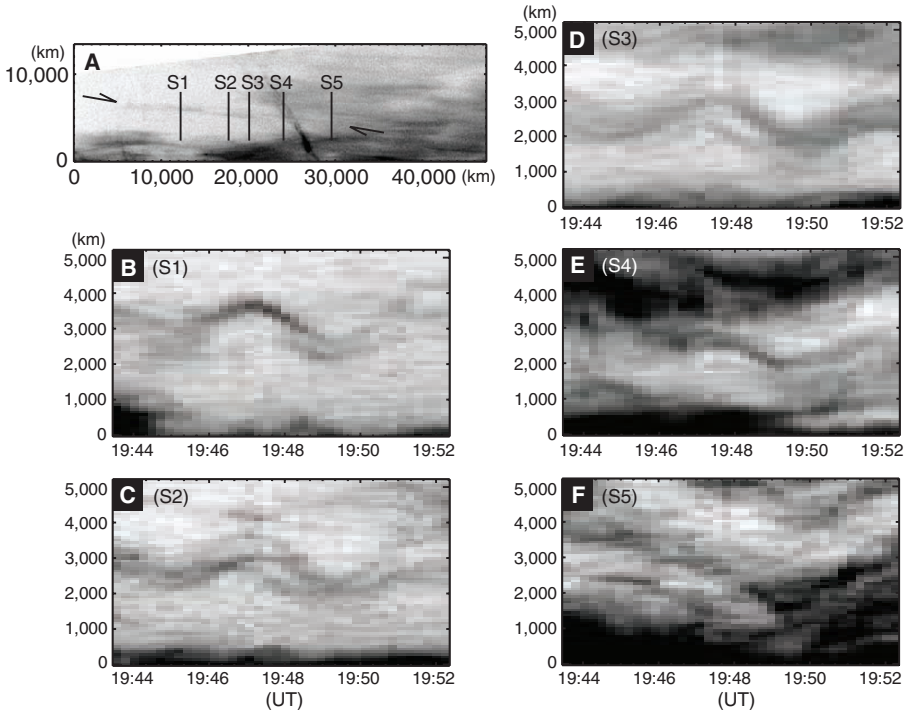


**Figure 21:** Example of a prominence thread undergoing synchronous oscillations along its entire length (all images are shown in negative contrast). (a) The ends of the considered thread are marked by the two arrows. S1 to S5 indicate the locations used to make the height versus time plots shown in panels (b) to (f). (b) – (f) Height-time plots for the locations indicated in (a). Maximum and minimum amplitudes occur at nearly the same time for all locations (from Okamoto *et al.*, 2007).

of the planes of oscillation of filament threads. In fact, Yi and Engvold (1991) found no center-to-limb variations of the velocity amplitude of threads displaying Doppler velocity oscillations, so they concluded that there did not seem to be a preferred direction of oscillatory motions in their data set.

Ning *et al.* (2009b) analyzed the oscillatory behaviour of 13 threads in a quiescent prominence observed with Hinode/SOT. They found that many prominence threads exhibited vertical and horizontal oscillatory motions and that the corresponding periods did not substantially differ for a given thread. In some parts of the prominence, the threads seemed to oscillate independently from one another, and the oscillations were strongly damped. Some of the oscillating threads presented a simultaneous drift in the plane of the sky with velocities from 1.0 to 9.2 km $s^{-1}$. The reported periods were short (between 210 to 525 s), with the dominant one appearing at 5 min. Peak to peak amplitudes were in the range 720 – 1440 km and the phase velocity varied between 5.0 and 9.1 km $s^{-1}$.

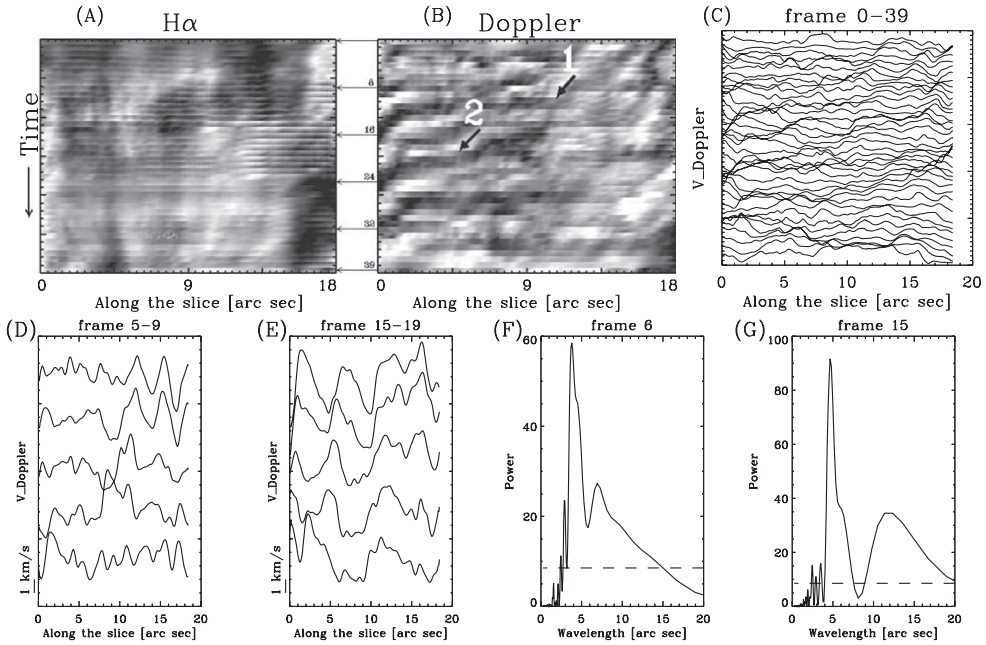


**Figure 22:** (a) and (b) Time-slice diagrams of the H$\alpha$ line intensity and Doppler shift along a filament thread. (c) Data of panel (b) shown as a set of curves instead of as a contour plot. Each curve represents the Doppler velocity along the thread for a fixed time (frame). (d) and (e) Signals from panel (c) for some selected times (frames). (f) and (g) Power spectra of the Doppler shift along the thread for two times. Large peaks help identify the wavelength of propagating oscillations (from Lin *et al.*, 2007).

# 4 Theoretical Aspects of Small Amplitude Oscillations: Periods and Spatial Distribution

The usual interpretation of small amplitude oscillations is that some external agent excites MHD waves in the form of periodic disturbances of the cold plasma. MHD waves can be propagating or standing. In the first case, there is a periodic disturbance of the particles of the prominence plasma that may propagate in the medium. In the second case, the wave is confined to a region with fixed boundaries, thus producing the positive interference of propagating waves. Theoretical models usually consider small amplitude perturbations superimposed on an equilibrium configuration. Then the properties of propagating/standing MHD waves are analyzed. In the case of standing waves, we usually refer to the MHD eigenmodes of the system or to the modes for short.

Following our previous discussion of observations (Section 3.4), oscillations may affect individual threads, groups of threads or even larger areas of a prominence. The wave information (period, wavelength, phase speed, damping time) obtained from the analysis of this kind of events has been presented in Sections 3.5 and 3.6. Given that the main purpose of studying prominence oscillations is to gain a more profound understanding of their nature via seismological studies, it is necessary to study these oscillations theoretically. The information one expects to derive from these works consists of the main wave properties (period, wavelength, phase speed, damping time, spatial distribution, ...). They can then be compared with the observationally determined values. The theory also allows us to determine the temporal variation of the perturbed magnetic field strength and its orientation, the perturbed density, temperature, etc., which means that these variables constitute another source of comparison with observations that will hopefully be exploited in the near future.

Theoretical works are here divided into five groups that reflect widely different choices of prominence equilibrium models: (a) simple, "toy" prominence models (Section 4.1); (b) models in which the prominence is represented as a plasma slab of finite width surrounded by the solar corona (Section 4.2); (c) line current prominence models (Section 4.3); (d) models of infinitely long prominence threads (Section 4.4); and (e) models concerned with the oscillations of prominence threads of finite length (Section 4.5).

## 4.1 Oscillations of very simple prominence models

The aim of the works discussed in this section is to follow elementary arguments to derive approximations for the oscillatory period and the polarization of plasma motions of the main modes of oscillation of a prominence. Some of the obtained results correspond to MHD modes studied in more detail in other works (see Section 4.2). One of these works (Joarder and Roberts, 1992b) is concerned with a prominence treated as a plasma slab embedded in the solar corona and with a magnetic field perpendicular to the prominence main axis (Figure 27). Waves are allowed to propagate along the slab. The coordinate system introduced by Joarder and Roberts (1992b) has the $x$-axis pointing across the prominence (i.e., parallel to the magnetic field), the $z$-axis in the direction of wave propagation and the $y$-axis along the prominence. Three MHD modes exist in this configuration: the fast, Alfvén, and slow modes, with motions polarized in the $z$-, $y$- and $x$-directions, respectively. Some of the simple analogies discussed next allow us to derive approximations for the period of these modes.

A very simplified view of a prominence (Roberts, 1991; Joarder and Roberts, 1992a) is to consider it as a concentrated mass, $M$, suspended on an elastic string (representing the sagged magnetic field that supports the prominence; Figure 23a). Such a model provides some insight into the period of the prominence oscillating vertically as a whole under the action of gravity and magnetic tension. The equilibrium state is simply one in which the gravitational force, $Mg$, is balanced by the upward component of the tension forces, $2T\sin\theta$, where $T$ is the tension in one

of the two strings and $\theta$ is the angle made by the string and the horizontal. Small amplitude oscillations of the mass about this equilibrium state have a period

$$P = 2\pi \left( \frac{L}{g} \tan\theta \right)^{\frac{1}{2}}, \tag{1}$$

with $2L$ the separation distance between the two anchor points, which is analogous to the distance between the photospheric feet of the magnetic tube supporting the prominence plasma. Roberts (1991) noted that for typical parameter values ($g = 274$ m s$^{-2}$, $2L = 50{,}000$ km, and $\theta$ between 3° and 30°), the period of these vertical oscillations is in the range 7 – 24 min, consistent with observationally reported values.

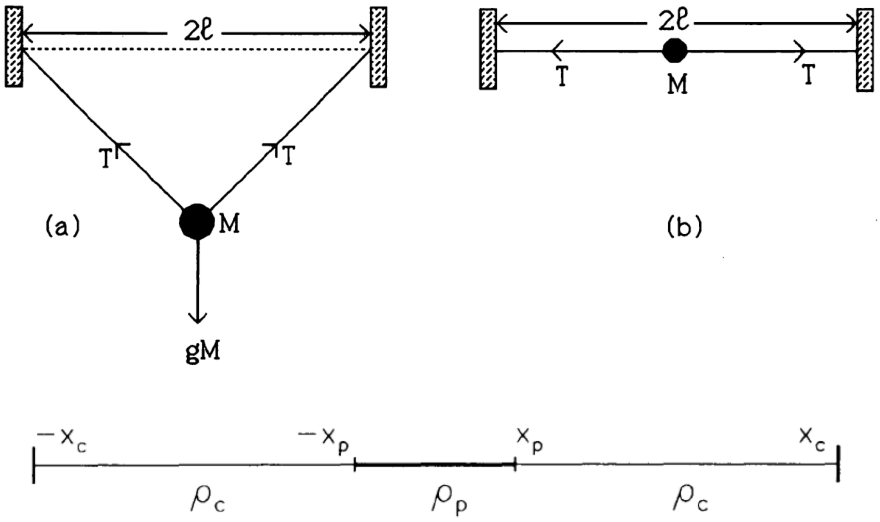


**Figure 23:** Simple models of a prominence. (a) Mass suspended from an elastic string under the influence of gravity and the tension force. (b) Mass suspended from a taut string subject solely to the tension force (from Roberts, 1991). (c) Taut string with density $\rho_c$ except for a central part with density $\rho_p$; gravity is also neglected (from Oliver *et al.*, 1993). The size of the system ($2\ell$ in panels (a) and (b) and $2x_c$ in panel (c)) is denoted by $2L$ in the text.

Roberts (1991) and Joarder and Roberts (1992b) considered a second model of interest (Figure 23b), that resembles the previous one except that now gravity is ignored. In this configuration there are two possible types of oscillation: either longitudinal or transversal. The frequencies of oscillation are given by

$$\frac{\omega L}{c_{\rm str}} \tan\left( \frac{\omega L}{c_{\rm str}} \right) = \frac{2\rho L}{M}, \tag{2}$$

where again $2L$ is the distance between the anchor points, $\rho$ is the mass density of the string (per unit length) and $c_{\rm str}$ is a natural wave speed of the string. To simplify matters one can assume that the mass of the string ($2\rho L$) is negligible in comparison with $M$, that is, $M \gg \rho L$. Translating this inequality to prominences, it is equivalent to assuming that the mass of the cold plasma in a magnetic tube is much larger than the coronal mass in the same tube; this assumption seems most reasonable. Then, Equation (2) reduces to a simple expression for the fundamental mode frequency,

$$\omega = \left( \frac{2T}{ML} \right)^{\frac{1}{2}}, \tag{3}$$

where it has been taken into account that the tension force is $T = \rho c_{\rm str}^2$. Although $M$ has been considered a point mass, one can assume that it has a short, but finite, width $2x_{\rm p}$. Then, the previous expression for the tension force applied to the prominence part of the structure is $T = Mc_{\rm pro}^2/(2x_{\rm p})$, with $c_{\rm pro}$ a natural prominence wave speed. Now, inserting this expression into Equation (3) we obtain for the period

$$P = 2\pi \frac{(Lx_{\rm p})^{\frac{1}{2}}}{c_{\rm pro}}. \tag{4}$$

For fast magnetoacoustic waves in a prominence (with transverse polarization of motions), $c_{\rm pro}$ can be taken as the fast speed,

$$c_{\rm f} = \left(v_{\rm A}^2 + c_{\rm s}^2\right)^{1/2}, \tag{5}$$

with $v_{\rm A}$ and $c_{\rm s}$ the Alfvén and sound speeds, respectively. These quantities are given by

$$c_{\rm s}^2 = \frac{\gamma RT}{\tilde{\mu}} \tag{6}$$

and

$$v_{\rm A}^2 = \frac{B^2}{\mu\rho}, \tag{7}$$

with $\gamma$ the ratio of specific heats, $R$ the gas constant, $\tilde{\mu}$ the mean atomic weight, $\mu$ the magnetic permeability of vacuum, and $T$, $\rho$, and $B$ the temperature, density, and magnetic field strength. For Alfvén modes (also characterized by transverse displacements in this simplified model) $c_{\rm pro} = v_{\rm A}$. The Alfvén velocity is the group velocity but not the phase velocity for Alfvén waves except for parallel propagation. On the other hand, for slow magnetoacoustic waves (with longitudinal polarization of motions), $c_{\rm pro}$ can be taken to be the cusp speed,

$$c_{\rm T} = \frac{v_{\rm A} c_{\rm s}}{\left(v_{\rm A}^2 + c_{\rm s}^2\right)^{1/2}}. \tag{8}$$

The fast speed in Equation (5) and the cusp speed in Equation (8) are in general different from the phase speed and the group speed for fast and slow magnetoacoustic waves. Only for very specific directions of propagation are these quantities phase and/or group speeds. Using the same parameters as above together with $v_{\rm A} = 28$ km s$^{-1}$, $c_{\rm s} = 15$ km s$^{-1}$ and a prominence width equal to one tenth the length of magnetic field lines (i.e., $2x_{\rm p} = 2L/10 = 5000$ km), Equation (4) yields the periods $P_{\rm fast} = 26$ min, $P_{\rm Alfven} = 30$ min, and $P_{\rm slow} = 63$ min, all of them within the range of observed intermediate- to long-period oscillations in prominences.

Oliver *et al.* (1993) (see also Roberts and Joarder, 1994) modified the mass loaded string model of Figure 23b by replacing the point mass $M$ by a denser central string of width $2x_{\rm p}$ (Figure 23c). To solve the wave equation it is necessary to impose the continuity of the displacement and its spatial derivative at the joints $x = \pm x_{\rm p}$. Here the $x$-axis is placed along the string with $x = 0$ the string centre. Then, upon imposing that the string is tied at its ends, the dispersion relation for even solutions about the centre of the string can be expressed as

$$\tan\frac{\omega x_{\rm p}}{c_{\rm pro}} = \left(\frac{\rho_{\rm c}}{\rho_{\rm p}}\right)^{\frac{1}{2}} \cot\frac{\omega(L - x_{\rm p})}{c_{\rm cor}}, \tag{9}$$

whereas the dispersion relation for odd solutions can be written as

$$\cot\frac{\omega x_{\rm p}}{c_{\rm pro}} = -\left(\frac{\rho_{\rm c}}{\rho_{\rm p}}\right)^{\frac{1}{2}} \cot\frac{\omega(L - x_{\rm p})}{c_{\rm cor}}. \tag{10}$$

In these formulas $c_{\rm pro}$ and $c_{\rm cor}$ represent the natural wave speeds of the prominence and coronal parts of the string and $\rho_{\rm p}$ and $\rho_{\rm c}$ their respective densities. These expressions contain a rich array of solutions representing oscillatory modes of the system with different properties. And since there are three characteristic wave modes (fast, Alfvén, and slow, with their specific fast, Alfvén, and tube speeds in the prominence and corona), each set of modes is repeated three times. For the sake of simplicity, we here keep the parameters $c_{\rm pro}$ and $c_{\rm cor}$ in the following expressions, although it must be understood that these two speeds need to be substituted by their corresponding $c_{\rm f}$, $v_{\rm A}$, or $c_{\rm T}$ to derive the frequencies of the fast, Alfvén, and slow solutions.

Equations (9) and (10) can be numerically solved to obtain the frequencies of the various solutions. Nevertheless, some simplifications can be done by taking into account that the prominence width is much shorter than the length of magnetic field lines ($x_{\rm p} \ll L$) and that the prominence density is much larger than the coronal one ($\rho_{\rm p} \gg \rho_{\rm c}$) (Joarder and Roberts, 1992b; Roberts and Joarder, 1994). Further assuming that $\rho_{\rm c}/\rho_{\rm p} \ll x_{\rm p}/L \ll 1$ the following expression for the period of the fundamental mode can be obtained from Equation (9)

$$\omega = \frac{c_{\rm pro}}{(L x_{\rm p})^{\frac{1}{2}}}. \tag{11}$$

It is not surprising that the period corresponding to this frequency is just the one given by Equation (4). Other solutions to Equation (9) can be obtained by simply assuming $\rho_{\rm c}/\rho_{\rm p} \ll 1$. They come in two sets (Joarder and Roberts, 1992b)

$$\omega = n\pi \frac{c_{\rm pro}}{x_{\rm p}}, \qquad n = 1, 2, 3, \ldots, \tag{12}$$

and

$$\omega = n\pi \frac{c_{\rm cor}}{L - x_{\rm p}}, \qquad n = 1, 2, 3, \ldots \tag{13}$$

On the other hand, Equation (10) has no low-frequency solution analogous to that of Equation (11). Instead, it has just two sets of solutions: one of them is identical to Equation (13) and the other one is similar to that given by Equation (12), namely

$$\omega = (2n+1)\frac{\pi}{2} \frac{c_{\rm pro}}{x_{\rm p}}, \qquad n = 0, 1, 2, \ldots \tag{14}$$

To understand the standing solutions supported by the string of Figure 23c, we now concentrate on their spatial distribution. Figures 24a and b display the two lowest frequency solutions of Equation (9), while Figures 24c and d show the two lowest frequency solutions of Equation (10). Their frequencies are approximately given by Equations (11), (12) with $n = 1$, (14) with $n = 0$, and (13) with $n = 1$, respectively. Let us refer to the parts of the string with density $\rho_{\rm c}$ and $\rho_{\rm p}$ as the external and internal regions. The eigenfunction in Figure 24d differs from the other three in that the displacement in the external region is an order of magnitude larger than in the internal region. For this reason it is termed an external mode, since its properties are dominated by the nature of the external part of the string (Joarder and Roberts, 1992b). One then is tempted to call the other three solutions in Figure 24 internal modes, but a simple experiment will prove this to be wrong (Oliver *et al.*, 1993). Let us gradually reduce the size of the internal part of the string (by reducing $x_{\rm p}$). Then internal mode frequencies (cf. Equations (12) and (14)) tend to infinity and in the limit $x_{\rm p} \to 0$ internal modes disappear and only external modes remain. It turns out that this process of gradually removing the density enhancement in the central part of the string does not eliminate the mode of Figure 24a, which is transformed into the fundamental mode of the string. Thus, this is not an internal mode. By a similar process (i.e., by letting $x_{\rm p} \to L$), the central part of the string can be progressively expanded so that we end up with a uniform

density $\rho_{\rm p}$. This makes external mode frequencies grow unbounded (cf. Equation (13)) and for $x_{\rm p} \to L$ only internal modes remain. In this process the mode of Figure 24a transforms into the fundamental mode of the string. Hence, this mode is not an external mode, either, and it owes its existence to the concurrent presence of both the internal and external parts of the string. For this reason Oliver *et al.* (1993) labelled this solution a hybrid mode. The hybrid mode frequency is approximately given by Equation (11), the internal mode frequencies by Equations (12) and (14) and the external mode frequencies by Equation (13).

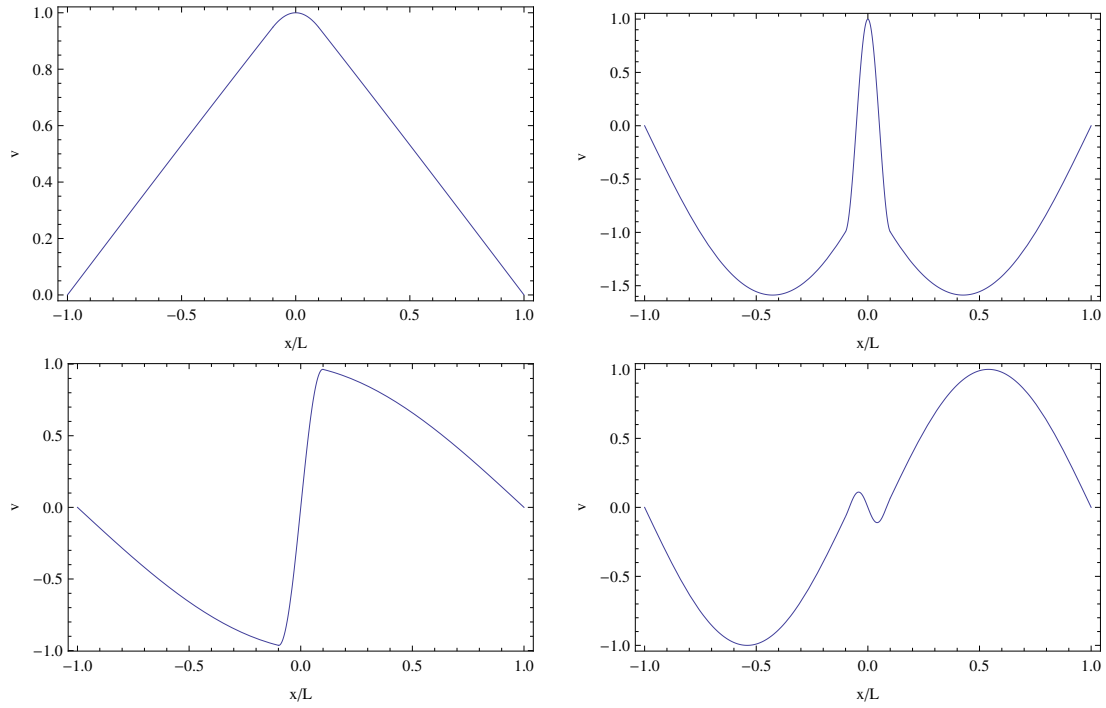


**Figure 24:** Spatial distribution of some normal modes of the string shown in Figure 23c. (a) Hybrid mode, (b) first internal even harmonic, (c) first internal odd harmonic, (d) first external odd harmonic. The spatial coordinate is given in units of $L$ and the string of density $\rho_{\rm p}$ is in the range $-0.1 \leq x \leq 0.1$. The wave speeds are $c_{\rm pro} = 15$ km s$^{-1}$ and $c_{\rm cor} = 166$ km s$^{-1}$, representative of prominence and coronal sound speeds, and the density ratio is $\rho_{\rm p}/\rho_{\rm c} = 11.25$.

This string analogy points out the basic nature of a prominence's modes of oscillation. Because there are in general three MHD modes, there is a fast hybrid mode, an infinite number of internal fast modes, and an infinite number of external fast modes (Joarder and Roberts, 1992b; Oliver *et al.*, 1993; Roberts and Joarder, 1994). Their respective frequencies are given by Equations (11), (12), (13) and (14) with $c_{\rm pro}$ and $c_{\rm cor}$, substituted by the prominence and coronal fast speeds. Something similar can be said about Alfvén and slow modes.

Anzer (2009) performed some simple estimates of the main oscillatory periods of a prominence using the Kippenhahn–Schlüter model (Kippenhahn and Schlüter, 1957) modified so as to include the corona in which the prominence is embedded (for a general solution see Poland and Anzer, 1971). In this configuration, see Figure 25, a curved magnetic field provides support of the cold plasma against gravity. Field lines outside the prominence do not bend downwards and so the magnetic field in the coronal environment does not present the desired arcade shape. For this reason, the role of the dense photosphere is played by two vertical rigid walls. Note that the configuration used by Anzer (2009) bears some resemblance to that of Figure 23a: the coronal

magnetic field is almost uniform and makes an angle $\theta$ with the horizontal direction. Hence, $\tan\theta = B_{z1}/B_x$, with $B_{z1}$ the magnetic field at the prominence boundary. A further similarity between the present model and the previous ones is that the density is analogous to that of Figure 23c.

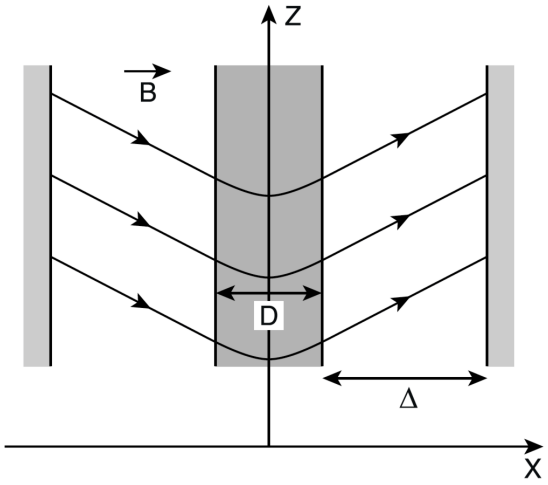


**Figure 25:** Sketch of a prominence configuration based on the Kippenhahn and Schlüter (1957) model. In the text the system size ($2\Delta$) and the prominence width ($D$) are denoted by $2L$ and $2x_{\rm p}$, respectively. Except for the filed line curvature, this configuration is identical to that of Figure 27 (from Anzer, 2009).

Instead of solving the MHD equations, Anzer (2009) took the clever approach of making educated guesses for the restoring forces acting over the prominence ($F(\xi)$) and then solving the equation

$$M\frac{d^2\xi}{dt^2} = F(\xi), \tag{15}$$

where $\xi$ is the plasma displacement and $M$ is the prominence column mass. For magnetically driven oscillations in the $x$-direction, caused by the magnetic pressure gradient, it is postulated that

$$F(\xi) = -M\frac{B_{z1}}{B_x}\frac{g}{L}\xi, \tag{16}$$

so that the corresponding oscillatory period is

$$P = 2\pi\left(\frac{B_x}{B_{z1}}\frac{L}{g}\right)^{\frac{1}{2}} = 2\pi\left(\frac{L}{g\tan\theta}\right)^{\frac{1}{2}}. \tag{17}$$

For oscillations in the $y$- and $z$-directions the restoring force is the magnetic tension of the stretched field lines. In both cases the restoring force is

$$F(\xi) = -M\frac{B_x}{B_{z1}}\frac{g}{L}\xi, \tag{18}$$

and the oscillatory period is

$$P = 2\pi\left(\frac{B_{z1}}{B_x}\frac{L}{g}\right) = 2\pi\left(\frac{L}{g}\tan\theta\right)^{\frac{1}{2}}. \tag{19}$$

It does not come as a surprise that this formula is identical to Equation (1).

Anzer (2009) noted that the field line inclination is expected to be very small and, therefore, $B_{z1}/B_x \ll 1$. As a consequence, the period of $x$-oscillations will be much larger than that of the other two modes, polarized in the $y$- and $z$-directions.

Anzer (2009) also investigated perturbations driven by the gas pressure. He assumed that the coronal magnetic field is so strong that the prominence cannot distort it by a large amount. Further assuming that the magnetic field is horizontal, then the difference in gas pressure on either side of the prominence-corona interface can drive oscillations in the $x$-direction. The restoring force is approximated by

$$F(\xi) = -M\frac{c_{\rm s}^2}{Lx_{\rm p}}\xi, \tag{20}$$

and consequently the period of this mode is

$$P = 2\pi\frac{(Lx_{\rm p})^{\frac{1}{2}}}{c_{\rm s}}. \tag{21}$$

This result coincides with that obtained from the simple string models of Figures 23b and c; see Equation (4).

Four oscillatory modes can be identified from these elementary considerations, but the restoring forces in the $x$-direction act in unison to create a single mode, so we are left with the familiar three MHD modes: fast, Alfvén, and slow.

Some values of the periods given by Anzer (2009) are similar to those in previous works: 200 min for the magnetically dominated oscillations in the $x$-direction, 430 min for the gas pressure driven oscillations and 20 min for the transverse, magnetically driven oscillations.

A further refinement of the string analogy (Joarder and Roberts, 1992b; Roberts and Joarder, 1994) can be introduced by noting that the magnetic field of a prominence is not at 90° with the prominence axis, contrary to the simple models of Figures 23 and 25. Instead, the prominence magnetic field makes an angle $\phi$, typically around 20°, with the long axis of the slab. This is not too important for the almost isotropic fast modes, but Alfvén and slow modes propagate mainly along field lines, which in a skewed magnetic configuration are longer than $2L$ by a factor $1/\sin\phi \approx 3$. Thus, the periods of these waves become larger by this same factor since the travel time needed for them to travel back and forth between the anchor points increases by $1/\sin\phi$. The result is that the hybrid Alfvén and slow modes can have periods up to 60 min and 5 h, respectively. It has been suggested that the last one may be the cause of the very long-period oscillations observed by Foullon *et al.* (2004); Pouget *et al.* (2006).

## 4.2 Oscillations of prominence slabs

In a series of three papers, Joarder and Roberts conducted analyses of the modes of oscillation of a magnetized prominence slab embedded in the corona. The influence of gravity was neglected and so the plasma variables (temperature, pressure, and density) are uniform both in the prominence and in the coronal region. In the first of these works (Joarder and Roberts, 1992a) a purely longitudinal magnetic field was taken (see Figure 26). The dispersion relation contains a variety of modes, which can be fast or slow, combined with kink or sausage and body or surface. Because of the strong difference of the prominence and coronal physical parameters, some eigensolutions are slow in the external medium and fast in the internal medium. Tabulated periods range from 9 h and 5 h to a few minutes. The first values had not been reported at the time this work was published, so emphasis was given by the authors to fast surface modes, with shorter periods around 1 h, and to 5-min and 3-min Pekeris and Love modes.

Joarder and Roberts (1992b) considered the purely transverse magnetic field of Figure 27. From the characteristic wavenumbers of the solutions in the $x$-direction, Joarder and Roberts (1992b)

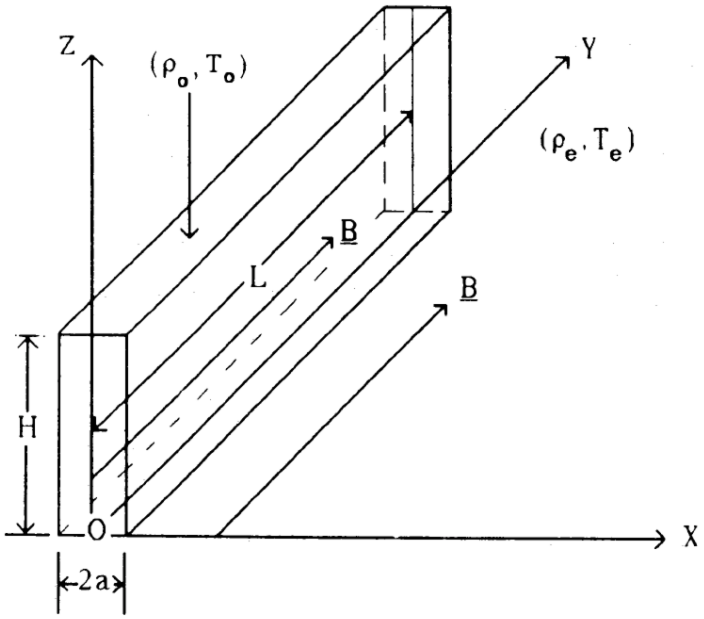


**Figure 26:** Sketch of the prominence slab model with longitudinal magnetic field used by Joarder and Roberts (1992a). These authors assumed that the coronal environment in which the prominence is embedded extends infinitely in the $x$-direction. In this figure the width of the prominence is denoted by $2a$, whereas in our text $2x_p$ is used.

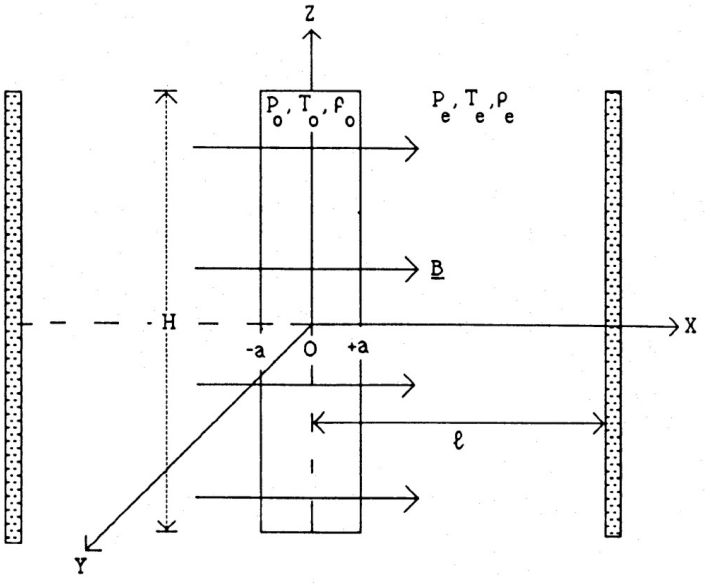


**Figure 27:** Schematic diagram of a prominence slab in a coronal environment. The magnetic field is perpendicular to the prominence axis and tied at the photosphere, represented by two rigid conducting walls at $x = \pm\ell$. Note that in the text the position of the photospheric walls is denoted by $x = \pm L$ (from Joarder and Roberts, 1992b).

created the distinction between internal and external modes (see Section 4.1 for a discussion of the features of these solutions). According to these authors, the former group of modes arises principally from the magnetoacoustic properties of the plasma slab, although these modes are somewhat influenced by the external material because of the presence of free interfaces between the prominence and corona. External modes are present, on the other hand, even in the absence of the prominence plasma but are modified because of the introduction of this cool, dense slab. The dispersion diagrams of kink and sausage modes are shown in Figure 28, where $c_{\rm sp}$ and $v_{\rm Ap}$ are the sound and Alfvén speeds in the prominence, while $c_{\rm sc}$ and $v_{\rm Ac}$ are their coronal counterparts. Moreover, Joarder and Roberts (1992b) also removed propagation along the prominence by setting $k_z = 0$. The mode frequencies are then those on the vertical axes of Figure 28. In this case the dispersion relations of kink and sausage modes are those discussed for a string with densities $\rho_{\rm c}$ and $\rho_{\rm p}$ (Figure 23c), namely Equations (9) and (10). Joarder and Roberts (1992b) gave the approximate solutions of Equations (11) to (14), which are in very good agreement with the results of Figure 28 for $k_z = 0$.

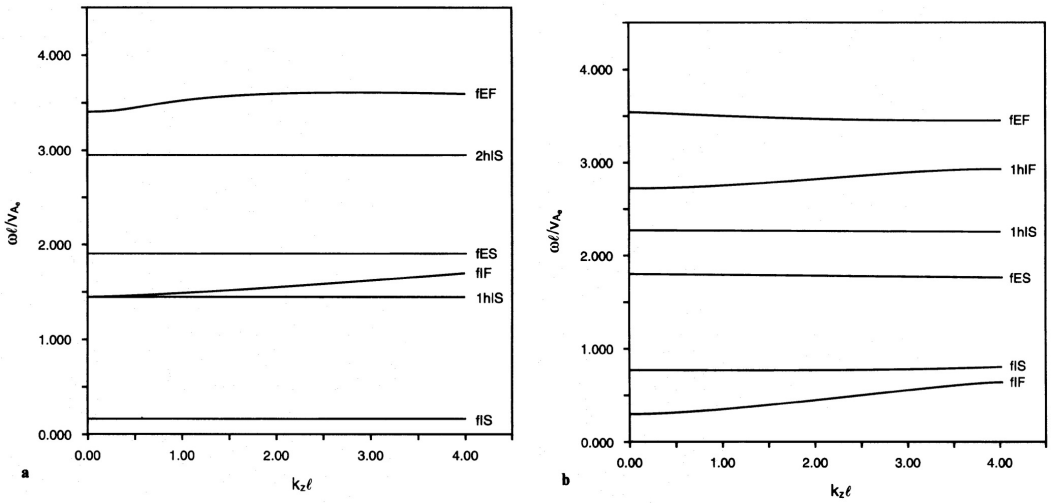


**Figure 28:** Dispersion diagram of magnetoacoustic (a) kink modes and (b) sausage modes in the equilibrium model represented in Figure 27. Meaning of labels at the right of each curve: modes are identified as fundamental (f), first harmonic (1h), second harmonic (2h), ...; internal or external (I or E); and fast or slow (F or S). Here $\omega$ and $k_z$ are the frequency and the wavenumber along the slab, while $v_{\rm Ae}$ is the coronal Alfvén speed and $L$ is half the length of the supporting magnetic field. Parameter values used: $v_{\rm Ap} = 28$ km s$^{-1}$, $c_{\rm sp} = 15$ km s$^{-1}$, $v_{\rm Ac} = 315$ km s$^{-1}$, $c_{\rm sc} = 166$ km s$^{-1}$ (from Joarder and Roberts, 1992b).

Oliver *et al.* (1993) provided more insight into the nature of internal and external modes while using the non-isothermal Kippenhahn–Schlüter solution represented in Figure 25. These authors followed the evolution of fast and slow modes in the dispersion diagram when the prominence is slowly removed by taking $x_{\rm p} \to 0$. They noted that the frequency of internal modes, both slow and fast, progressively grows until the modes disappear from the dispersion diagram and, therefore, only external modes remain. The presence of the prominence region thus provides physical support for the existence of internal modes. The same is true for external modes when the corona is gradually removed by making $x_{\rm p} \to L$. A clear distinction then arises between the two types of modes, although it turns out that the fundamental mode is internal and external at the same time, since it survives both when the prominence and the corona are eliminated. For this reason, this mode with mixed internal and external properties was called hybrid by Oliver *et al.* (1993) and later string by Joarder and Roberts (1993b) because it arises in the string analogy. Nevertheless, internal and

external modes are also present in the string analogy (Section 4.1), so perhaps hybrid mode is a better denomination for this solution.

From Oliver *et al.* (1993) it also appears that the amplitude of perturbations in the prominence is rather small for external modes, a feature that is also present in the string solutions of Figure 24. For this reason it was postulated that they would probably be difficult to detect in solar prominences and that the reported periodic variations are produced by the hybrid and internal modes. In addition, the frequency of internal modes is shown to depend on prominence properties only, while that of hybrid and external modes depends on other physical variables such as the length of field lines. This is in agreement with the approximate Equations (11) to (14).

The essential difference between the equilibrium models in Joarder and Roberts (1992b) and in Oliver *et al.* (1993) is that gravity is neglected in the former, which results in straight magnetic field lines, while it is a basic ingredient in the later, which results in the curved shape of field lines characteristic of the Kippenhahn–Schlüter equilibrium model. Despite the different shape of field lines, the main features of the oscillatory spectrum are similar and so the influence of gravity and field line shape on the properties of the MHD modes is not too relevant in this kind of configurations.

A study of the oscillatory modes of the Kippenhahn and Schlüter (1957) prominence model was undertaken by Oliver *et al.* (1992). The equilibrium model is represented in Figure 25 although the corona is omitted. This implies that this work only provides a restricted account of the MHD modes of a slab prominence since there are no hybrid and external solutions in the absence of the corona. Oliver *et al.* (1992) noted that the three MHD modes possess different velocity orientations. The fast mode is characterized by vertical motions. The Alfvén mode by motions along the filament long axis, and the slow mode by plasma displacements parallel to the equilibrium magnetic field, which in this configuration is practically horizontal and transverse to the prominence. The immediate consequence of this association between modes and velocity polarization is that periodic variations in the Doppler shift are more likely to be detected in filaments near the disk centre for fast modes and in limb prominences for Alfvén and slow modes, depending on the orientation of the prominence with respect to the observer. These features of the MHD modes are retained in other models in which the equilibrium magnetic field is assumed perpendicular to the filament axis (Joarder and Roberts, 1992b, 1993a; Oliver *et al.*, 1993; Oliver and Ballester, 1995, 1996). Nevertheless, the distinction between the three MHD modes is lost when the observed longitudinal magnetic field component is taken into account (Joarder and Roberts, 1993b). Probably, there are no characteristic oscillatory directions associated to the various modes (unfortunately, the issue of velocity polarization in a skewed magnetic equilibrium model has not yet been addressed in the context of prominence oscillations). The actual velocity field in prominences can be substantially more complex than that indicated by investigations based on models with magnetic field purely transverse to the prominence slab.

It is well-known (Leroy, 1988, 1989) that magnetic lines are actually oriented at a rather small angle (around 20°) with the prominence axis. Joarder and Roberts (1993b) took this observational fact into account by adding a longitudinal magnetic field component to the equilibrium model used in Joarder and Roberts (1992b); see Figure 29. Now, the $xy$-plane is defined to contain the assumed horizontal magnetic field. Then, it is not possible to place the $z$-axis parallel to the wavenumber along the prominence axis, so now the $k_y$ and $k_z$ components must be considered. The assumptions of transverse field and propagation of perturbations in the $z$-direction made in the works discussed above simplify the MHD wave equations since the Alfvén mode is decoupled from the slow and fast modes, which can be studied separately with a subsequent reduction in complexity of the mathematical problem. The problem considered by Joarder and Roberts (1993b) contains coupled fast, Alfvén and slow modes. The resulting dispersion diagram (Figure 30) displays a very rich mode structure with plenty of mode couplings, which anticipates the complex nature of actual prominence MHD modes. Unfortunately, the physical properties of perturbations (velocity

polarization, importance of the various restoring forces, perturbations of the equilibrium variables, ...) for the modes in the dispersion diagram have not been examined yet. Oscillation periods up to 4 h (for the slow hybrid mode) are present in this configuration.

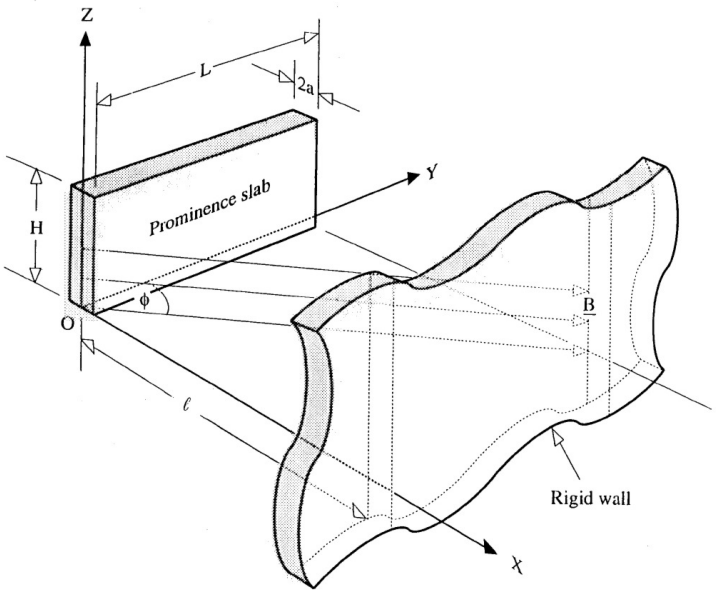


**Figure 29:** Schematic diagram of a prominence slab in a coronal environment. The magnetic field makes an angle $\phi$ with the prominence axis and is tied at the photosphere, represented by two rigid, perfectly conducting walls (from Joarder and Roberts, 1993b).

The previous results rely on models in which the prominence and coronal temperatures are uniform, with a sharp jump of this physical variable from the cool to the hot region at an infinitely thin interface. A smoothed temperature transition between the two domains, representing the prominence-corona transition region (PCTR), was used by Oliver and Ballester (1996) to investigate the MHD modes of a more realistic configuration. Despite the presence of the PCTR in the equilibrium model, internal, external, and hybrid modes are still supported, just like in configurations with two uniform temperature regions. Nevertheless, the PCTR results in a slight frequency shift and in the modification of the spatial velocity distribution so as to decrease the oscillatory amplitude of internal modes inside the prominence. Hybrid modes are not so much affected by the presence of the PCTR because their characteristic wavelength is much longer than the width of the PCTR. Then, the conclusion is that the PCTR may influence the detectability of periodic prominence perturbations arising from internal modes.

Some two-dimensional equilibrium models were considered by Galindo Trejo (1987, 1989a,b, 1998, 2006). The focus of these works was in the stability properties of prominence equilibrium configurations (using the MHD energy principle of Bernstein *et al.*, 1958) and for this reason the author concentrated in the lowest eigenvalue squared. This means that information about all other modes of the system is absent. Galindo Trejo (1987) considered four prominence models, namely those by Kippenhahn and Schlüter (1957), Dungey (1953), Menzel (1951), and Lerche and Low (1980). All these models are isothermal, i.e., they do not incorporate the corona around the prominence plasma. This implies that the important hybrid modes are absent in the analysis. In spite of this, some interesting results were obtained by Galindo Trejo (1987). Here we only mention the most relevant ones. For example, the fundamental mode of the Kippenhahn–Schlüter

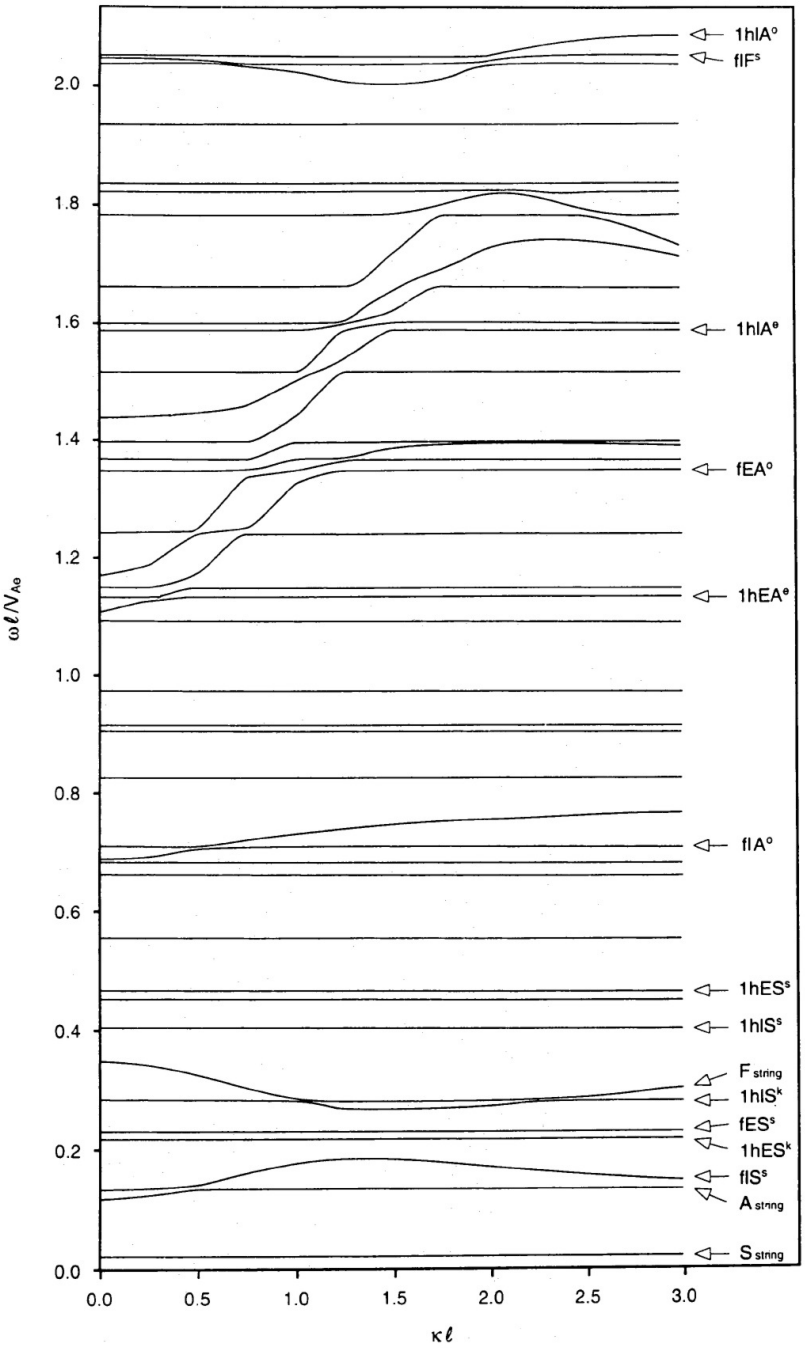


**Figure 30:** Dispersion diagram of magnetoacoustic modes in the equilibrium structure of Figure 29. Meaning of labels at the right of each curve: modes are identified as string, fundamental (f), first harmonic (1h), second harmonic (2h), ...; internal or external (I or E); and fast, Alfvén or slow (F, A or S) according to the mode's nature for $\kappa \ll 1$. Here $\omega$ and $\kappa$ are the frequency and the wavenumber modulus, while $v_{\rm Ae}$ is the coronal Alfvén speed and $\ell$ is half the length of the supporting magnetic field. Parameter values used: $v_{\rm Ap} = 74$ km s$^{-1}$, $c_{\rm sp} = 15$ km s$^{-1}$, $v_{\rm Ac} = 828$ km s$^{-1}$, $c_{\rm sc} = 166$ km s$^{-1}$ (from Joarder and Roberts, 1993b).

configuration, whose period is 16 min, has motions polarized mainly across the prominence slab, so it can be associated with the internal slow mode. On the other hand, the fundamental mode of Dungey's model has horizontal motions mostly along the prominence axis (such as corresponds to Alfvén waves) which are more important at the top of the prominence than at the bottom. The oscillatory period ranges from 55 to 80 min. In the case of Menzel's model, the lowest frequency eigenmode has a period of 40 min and motions whose amplitude increases with height and oriented across the prominence. The eigenmode of Lerche & Low's solution presents a greater range of periods (17 – 50 min) and, once more, with horizontal plasma displacements transverse to the prominence axis. Two improvements of this elaborated work can be done: the inclusion of the coronal plasma and the consideration of the oscillatory properties of other modes.

In two subsequent papers the stability of the prominence model of Low (1981) was investigated. In the first one (Galindo Trejo, 1989a) a uniform magnetic field component along the prominence axis was used, whereas in the second one (Galindo Trejo, 1989b) this quantity is not uniform. The author concluded that, as long as this magnetic field component is weak, these different choices of the magnetic configuration do not influence much the period of the fundamental mode, which is in the range 3 – 7 min. The spatial distribution of motions is similar to that found by Galindo Trejo (1987) for Menzel's and Lerche & Low's equilibrium models.

The following paper of this series (Galindo Trejo, 1998) is concerned with the prominence model of Osherovich (1985), which is characterized by a surrounding horizontal magnetic field connected with the prominence field. Different values of the equilibrium parameters were used and as a result the fundamental mode has periods that range from 4 to 84 min. Galindo Trejo (1998) found that for small values of the longitudinal magnetic field component large velocity amplitudes predominate in the upper part of the prominence, while the opposite happens for a stronger longitudinal component. The magnetic field shear is also relevant: for a moderate (and hence non-uniform) shear, the fundamental eigenmode is in the intermediate-period range and for a uniform shear long periods are obtained.

Galindo Trejo (2006) investigated the equilibrium solution of Osherovich (1989), that is characterized by an external vertical magnetic field that allows the prominence to be placed on the boundary between two regions of opposite photospheric magnetic polarity. A wide range of periods was obtained in this work (9 – 73 min). Also, horizontal oscillatory motions either along the prominence or almost across it were found. Therefore, it seems that in most configurations studied by Galindo Trejo the fundamental oscillatory mode is a slow mode.

## 4.3 Oscillations of line current models

A completely different approach, based on line current models of filaments, was taken by van den Oord and Kuperus (1992), Schutgens (1997a,b), and van den Oord *et al.* (1998) in order to study filament vertical oscillations. They used the model introduced by Kuperus and Raadu (1974), in which the prominence is treated as an infinitely thin and long line, i.e., without internal structure. The interaction of the filament current with the surrounding magnetic arcade and photosphere was taken into account. Furthermore, both normal (NP) and inverse polarity (IP) configurations were considered. When a perturbation displaces the whole line current representing the filament, that remains parallel to the photosphere during its motion, the coronal magnetic field is also disturbed and the photospheric surface current is modified. This restructuring affects the magnetic force acting on the filament current. As a consequence, either this force enhances the initial perturbation and the original equilibrium becomes unstable, or the opposite happens and the system is stable against the initial disturbance. As a further complication, van den Oord and Kuperus (1992), Schutgens (1997a,b), and van den Oord *et al.* (1998) took into account the finite travel time of the perturbations between the line current and the photosphere and investigated the effect of these time delays on the filament dynamics. For both NP and IP configurations, exponentially growing or

decaying solutions were found, which means that perturbations are amplified and the equilibrium becomes unstable, or that oscillations are damped in time and the equilibrium is stable.

Schutgens and Tóth (1999) considered an IP magnetic configuration in which the prominence is not infinitely thin but is represented by a current-carrying cylinder. They solved numerically the magnetohydrodynamic equations assuming that the temperature has a constant value ($10^6$ K) everywhere. The inner part of the filament is disturbed by a suitable perturbation that causes the prominence to move like a rigid body in the corona, both vertically and horizontally, undergoing exponentially damped oscillations. Horizontal and vertical motions can be studied separately since they are decoupled. It turns out that the period and damping time of horizontal oscillations are much larger than those of vertical oscillations. Some remarks about the damping mechanism at work in these models is presented in Section 5.6.

## 4.4 Fine structure oscillations (infinitely long thread limit)

Prominence models considered in Sections 4.1, 4.2, and 4.3 are very simplified representations of solar prominences. They provide us with information about a prominence global oscillatory behaviour, but high resolution observations (see Sections 3.4 and 3.6.4) have given us detailed information about the local oscillatory behaviour of the fine, internal structure of filaments. This has prompted the study of thread oscillations. Two situations can be considered: the simplest one is that of short waves propagating along a thread. By short we mean that the wavelength is much shorter than the thread length, so we refer to this problem as the infinitely long thread limit. On the other hand, the second situation includes propagating waves whose wavelength is comparable to or larger than the length of the thread and standing modes, whose wavelength is of the order of the length of the supporting magnetic tube and thus much larger than the thread length; the works concerned with this second kind of problem are presented in Section 4.5. Other important ingredients uncovered by observations (Sections 3.4 and 3.6.4) are the collective behaviour and the presence of flows in some oscillating threads. These features have been incorporated into some investigations and will be also discussed here.

### 4.4.1 Individual thread oscillations

A simple thread model consists of an infinitely long cylinder filled with cold, dense plasma and embedded in the hotter and less dense corona; field line curvature is neglected. The magnetic field is parallel to the cylinder axis and uniform everywhere (Figure 31).

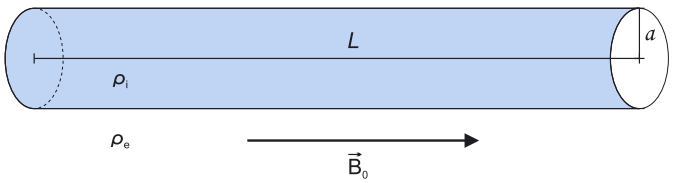


**Figure 31:** Sketch of an infinitely long thread immersed in the solar corona (from Lin *et al.*, 2009).

The MHD modes of this structure have been extensively studied in the context of coronal and photospheric magnetic tube oscillations (Spruit, 1982; Edwin and Roberts, 1983; Cally, 1986). The mode of interest here is the kink mode because it is the only one that produces a significant transverse displacement of the thread, which is the observed behavior of oscillating threads. In the absence of mass flows and assuming that the thread radius is much smaller than the wavelength,

the kink frequency is given by

$$\omega_{\rm k} = k_z \sqrt{\frac{\rho_{\rm f} v_{\rm Ap}^2 + \rho_{\rm c} v_{\rm Ac}^2}{\rho_{\rm p} + \rho_{\rm c}}} = k_z v_{\rm Ap} \sqrt{\frac{2\zeta}{1+\zeta}}, \tag{22}$$

with $k_z$ the axial wavenumber, $\rho_{\rm p}$ and $\rho_{\rm c}$ the prominence thread and coronal densities, $\zeta = \rho_{\rm p}/\rho_{\rm c}$ the density contrast, and $v_{\rm Ap,c} = B/\sqrt{\mu\rho_{\rm p,c}}$ the prominence thread and coronal Alfvén velocities. In terms of the density contrast, the period of kink oscillations with wavelength $\lambda = 2\pi/k_z$ can then be written as

$$P = \frac{\sqrt{2}}{2} \frac{\lambda}{v_{\rm Ap}} \left( \frac{1+\zeta}{\zeta} \right)^{1/2}. \tag{23}$$

Note that the factor containing the density contrast varies between $\sqrt{2}$ and 1 when $\zeta$ is allowed to vary between a value slightly larger that 1 (extremely tenuous thread) and $\zeta \to \infty$. This defines a narrow range of Alfvén speed values when the inverse problem is solved for plasma diagnostic purposes (see Section 6). One can plug typical parameter values into Equation (23) and periods ranging from 30 s to a few minutes are obtained. This result is in agreement with the observed periods of traveling waves in threads (see Section 3.6.4).

This formula for $P$ is based on some assumptions, namely that the thread is much longer than the wavelength, which in turn is much larger than the thread radius (this last approximation is also know as the thin tube limit). Short-wavelength propagating waves in threads have been detected by Lin *et al.* (2007) (see Section 3.6.4 and Figure 22). The length of the fine structure is around 20 arcsec, the reported wavelength is 3.8 arcsec, and the radius of threads is typically between 0.1 and 0.15 arcsec. We can appreciate that the assumptions made to derive Equation (23) are satisfied in this event.

Nakariakov and Roberts (1995) studied the magnetosonic modes of a magnetic slab when flows are present, while Soler *et al.* (2008) considered non adiabatic waves and included a mass flow parallel to the magnetic field in the thread model of Figure 32, which is identical to that of Figure 31 except for the inclusion of plasma flows. Without loss of generality the flow speed in the corona was neglected in this last work, while typical values observed in prominences were taken for the flow speed in the thread (namely $U_{\rm p} \leq 30$ km s$^{-1}$). In the absence of flow, the complex oscillatory frequencies for a fixed, real and positive wavenumber $k_{\rm z}$ appear in pairs, $\omega_1 = \omega_{\rm R} + i\omega_{\rm I}$ and $\omega_2 = -\omega_{\rm R} + i\omega_{\rm I}$. The solution $\omega_1$ corresponds to a wave propagating towards the positive $z$-direction (parallel to magnetic field lines). The $\omega_2$ solution corresponds to a wave that propagates toward the negative $z$-direction (antiparallel to magnetic field lines). Both solutions have exactly the same physical properties in the absence of flows. In the presence of flow, the frequencies are Doppler shifted. In addition, the symmetry between parallel and antiparallel propagation is broken. For instance, for strong enough flows, slow waves can only propagate parallel to the flow direction, antiparallel propagation being forbidden. Figure 33 presents the period of the slow, fast and thermal modes as a function of the flow speed in the thread. For $U_{\rm p} \neq 0$ the fast and slow waves acquire different periods that diverge as $U_{\rm p}$ is increased. For $U_{\rm p} \sim 8.5$ km s$^{-1}$ the antiparallel slow wave becomes a backward wave, which causes its period to grow dramatically near this flow velocity. The influence of the flow on the fast mode is not so severe, while the thermal mode has a finite period that takes very large values.

### 4.4.2 Collective thread oscillations

Some authors have reported that groups of threads oscillate in unison (e.g., Yi *et al.*, 1991) and that large areas of a prominence present in-phase oscillations (e.g., Terradas *et al.*, 2002; Lin *et al.*, 2007), which may be also taken as a sign of collective thread behaviour (see Sections 3.4, 3.6.3, and 3.6.4). Similar collective oscillations have been observed in coronal loops (Verwichte

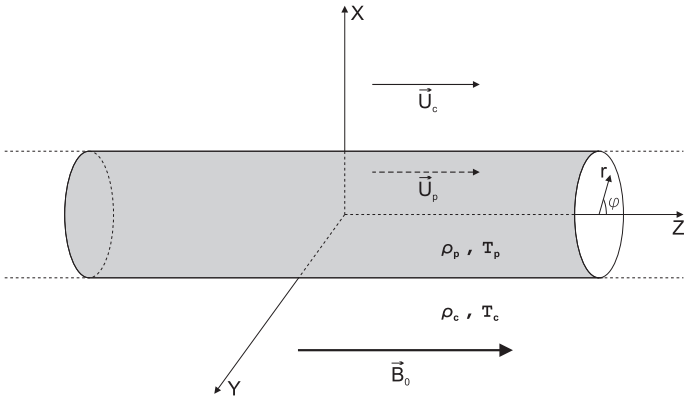


**Figure 32:** Sketch of an infinitely long thread immersed in the solar corona. The respective flow speeds in the thread and the corona are denoted by $U_\mathrm{p}$ and $U_\mathrm{c}$ (from Soler *et al.*, 2008).

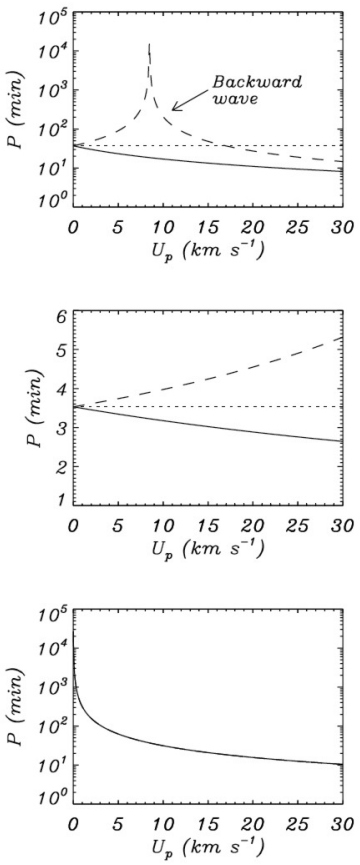


**Figure 33:** Period of the fundamental oscillatory modes of an infinitely long thread versus the mass flow, $U_\mathrm{p}$. The top, middle, and bottom panels correspond to the slow, kink, and thermal modes. Different line styles correspond to waves propagating in the absence of flow (dotted), parallel waves (solid), and anti-parallel waves (dashed). The wavenumber is given by $k_z a = 10^{-2}$, which is consistent with the wavelength of observed propagating waves in prominences (Section 3.6); $a$ is the thread radius (from Soler *et al.*, 2008).

*et al.*, 2004) and their properties have been studied by, e.g., Murawski (1993), Luna *et al.* (2008), Van Doorsselaere *et al.* (2008b), and Robertson and Ruderman (2011). To model this situation, an equilibrium model made of two homogeneous and infinitely long prominence threads embedded in the coronal medium has been considered (see Figure 34).

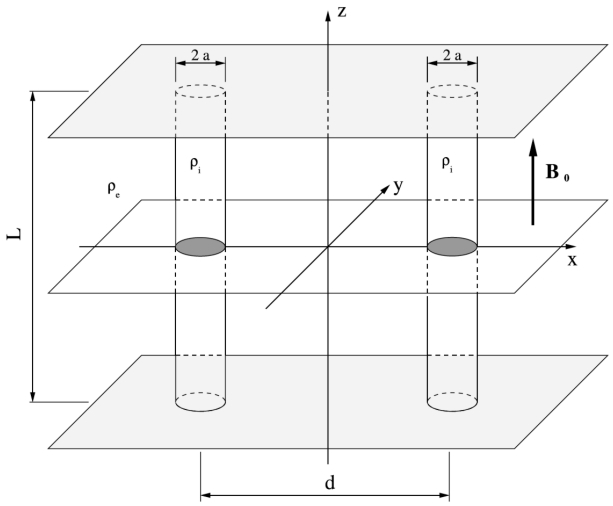


**Figure 34:** Sketch of an equilibrium model made of two infinitely long threads embedded in the solar corona (from Luna *et al.*, 2008).

When identical threads are considered, the system exhibits four kink-like transverse oscillatory modes (Luna *et al.*, 2008; Soler *et al.*, 2009a). These modes are denoted by $S_x$, $A_x$, $S_y$ and $A_y$. The $S$ and $A$ denote symmetry or antisymmetry of the total pressure perturbation with respect to the $yz$-plane. The subscript describes the main direction of polarization of motions, that is in the $xy$-plane; the choice of the coordinate axes is shown in Figure 34 and the spatial distribution of the modes is displayed in Figure 35. In addition to the kink-like modes, Soler *et al.* (2009a) studied the collective slow modes and obtained only two fundamental collective solutions, one symmetric and the other antisymmetric with respect to the $yz$-plane, with motions mainly polarized along the $z$-direction (Figure 35).

A measure of the interaction between threads is the frequency of their normal modes. If the modes have frequencies similar to that of the isolated cylinder, then the threads oscillate independently from one another. If the frequencies are significantly different, the threads oscillate in a collective manner. The left panel of Figure 36 displays the real part of the frequency of the four kink-like solutions as a function of the distance between cylinders. For large separations, i.e., for a distance between threads larger than about 6 or 7 radii, the collective kink mode frequencies are almost identical to the individual kink frequency. This is a signature of a weak interaction between threads, which behave as independent structures. On the other hand, for short thread separations the four frequencies separate in two branches as a consequence of a strong interaction between the cylinders. Therefore, the collective behaviour of oscillations becomes stronger when the threads are closer. In the case of slow modes the interaction between threads is almost negligible and as a result the frequencies of the $S_z$ and $A_z$ modes are almost identical to the individual slow mode frequency (cf. right panel of Figure 36) in the whole range of thread separations. This is in agreement with the fact that transverse motions (responsible for the interaction between threads) are not significant for slow modes in comparison with their longitudinal motions. Therefore, the $S_z$ and $A_z$ modes essentially behave as individual slow modes, contrary to kink-like modes, which display a more significant collective behaviour.

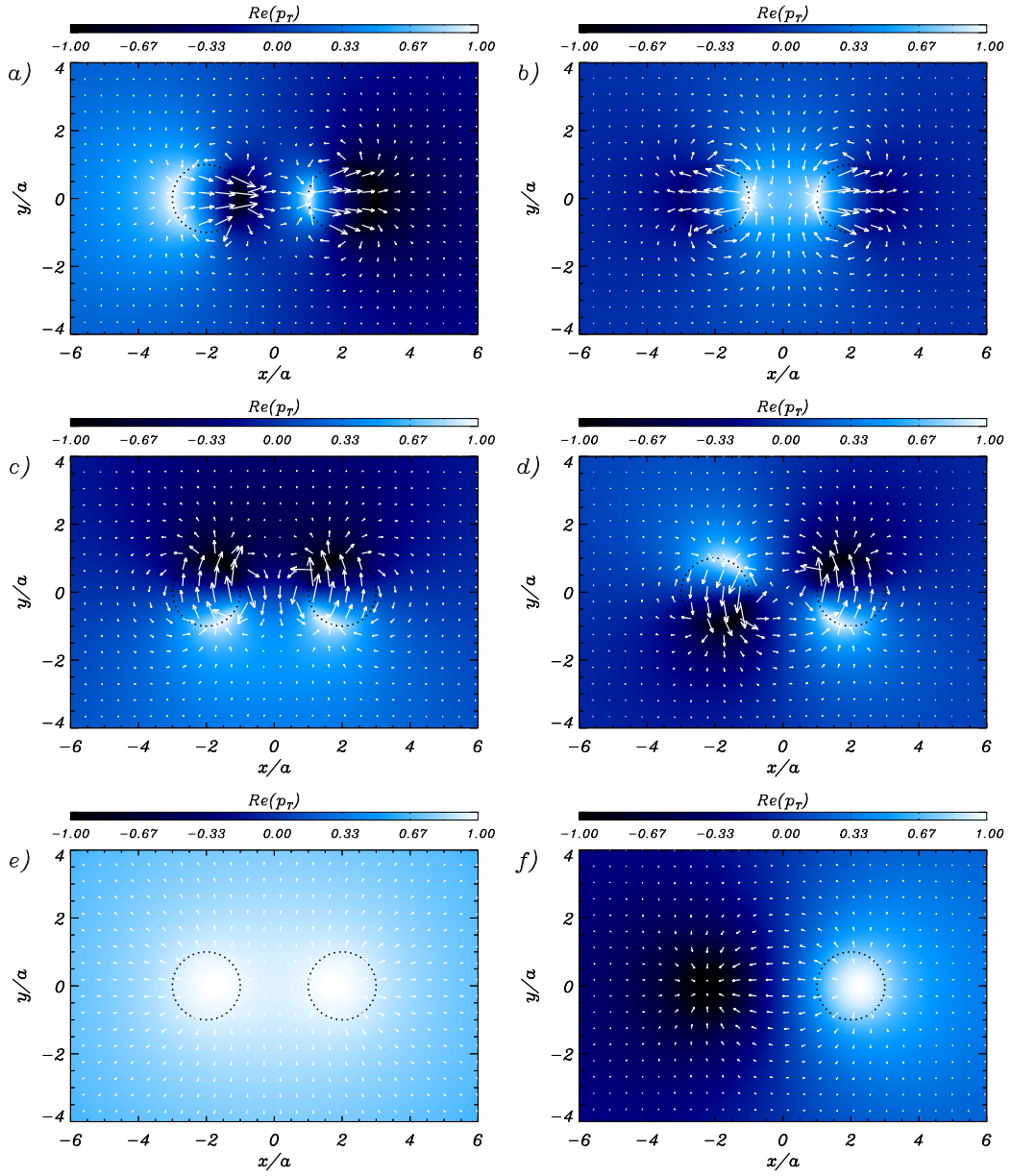


**Figure 35:** Fundamental normal modes of two parallel and infinitely long threads (Figure 34). Total pressure perturbation field (contour plot in arbitrary units) and transverse Lagrangian displacement vector field (arrows) in the $xy$-plane for the wave modes (a) $S_x$, (b) $A_x$, (c) $S_y$, (d) $A_y$, (e) $S_z$, and (f) $A_z$ for a separation between threads $d = 4a$ and a longitudinal wavenumber $k_z a = 10^{-2}$, where $a$ is the thread radius. The prominence thread boundaries are denoted by dotted circles (from Soler *et al.*, 2009a).

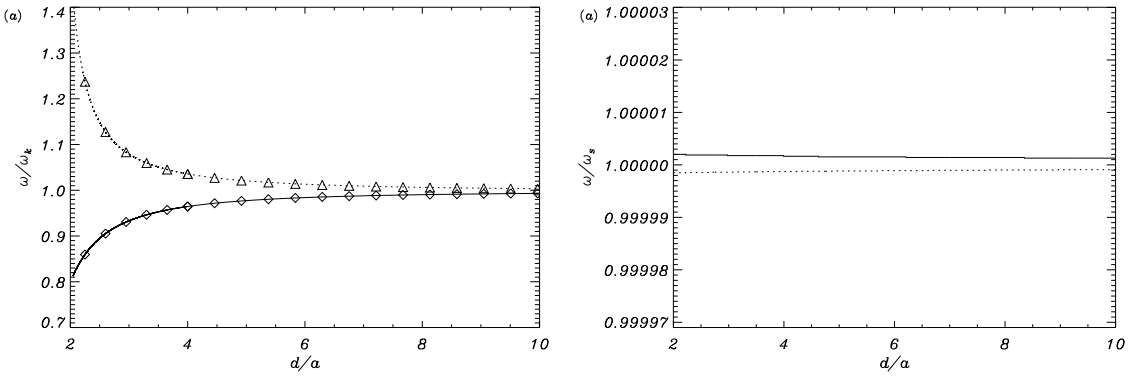


**Figure 36:** Fundamental normal modes of two parallel and infinitely long threads (Figure 34). *Left:* Ratio of the frequency of the four collective kink-like modes, $\omega$, to the frequency of the individual kink mode, $\omega_{\rm k}$, as a function of the normalized distance between strand axes. Meaning of symbols: $S_x$ (solid line), $A_x$ (dotted line), $S_y$ (triangles), and $A_y$ (diamonds). *Right:* Ratio of the frequency of the two collective slow modes, $\omega$, to the frequency of the individual slow mode, $\omega_{\rm s}$ for the $S_z$ (solid line) and $A_z$ (dotted line) (from Soler *et al.*, 2009a).

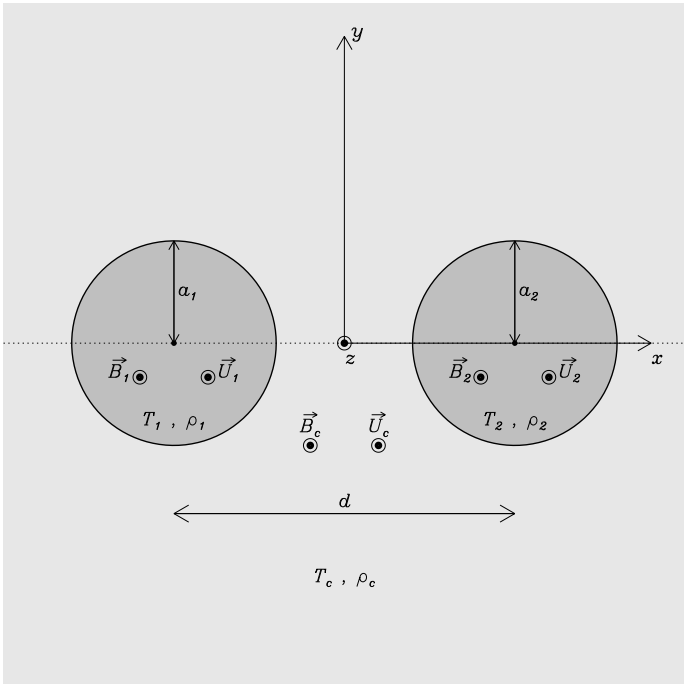


**Figure 37:** Cross-section of a two-thread model analogous to that of Figure 34 with the addition of mass flows along the cylinders (from Soler *et al.*, 2009a).

Soler *et al.* (2009a) assessed the effect of material flows along two threads on the behaviour of collective modes (see Figure 37 for a sketch of the model). Arbitrary flows $U_1$ and $U_2$ were assumed in both cylinders, while coronal flows were neglected. The first main conclusion of this work is that the flows do not eliminate wave modes with collective dynamics (i.e., those that produce significant perturbations in the two threads), even in the case $U_1 \neq U_2$. Nevertheless, the requisite for retaining the collective dynamics is that the Doppler-shifted individual frequencies of the threads must be very similar. In the case of kink-like modes the Doppler-shifted frequencies are given by

$$\Omega_{\rm k1} = \omega_{\rm k1} + U_1 k_z, \tag{24}$$

$$\Omega_{\rm k2} = \omega_{\rm k2} + U_2 k_z, \tag{25}$$

where $\omega_{\rm k1}$ and $\omega_{\rm k2}$ are the kink frequencies of each thread, which are not equal if the thread densities differ. In the limit $\lambda \gg a$, with $a$ the tube radius, these frequencies are given by Equation (22). Now, the requirement for the two threads to oscillate in phase rather than independently is $\Omega_{\rm k1} \sim \Omega_{\rm k2}$. Using Equation (22) and making the reasonable assumption that the density contrast in both cylinders is much larger than one, Soler *et al.* (2009a) obtained

$$U_1 - U_2 \approx \pm\sqrt{2}\,(v_{\rm A2} - v_{\rm A1})\,, \tag{26}$$

where the + sign is for parallel waves and the − sign is for anti-parallel propagation. A similar analysis can be performed for slow modes to obtain,

$$U_1 - U_2 \approx \pm\,(c_{\rm s2} - c_{\rm s1})\,. \tag{27}$$

which points out that the coupling between slow modes occurs at different flow velocities than the coupling between kink modes. Therefore, the simultaneous existence of collective slow and kink-like solutions in systems of non-identical threads is difficult. In the above equations, $v_{\rm A1,2}$ and $c_{\rm s1,2}$ correspond to Alfvén and sound speeds in both threads, respectively.

Soler *et al.* (2009a) extracted another conclusion from Equations (26) and (27): the difference between the Alfvén (sound) speed of the threads determines the difference of the flow speeds for the existence of collective behaviour of kink (slow) modes. Therefore, when flows are present in the equilibrium, collective motions can be found even in systems of non-identical threads for very specific combinations of the two flow velocities. These velocities are within the observed values in prominences if threads with not too different temperatures and densities are considered. However, since the flow velocities required for collective oscillations must take very particular values, such a special situation may rarely occur in prominences. This conclusion has important repercussions for future prominence seismological applications, given that if collective oscillations are observed in large areas of a prominence, threads in such regions should possess very particular combinations of temperatures, densities, magnetic field strengths and flows.

## 4.5 Fine structure oscillations (finite length threads)

Filament threads have been modeled as magnetic flux tubes anchored in the solar photosphere (Ballester and Priest, 1989; Rempel *et al.*, 1999) which are stacked one on top of one another in the vertical and horizontal directions, giving place to the filament body.

Many observations of oscillatory events in threads (see Section 3.6.4) cannot be accounted for by the simple models of Section 4.4 because the obtained results rely on the assumption that the thread length is much larger than the wavelength. Exceptions to this hypothesis are standing waves and propagating waves whose wavelength is of the order of or larger than the thread length. In the models presented in this section a thread is envisaged as a cold, dense condensation that fills the central part of a magnetic tube containing hot coronal plasma and anchored in the solar

photosphere. Although this structure has been modeled with some complexity (Ballester and Priest, 1989; Rempel *et al.*, 1999), only oscillations of much simpler thread configurations have been investigated so far. Because the reported thread oscillations are transverse, we here concentrate on works that investigate this kind of motions.

Joarder *et al.* (1997) considered a thin thread with finite width and length in Cartesian geometry (Figure 38). The thread is infinitely deep since the equilibrium configuration is invariant along the $y$-axis. The influence of the plasma pressure was neglected (i.e., the zero-$\beta$ limit was taken) and consequently the slow mode is absent from their analysis. Joarder *et al.* (1997) obtained the dispersion relations for Alfvén and fast modes, and restricted their study to the oscillatory frequencies, omitting other properties that are also relevant for the understanding of oscillations such as the spatial structure and the polarization of perturbations.

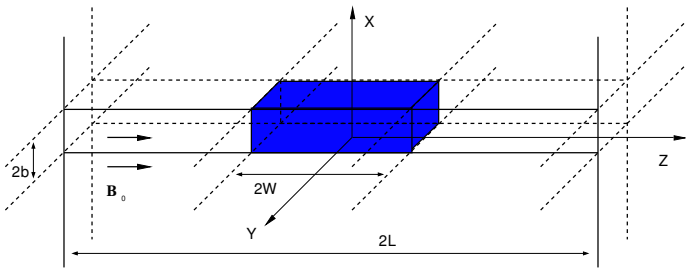


**Figure 38:** Sketch of the thread equilibrium model used by Joarder *et al.* (1997), Díaz *et al.* (2001), and Díaz *et al.* (2003). The blue zone of length $2W$ represents the cold part of the flux tube, i.e., the prominence thread. The length of the magnetic structure is $2L$ and the thread thickness (equivalent to its diameter) is $2b$. The magnetic field is uniform and parallel to the $z$-axis, and the whole configuration is invariant in the $y$-direction (from Díaz *et al.*, 2001).

Using the same two-dimensional configuration, Díaz *et al.* (2001) performed an analytical and numerical study of the behaviour of fast modes when a proper treatment of the boundary conditions at the different interfaces of this thread configuration is included. The main conclusion is that prominence threads can only support a few non-leaky modes of oscillation, those with the lowest frequencies. Also, for reasonable values of the thread length, the spatial structure of the fast fundamental even and odd kink modes is such that the velocity amplitude outside the thread takes large values over long distances (Figure 39). Fast kink modes are associated to normal motions with respect to the thread length (i.e., in the $x$-direction; see Figure 38). The fundamental kink mode (simply referred to as the kink mode) has a velocity maximum at the thread centre, while its first harmonic (that is, the fundamental odd kink solution) has a node in the same position.

Later on, Díaz *et al.* (2003) included wave propagation in the $y$-direction (see Figure 38) making the model fully three-dimensional, and two important features appeared. The first is that the cut-off frequency, that separates confined and leaky modes, varies with the longitudinal wavenumber ($k_y$), which allows the structure to trap more modes. The second one is that a much better confinement of the wave energy is obtained compared to the $k_y = 0$ case (see Figure 40). An interesting issue concerning these results obtained using Cartesian threads is that large velocity amplitudes are found in the corona, which seems to favour collective thread oscillations in front of individual oscillations.

Since cylindrical geometry is more suitable to model prominence threads, Díaz *et al.* (2002) considered a straight cylindrical flux tube with a cool region representing the prominence thread, which is confined by two symmetric hot regions (Figure 41). With this geometry the fundamental sausage mode ($m = 0$, with $m$ the azimuthal wavenumber) and its harmonics are always leaky. However, for all other modes ($m > 0$), at least the fundamental solution lies below the cut-off

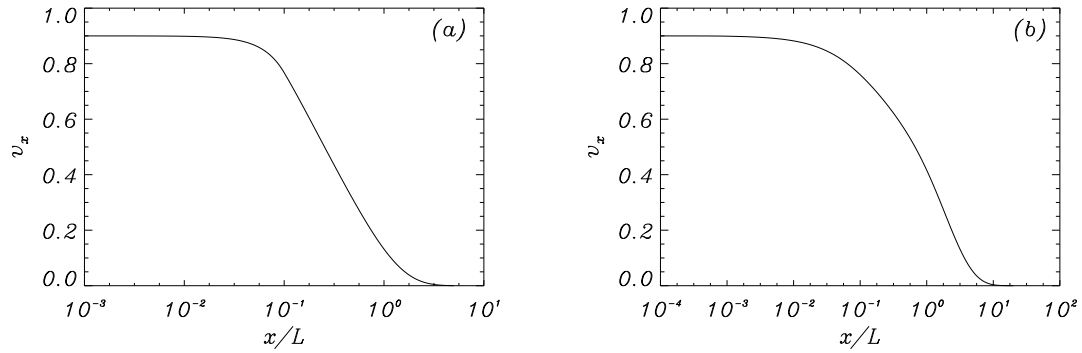


**Figure 39:** Kink mode normal velocity component across the axis of the Cartesian prominence thread depicted in Figure 38. Solutions are symmetric about the thread axis ($x = 0$) and so they are only shown for $x \geq 0$. The length of magnetic field lines is $2L = 200{,}000$ km. (a) In a very thick thread (with a "radius" of 10,000 km) the perturbation is essentially confined to the thread itself, i.e., to $0 \leq x/L \leq 0.1$. (b) In an actual thread (with a "radius" of 100 km) the velocity displays a large amplitude beyond the thread boundary, at $x/L = 0.001$. This means that wave energy spreads into the surrounding coronal medium (from Díaz *et al.*, 2001).

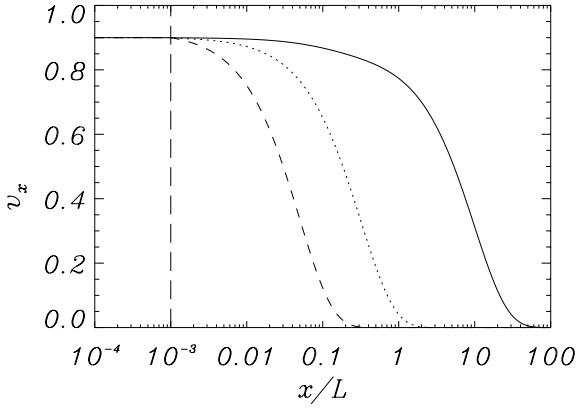


**Figure 40:** Normal velocity component (in arbitrary units) of the kink mode in the direction across the thread axis. The ratio of the thread "diameter" to the length of magnetic field lines is $b/L = 0.001$, while the ratio of the thread length to the field lines length is $W/L = 0.1$. The solid, dotted, and dashed lines correspond to $k_y L = 0$ (curve of Figure 39b), $k_y L = 3$, and $k_y L = 20$. All other parameter values are those of Figure 39. The thread boundary is marked by a vertical dashed line (from Díaz *et al.*, 2003).

frequency. Hence, if any of these modes is excited the oscillatory energy in the prominence plasma does not vary in time after the initial transient has elapsed. Regarding the spatial structure of perturbations, in cylindrical geometry the modes are always confined to the dense part of the flux tube (Figure 42). Therefore, an oscillating cylindrical thread is less likely to induce oscillations in its neighbouring threads than a Cartesian one.

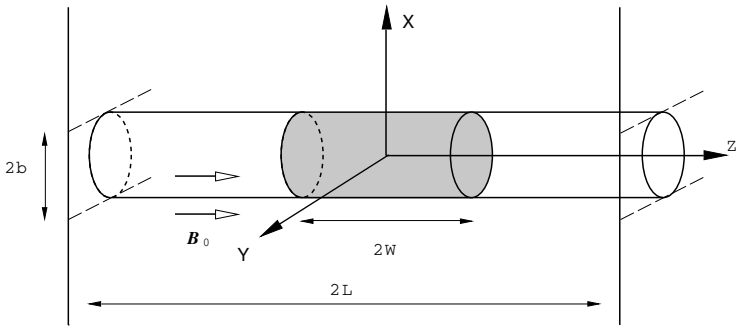


**Figure 41:** Sketch of the equilibrium configuration of a thread in a cylindrical coronal magnetic tube. The gray zone of length $2W$ represents the cold part of the flux tube, i.e., the prominence thread. The length of the magnetic structure is $2L$ and the thread radius is $b$. The magnetic field is uniform and parallel to the $z$-axis, and the whole configuration is invariant in the $\varphi$-direction (from Díaz *et al.*, 2002).

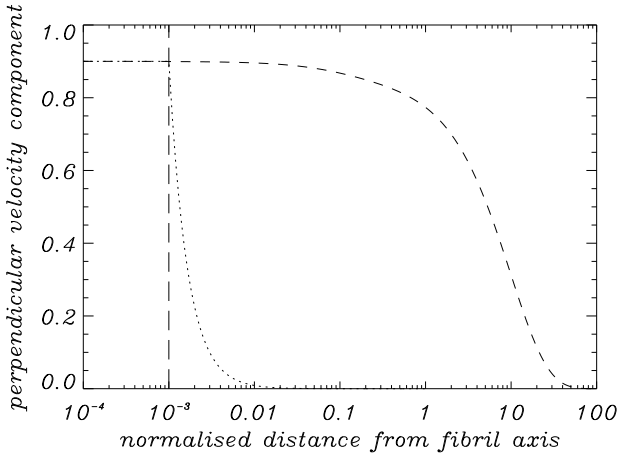


**Figure 42:** Cut of the normal velocity component in Cartesian geometry (dashed line, i.e., curve of Figure 39b) and the radial velocity component in cylindrical geometry (dotted line) in the direction across the thread axis. These solutions correspond to the (fundamental) kink mode in a prominence thread with the parameter values used in Figure 40. The vertical long dashed line marks the thread boundary (from Díaz *et al.*, 2002).

To study the oscillations of the above mentioned configurations, Díaz *et al.* (2001, 2002) developed a very general, although cumbersome procedure. However, Dymova and Ruderman (2005) considered the same problem and to simplify its study took advantage of the fact that the observed thickness of oscillating threads is orders of magnitude shorter than their length. Taking this into account, Dymova and Ruderman (2005) used the so-called thin flux tube (TT) approximation, that enables a simpler solution for the MHD oscillations of longitudinally inhomogeneous magnetic

tubes. Once the partial differential equation for the total pressure perturbation is obtained, a different scaling (stretching of radial and longitudinal coordinates) of this equation inside the tube and in the corona can be performed. Following this procedure, two different equations for the total pressure perturbation inside and outside the flux tube, with well known solutions, are obtained. After imposing boundary conditions, the analytical dispersion relations for even and odd modes were derived and a parametric study was performed. A comparison between the numerical values of the periods obtained with this approach and that of Díaz *et al.* (2002) points out differences of the order of 1%. The only drawback of the method of Dymova and Ruderman (2005) is that it can be only applied to the fundamental mode with respect to the radial dependence.

Taking into account observations by, e.g., Lin (2005), which suggest in-phase oscillations of neighbouring threads in a filament, Díaz *et al.* (2005) studied multi-thread systems in Cartesian geometry. The equilibrium configuration consists of a collection of two-dimensional threads modeled as in Díaz *et al.* (2001) and separated by an adjustable distance $2c$ (Figure 43). An inhomogeneous filament composed of five threads was constructed (Figure 44) with thread density ratios thought to represent the density inhomogeneity of a prominence. The separations between threads were chosen randomly within a realistic range. The thread separations were then changed with respect to the values of Figure 44 by a certain factor and the kink modes were computed. Their frequencies are displayed in Figure 45, where $c_{\rm ref}$ is a reference value representative of the separations between threads. When the separations are small, i.e., for $c_{\rm ref}/L \ll 1$, there is a strong interaction between threads since the perturbed velocity in a given thread can easily extend over its neighbours. As a result, there is only one even non-leaky mode: the one producing in-phase oscillations of all threads. The other extreme of Figure 45, i.e., $c_{\rm ref}/L \gg 1$, corresponds to very large separations. In this situation all threads oscillate independently and the individual kink mode frequencies are recovered. Note that realistic thread separations correspond to $c_{\rm ref}/L \sim 10^{-3}-10^{-2}$, for which only the kink mode mentioned before is supported by the system. Its frequency is lower than the individual kink mode frequencies. Although these results show some agreement with observations about the collective oscillations of threads, the use of Cartesian geometry favours this kind of combined behaviour and so a similar study based on a cylindrical model is also of interest.

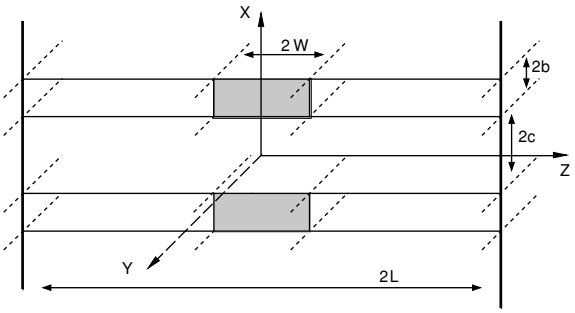


**Figure 43:** Sketch of a multi-thread equilibrium configuration. The grey zone represents the cold part of the magnetic tube, i.e., the prominence. The magnetic field is uniform and parallel to the $z$-axis, and the whole configuration is invariant in the $y$-direction (from Díaz *et al.*, 2005).

Díaz and Roberts (2006) studied the properties of the fast MHD modes of a periodic, Cartesian thread model (see Figure 1 of Díaz and Roberts 2006). This configuration provides a bridge between a structure with a limited number of threads (studied by Díaz *et al.*, 2005, see Figure 43) and a homogeneous prominence with a transverse magnetic field (investigated by Joarder and Roberts, 1992b, see Figure 27). Díaz and Roberts (2006) found that for thread separations of the order of their thickness the only confined modes are those in which large numbers of threads are constrained to oscillate nearly in phase. The spatial structure of these solutions is similar to that

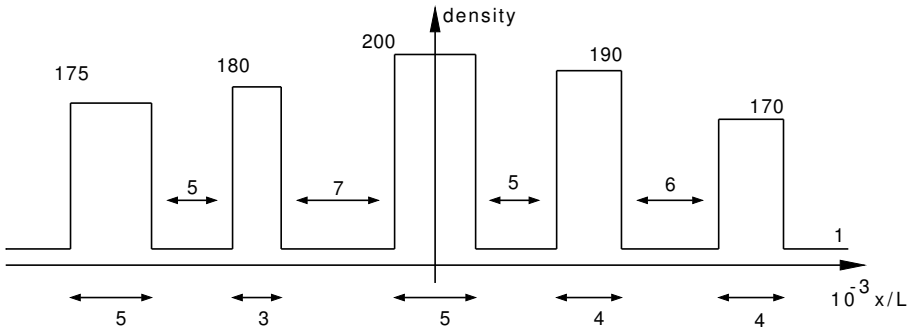


**Figure 44:** Sketch of the density profile in the direction $z = 0$ of an inhomogeneous multi-thread system. The density values of the are normalized to the coronal value. Between and under the threads the dimensionless separation, $2c/L$, and "diameter", $2b/L$, are given (from Díaz *et al.*, 2005).

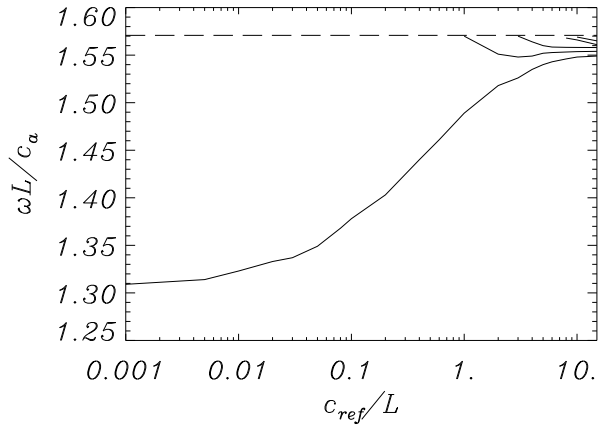


**Figure 45:** Dimensionless frequency versus the dimensionless reference separation between threads in a multi-thread system. In this figure $c_a$ is the Alfvén speed in the corona (from Díaz *et al.*, 2005).

of the propagating modes of a homogeneous prominence, with small-scale deviations due to the presence of the dense threads. Their period is equal to $\sqrt{f}P$, with $P$ the period of the prominence slab and $f$ the filling factor. The system with a limited number of threads has an even shorter period and a comparison between the different configurations considered by Díaz and Roberts (2006) gives periods of 23.6 min for the homogeneous prominence, between 12.1 and 19.3 min for the system of periodic threads and 5.3 for the four-thread configuration studied by Díaz *et al.* (2005). Hence, the main conclusion of Díaz and Roberts (2006) is that prominence fine structure plays an important role and cannot be neglected.

Terradas *et al.* (2008) modeled the transverse oscillations of flowing prominence threads observed by Okamoto *et al.* (2007) with HINODE/SOT (Section 3.6.4). The kink oscillations of a flux tube containing a flowing dense part, which represents the prominence material, were studied from both the analytical and the numerical point of view. In the analytical case, the Dymova and Ruderman (2005) approach with the inclusion of flow was used, while in the numerical calculations the linear ideal MHD equations were solved. The results point out that for the observed flow speeds there is almost no difference between the oscillation periods when static versus flowing threads are considered, and that the oscillatory period matches that of a kink mode. In addition, to obtain information about the Alfvén speed in oscillating threads, a seismological analysis as described in Section 6.6 was also performed. Also motivated by the observations by Okamoto *et al.* (2007), Soler and Goossens (2011) have further studied the properties of kink MHD waves propagating in flowing threads. In good agreement with Terradas *et al.* (2008), the period is seen to be slightly affected by mass flows. When the thread is located near the center of the supporting magnetic tube, and for realistic flow velocities, the effect of the flow on the period is estimated to fall within the error bars from observations. On the other hand, as the thread approaches the footpoint of the magnetic structure, flows introduce differences up to 50% in comparison to the static case. The variation of the amplitude of kink waves due to the flow is additionally analysed by Soler and Goossens (2011). It is found that the flow leads to apparent damping or amplification of the oscillations. During the motion of the prominence thread along the magnetic structure, the amplitude grows as the thread gets closer to the center of the tube and decreases otherwise. This effect might be important, since it would modify the actual observed attenuation, if any physical damping mechanisms is present.

Theoretical models described in this section have considered prominence plasmas as either slabs or cylindrical magnetic flux tubes. Slab models were intended to study the global oscillation properties of prominences, while flux tube models seem to be more appropriate for their application to the fine structure of prominences. Nevertheless, the properties of modes of oscillation like the kink mode have often been first studied in Cartesian geometry and then in cylindrical configurations. A few differences that arise are relevant when comparing the theoretical results to observations.

The theoretical frequencies for the kink mode in Cartesian geometry are above the value obtained for a cylindrical equivalent with the same physical properties. This has been shown by Arregui *et al.* (2007b), in the context of coronal loop oscillations. By assuming that a kink mode in a cylinder can be modeled in Cartesian geometry by adding a large perpendicular wavenumber, these authors show that in that limit the cylindrical kink mode frequency is recovered. A similar analogy was used by Hollweg and Yang (1988) who derived an expression for the damping time of a surface wave in Cartesian geometry and applied their result to coronal loops in the limit of large perpendicular wave number.

The spatial distribution of the eigenfunctions also differ when one compares, e.g., the kink mode properties in Cartesian and cylindrical geometry. The drop-off rate of the transverse velocity component is faster in cylindrical flux tubes than in slabs. A cylinder is a much better wave guide. For this reason, an oscillating cylindrical thread is less likely to induce oscillations in its neigboring threads than a Cartesian thread.

# 5 Theoretical Aspects of Small Amplitude Oscillations: Damping Mechanisms

Temporal and spatial damping is a recurrently observed characteristic of prominence oscillations (see Section 3.5). Several theoretical mechanisms have been proposed in order to explain the observed damping. Direct dissipation mechanisms seem to be inefficient, as shown by Ballai (2003), who estimated, through order of magnitude calculations, that several isotropic and anisotropic dissipative mechanisms, such as viscosity, magnetic diffusivity, radiative losses, and thermal conduction cannot in general explain the observed wave damping. The time and spatial damping of linear non-adiabatic MHD waves has been considered by Carbonell *et al.* (2004, 2009), Terradas *et al.* (2001), Terradas *et al.* (2005), Carbonell *et al.* (2006), and Soler *et al.* (2007, 2008). The overall conclusion from these studies is that thermal mechanisms can only account for the damping of slow waves in an efficient manner, while fast waves remain almost undamped. Since prominences can be considered as partially ionized plasmas, a possible mechanism to damp fast and Alfvén waves could be ion-neutral collisions (Forteza *et al.*, 2007, 2008), although the ratio of the damping time to the period does not completely match the observations. Besides non-ideal mechanisms, another possibility to attenuate fast waves in thin filament threads comes from resonant wave damping (see, e.g., Goossens *et al.*, 2010), which needs the presence of a smooth radial profile of the Alfvén speed. This phenomenon is well studied for transverse kink waves in coronal loops (Goossens *et al.*, 2006; Goossens, 2008) and provides a plausible explanation for quickly damped transverse loop oscillations first observed by TRACE (Aschwanden *et al.*, 1999; Nakariakov *et al.*, 1999).

The time scales of damping produced by these different mechanisms should be compared with those obtained from observations, that indicate that the ratio of the damping time to the period, $\tau_{\rm d}/P$, is of the order of 1 to 4. The theoretical approach of many works about the damping of prominence oscillations has been to first study a given damping mechanism in a uniform and unbounded medium and, thereafter, to introduce structuring and non-uniformity. This has led to an increasing complexity of theoretical models in such a way that some of them now combine different damping mechanisms. Detailed reports on theoretical studies of small amplitude oscillations in prominences and their damping can be found in Oliver (2009), Ballester (2010), and Arregui and Ballester (2011). Here, we collect the most significant aspects of the theoretical mechanisms that have been proposed to explain the observed time-scales.

## 5.1 Damping of oscillations by thermal mechanisms

In a seminal paper, Field (1965) studied the thermal instability of a dilute gas in mechanical and thermal equilibrium. Using this approach, the time damping of magnetohydrodynamic waves in bounded Kippenhahn–Schlüter and Menzel prominence models was studied by Terradas *et al.* (2001). Similar studies using prominence slabs embedded in the solar corona were undertaken by Soler *et al.* (2007) and Soler *et al.* (2009b).

### 5.1.1 Non-adiabatic magnetoacoustic waves in prominence slabs

Terradas *et al.* (2001) studied the radiative damping of quiescent prominence oscillations. They adopted a relatively simple non-adiabatic damping mechanism, by including a radiative loss term based on Newton's law of cooling with constant relaxation time. The influence of this type of radiative dissipation on the normal modes of Kippenhahn–Schlüter and Menzel quiescent prominence models was analyzed. The normal modes of these configurations had previously been investigated by Oliver *et al.* (1992) and Joarder and Roberts (1993a); cf. Section 4.2. In a Kippenhahn–Schlüter prominence model, the fundamental slow mode is unaffected by radiation, but its harmonics are strongly damped. On the other hand, in a Menzel prominence configuration all slow modes are

characterized by short damping times. The damping time depends on the curvature of field lines, in such a way that more curved models produce larger damping times. In both prominence models, fast modes are practically unaffected by radiative losses and have very long damping times.

A more involved analysis was performed by Soler *et al.* (2007) by including thermal conduction, optically thin or thick radiation, and heating in the energy equation. The prominence was modeled as a plasma slab embedded in an unbounded corona and with a magnetic field oriented along the direction parallel to the slab axis (see Figure 26); this is the equilibrium configuration of Joarder and Roberts (1992a), whose normal modes have been discussed in Section 4.2. Soler *et al.* (2007) found that radiation losses have a different effect on magnetoacoustic waves depending on their wavenumber. For typical values of observed wavelengths, the internal slow mode is attenuated by radiation from the prominence plasma, the fast mode by the combination of prominence radiation and coronal conduction and the external slow mode by coronal conduction. This study highlights the relevance of the coronal physical properties on the damping properties of fast and external slow modes, whereas this aspect does not affect the internal slow modes at all. For thin slabs, representing a fine thread, Soler *et al.* (2007) found that the fast mode is less attenuated, whereas both internal and external slow modes are not affected by non-adiabatic damping mechanisms.

Damping of magnetoacoustic waves in slab prominence models with a transverse magnetic field (see Figure 27 and Section 4.2 for a description of the normal modes) were studied by Soler *et al.* (2009b). The most relevant damping processes are coronal thermal conduction and radiative losses from the prominence plasma. In terms of the spatial distribution of the studied normal modes, it was found that both mechanisms govern together the attenuation of hybrid modes, whereas prominence radiation is responsible for the damping of internal modes and coronal conduction essentially dominates the attenuation of external modes. In terms of the different magnetohydrodynamic wave types, slow modes were found to be efficiently damped, with damping times compatible with observations. On the contrary, fast modes are less attenuated by non-adiabatic effects and their damping times are several orders of magnitude larger than those observed. The inclusion of the coronal medium in the analysis causes a decrease of the damping times compared to those of an isolated prominence slab, but this effect is still insufficient to obtain fast mode damping times compatible with observations.

### 5.1.2 Non-adiabatic magnetoacoustic waves in a single thread with mass flows

Soler *et al.* (2008) investigated the effects of both mass flow and non-adiabatic processes on the oscillations of an individual prominence thread modeled as an infinite homogeneous cylinder Figure 32). Thermal conduction and radiative losses were taken into account as damping mechanisms. For a discussion of the oscillatory features of this system, see Section 4.4.1.

The analysis of the damping time-scales for the different wave types shows that slow and thermal modes are efficiently attenuated by non-adiabatic mechanisms. On the contrary, fast kink modes are much less affected and their damping times are much larger than those observed. These results are compatible with the known damping properties of these waves in the absence of flows.

In addition, Soler *et al.* (2008) analyzed how mass flows affect these damping properties. Figure 46 shows the dependence of the period, damping time, and their ratio as a function of the flow velocity for the slow, fast and thermal modes (for a discussion of the thermal mode, see Carbonell *et al.*, 2009). Note that the left column of this figure has been already presented in Figure 33, but it is retained here to facilitate our explanation. Flow velocities in the range $0-30$ km s$^{-1}$, that correspond to the observed flow speeds in quiescent prominences, were considered. The damping time of slow and thermal modes is found to be independent of the flow velocity, but the attenuation of the fast kink mode is affected by the flow. The larger the flow velocity, the more attenuated the parallel fast kink wave, whereas the opposite occurs for the anti-parallel solution. This behaviour is due to the weak coupling of the fast modes to external slow modes (Soler *et al.*, 2008).

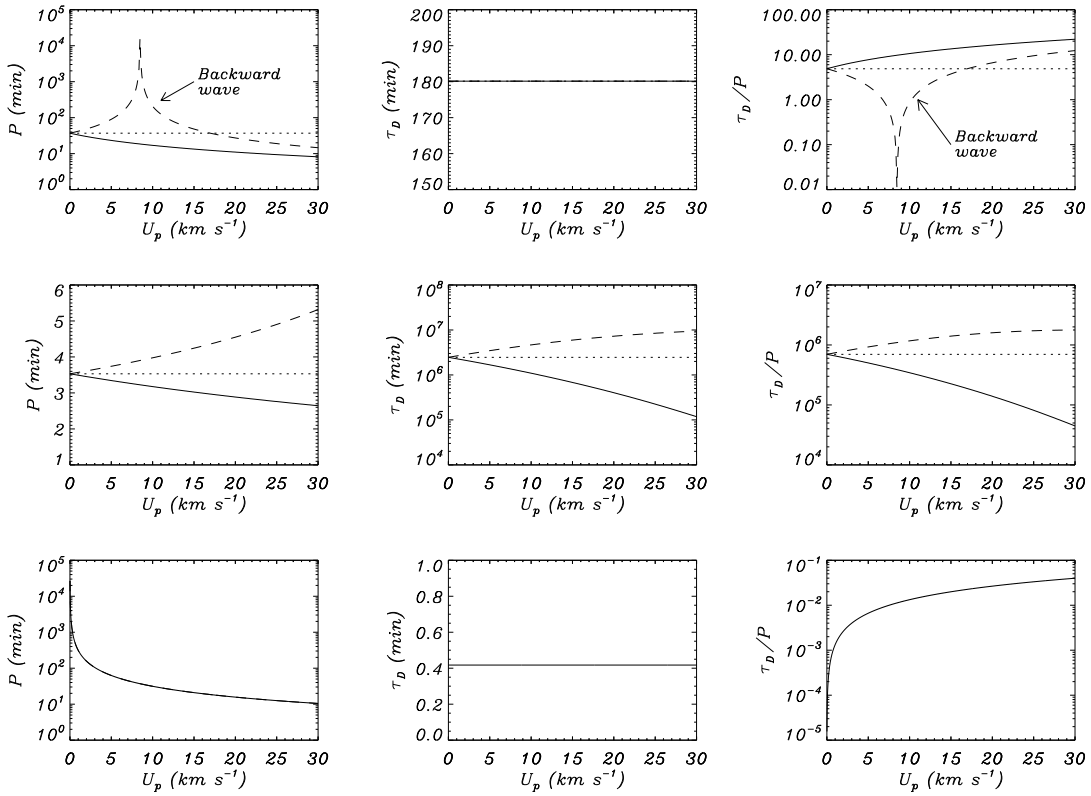


**Figure 46:** Wave damping by thermal effects in a uniform, infinitely long thread (Figure 32). Period *(left)*, damping time *(center)*, and ratio of the damping time to the period *(right)* versus the flow velocity for the fundamental oscillatory modes. The upper, middle, and lower panels correspond to the slow, fast kink, and thermal modes, respectively. Different line styles represent parallel waves (solid line), anti-parallel waves (dashed line), and solutions in the absence of flow (dotted line) (from Soler *et al.*, 2008).

Although the presence of steady mass flows improves the efficiency of non-adiabatic mechanisms on the attenuation of transverse kink oscillations for propagation parallel to the flow, its effect is still not enough to obtain damping times compatible with observations.

### 5.1.3 Non-adiabatic magnetoacoustic waves in a two-thread system with mass flows

The oscillatory properties, namely the frequency and spatial distribution, of fast and slow magnetoacoustic waves in a system made of two infinite threads with mass flows are described in Section 4.4.2; see Figure 37 for a sketch of the equilibrium configuration. Soler *et al.* (2009a) evaluated the damping time-scales caused by non-adiabatic effects as a function of the distance between the thread axes. The left panel of Figure 47 shows that the ratio of the damping time to the period of the four kink modes is very large, so that dissipation by non-adiabatic mechanisms is not efficient enough to damp these modes. Hence, the collective nature of the transverse oscillations in a system of two identical threads does not change the conclusion about the irrelevance of thermal mechanisms to account for the damping of fast modes already obtained for one thread.

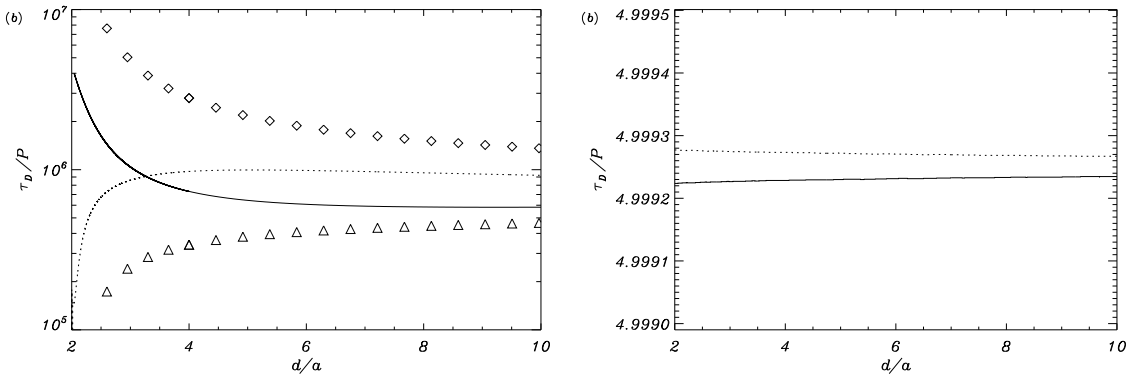


**Figure 47:** Wave damping by thermal effects in a two-thread system. *Left:* Ratio of the damping time to the period versus the distance between the thread axes of the $S_x$ (solid line), $A_x$ (dotted line), $S_y$ (triangles), and $A_y$ (diamonds) kink-like modes. *Right:* The same for the $S_z$ (solid line) and $A_z$ (dotted line) slow wave modes (from Soler *et al.*, 2009a).

As concluded in Section 5.1.2, slow wave damping can be explained by thermal mechanisms. The right panel of Figure 47 shows the damping ratios of the $S_z$ and $A_z$ solutions versus the distance between the two threads. Slow modes in a threaded prominence are efficiently attenuated by non-adiabatic mechanisms. Note that $\tau_{\rm d}/P$ is almost independent of the thread separation and the mode because the two threads oscillate independently in the $S_z$ and $A_z$ modes. Time-scales $\tau_{\rm d}/P \approx 5$ are obtained, which is in agreement with previous studies (Soler *et al.*, 2007, 2008) and consistent with observations.

Soler *et al.* (2009a) concluded that collective slow modes are efficiently damped by thermal mechanisms, with damping ratios similar to those reported in observations, while collective fast waves are poorly damped. This is a key point since efficiently damped transverse oscillations have been observed, which could suggest that other attenuation mechanisms could be at work.

## 5.2 Damping of oscillations by ion-neutral collisions

Since the temperature of prominences is typically of the order of $10^4$ K, the prominence plasma is only partially ionized. The exact ionization degree of prominences is unknown and the reported

ratio of electron density to neutral hydrogen density (see, e.g., Patsourakos and Vial, 2002) covers about two orders of magnitude (0.1 – 10). Partial ionization brings the presence of neutrals in addition to electrons and ions, thus collisions between the different species are possible. Because of the occurrence of collisions between electrons with neutral atoms and ions, and more importantly between ions and neutrals, Joule dissipation is enhanced when compared with the fully ionized case. A partially ionized plasma can be represented as a single-fluid in the strong coupling approximation, which is valid when the ion density in the plasma is low and the collision time between neutrals and ions is short compared with other time-scales of the problem. Using this approximation it is possible to describe the very low frequency and large-scale fluid-like behaviour of plasmas (Goossens, 2003).

Partial ionization affects the induction equation, which contains additional terms due to the presence of neutrals and a non-zero resistivity (Soler *et al.*, 2009d). These terms account for the processes of ohmic diffusion, with coefficient $\eta$; ambipolar diffusion, with coefficient $\eta_{\rm A}$; and Hall's magnetic diffusion, with coefficient $\eta_{\rm H}$. They govern collisions between the different plasma species. Ohmic diffusion is mainly due to electron-ion collisions and produces magnetic diffusion parallel to the magnetic field lines; ambipolar diffusion is mostly caused by ion-neutral collisions and Hall's effect is enhanced by ion-neutral collisions since they tend to decouple ions from the magnetic field, while electrons remain able to drift with the magnetic field (Pandey and Wardle, 2008). The ambipolar diffusivity can be expressed in terms of Cowling's coefficient, $\eta_{\rm C}$, that accounts for diffusion perpendicular to magnetic field lines, as

$$\eta_{\rm A} = \frac{\eta_{\rm C} - \eta}{B^2}, \tag{28}$$

with $B$ the magnetic field strength. For a fully ionized plasma, $\eta_{\rm C} = \eta$ and there is no ambipolar diffusion, so magnetic diffusion is isotropic. Due to the presence of neutrals, $\eta_{\rm C} \gg \eta$, which means that perpendicular magnetic diffusion is much more efficient than longitudinal magnetic diffusion in a partially ionized plasma. It is important to note that $\eta_{\rm C} \gg \eta$ even for a small relative density of neutrals.

### 5.2.1 Homogeneous and unbounded prominence medium

Several studies have considered the damping of MHD waves in partially ionized plasmas of the solar atmosphere (De Pontieu *et al.*, 2001; James *et al.*, 2003; Khodachenko *et al.*, 2004; Leake *et al.*, 2005). In the context of solar prominences, Forteza *et al.* (2007) derived the full set of MHD equations for a partially ionized, one-fluid hydrogen plasma and applied them to the study of the time damping of linear, adiabatic fast and slow magnetoacoustic waves in an unbounded prominence medium. This study was later extended to the non-adiabatic case by including thermal conduction by neutrals and electrons and radiative losses (Forteza *et al.*, 2008). The main effects of partial ionization on the properties of MHD waves manifest through a generalized Ohm's law, which adds some extra terms in the resistive magnetic induction equation, in comparison to the fully ionized case. Forteza *et al.* (2007) considered a uniform and unbounded prominence plasma and found that ion-neutral collisions are more important for fast waves, for which the ratio of the damping time to the period is in the range 1 to $10^5$, than for slow waves, for which values between $10^4$ and $10^8$ are obtained. Fast waves are efficiently damped for moderate values of the ionization fraction, while in a nearly fully ionized plasma, the small amount of neutrals is insufficient to damp the perturbations.

A hydrogen plasma was considered in the above studies, but 90% of the prominence chemical composition is hydrogen and the remaining 10% is helium. The effect of including helium in the model of Forteza *et al.* (2008) was assessed by Soler *et al.* (2010b). The species present in the medium are electrons, protons, neutral hydrogen, neutral helium (He I) and singly ionized helium (He II), while the presence of He III is neglected (Gouttebroze and Labrosse, 2009).

The hydrogen ionization degree is characterized by $\tilde{\mu}_{\rm H}$, which varies between 0.5 for fully ionized hydrogen and 1 for fully neutral hydrogen. The helium ionization degree is characterized by $\delta_{\rm He} = \frac{\xi_{\rm He\,II}}{\xi_{\rm He\,I}}$, where $\xi_{\rm He\,II}$ and $\xi_{\rm He\,I}$ denote the relative densities of single ionized and neutral helium, respectively. Figure 48 displays $\tau_{\rm d}/P$ as a function of the wavenumber, $k$, for the Alfvén, fast and slow waves, and the results corresponding to several helium abundances are compared for hydrogen and helium ionization degrees of $\tilde{\mu}_{\rm H} = 0.8$ and $\delta_{\rm He} = 0.1$, respectively. We can observe that the presence of helium has a minor effect on the results.

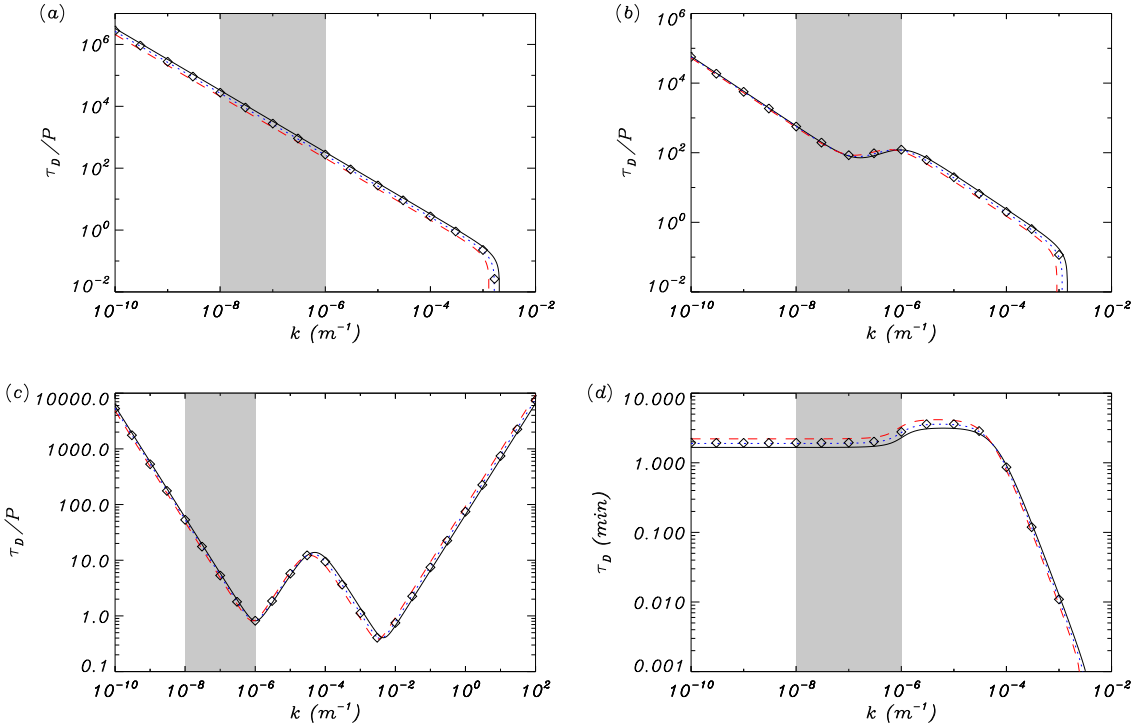


**Figure 48:** Wave damping by ion-neutral effects in a uniform medium. (a) – (c) Ratio of the damping time to the period, $\tau_{\rm d}/P$, versus the wavenumber, $k$, corresponding to the Alfvén wave, fast wave and slow wave, respectively. (d) Damping time, $\tau_{\rm d}$, of the thermal wave versus the wavenumber, $k$. The different linestyles represent the following abundances: $\xi_{\rm He\,ii} = 0\%$ (solid line), $\xi_{\rm He\,ii} = 10\%$ (dotted line), and $\xi_{\rm He\,ii} = 20\%$ (dashed line). In all computations, $\tilde{\mu}_{\rm H} = 0.8$ and $\delta_{\rm He} = 0.1$. The results for $\xi_{\rm He\,ii} = 10\%$ and $\delta_{\rm He} = 0.5$ are plotted by means of symbols for comparison. The shaded regions correspond to the range of typically observed wavelengths of prominence oscillations. In all the figures the angle between the wavevector and the magnetic field is $\pi/4$ (from Soler *et al.*, 2010b).

The thermal mode is a purely damped, non-propagating disturbance ($\omega_{\rm R} = 0$), so only the damping time, $\tau_{\rm d}$, is plotted (Figure 48d). We observe that the effect of helium is different in two ranges of $k$. For $k > 10^{-4}$ m$^{-1}$, thermal conduction is the dominant damping mechanism, so the larger the amount of helium, the shorter $\tau_{\rm d}$ because of the enhanced thermal conduction by neutral helium atoms. On the other hand, radiative losses are more relevant for $k < 10^{-4}$ m$^{-1}$. In this region, the thermal mode damping time grows as the helium abundance increases. Since these variations in the damping time are very small, we again conclude that the damping time obtained in the absence of helium does not significantly change when helium is taken into account. Therefore, the inclusion of neutral or single ionized helium in partially ionized prominence plasmas

does not modify the behaviour of linear, adiabatic or non-adiabatic MHD waves already found by Forteza *et al.* (2007) and Forteza *et al.* (2008).

### 5.2.2 Cylindrical filament thread model

Soler *et al.* (2009c) applied the equations derived by Forteza *et al.* (2007) to the study of MHD waves in a partially ionized filament thread modeled as an infinite cylinder with radius $a$ embedded in the solar corona (see Figure 32). As in Forteza *et al.* (2007), the one-fluid approximation for a hydrogen plasma was considered. The internal and external media are characterized by their densities, temperatures, and their own relative densities of neutrals, ions and electrons. The contribution of the electrons is neglected. The coronal medium is considered as fully ionized, while the ionization fraction in the prominence plasma, $\tilde{\mu}_{\rm p}$, is allowed to vary.

In their analysis, Soler *et al.* (2009c) neglected Hall's term since it can be ignored when the plasma is magnetized, i.e., when ions and electrons are tightly bound to the magnetic field. The condition to neglect Hall's term can be written in terms of the ion-gyrofrequency ($\omega_i$) and the ion-neutral collision time ($\tau$) as $\omega_i \tau \gg 1$, which once expanded gives,

$$\frac{eB}{m_i}\sqrt{\frac{\pi m_i}{16 k_B T}}\frac{1}{n_n \Sigma_{in}} \gg 1, \tag{29}$$

where $\Sigma_{in}$ is the ion-neutral cross-section and $n_n$ the neutrals number density (Leake *et al.*, 2005; Pandey and Wardle, 2008). Using prominence conditions ($\rho = 5 \times 10^{-11}$ kg m$^{-3}$, $B = 10$ G, $T = 8000$ K, $\tilde{\mu}_{\rm p} = 0.8$), we obtain the numerical value $\omega_i \tau = 467$, which fully justifies the neglect of Hall's term. Parallel and perpendicular magnetic diffusion can be evaluated by defining the corresponding Reynolds numbers as $R_{\rm m\parallel} = c_{\rm sp} a/\eta$ and $R_{\rm m\perp} = 4\pi^2 c_{\rm sp}/\eta_{\rm C} k_z^2 a$, where the typical velocity scale has been associated to the sound speed in the prominence, $c_{\rm sp}$. The parallel Reynolds number is independent of the wavenumber, while the relative importance of Cowling's diffusion increases with $k_z$, the longitudinal wavenumber. In the range of observed wavelengths ($k_z a \sim [10^{-3} - 10^{-1}]$) both Cowling's and ohmic diffusion could therefore be important. Soler *et al.* (2009c) analyzed separately the effect(s) of partial ionization in Alfvén, fast kink and slow waves.

For torsional Alfvén waves, Soler *et al.* (2009c) found that wave propagation is constrained between two critical wavenumbers (top panels of Figure 49). These critical wavenumbers are, however, outside the range of the observed wavelengths, in which $\tau_{\rm d}/P$ is in the range $10 - 100$ and so is considerably larger than the observed damping rate. Nevertheless, a prominence ionization fraction larger than the maximum one considered here (namely $\tilde{\mu}_{\rm p} > 0.95$) can yield $\tau_{\rm d}/P = 1 - 10$, in agreement with observations. For short wavenumbers, the values of the damping time over the period are independent of the ionization degree, while for large wavenumbers they become smaller for larger values of $\tilde{\mu}_{\rm p}$. This behaviour is explained in Soler *et al.* (2009c) by considering solutions to the dispersion relation in which one of the two possible damping mechanisms, i.e., partial ionization or ohmic dissipation, is neglected. Soler *et al.* (2009c) observed that ohmic diffusion dominates for small wavenumbers. Nevertheless, for large wavenumbers Cowling's diffusion dominates over ohmic dissipation and so a larger number of neutrals decreases the damping time: the larger $\tilde{\mu}$ in the thread, the shorter $\tau_{\rm d}$ and, consequently, the smaller $\tau_{\rm d}/P$.

The presence of critical wavenumbers is also found in the case of transverse kink waves (middle panels of Figure 49). Within the range of observed wavelengths, the phase speed closely corresponds to its ideal counterpart, $c_{\rm k} = \omega/k_z$, so non-ideal effects are irrelevant for wave propagation. The behaviour of the damping rate as a function of wavelength and ionization fraction is seen to closely resemble the result obtained for Alfvén waves, with $\tau_{\rm d}/P > 10$ in the range of observed wavelengths. Therefore, neither ohmic diffusion nor ion-neutral collisions seem to provide damping times as short as those observed for kink waves in filament threads. Only for an almost neutral plasma, with $\tilde{\mu}_{\rm p} > 0.95$, the obtained damping rates are compatible with the observed time-scales.

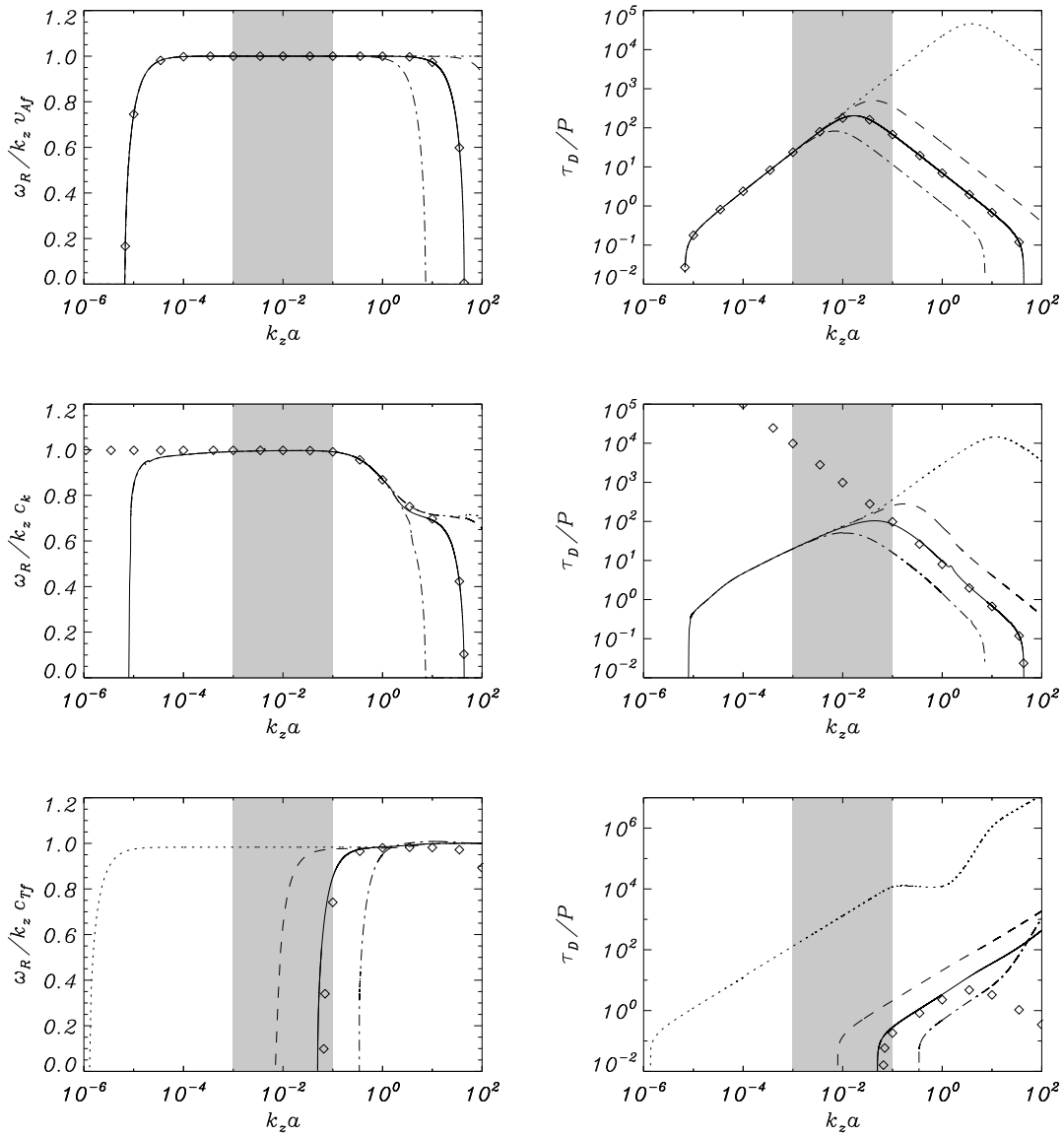


**Figure 49:** Wave damping by ion-neutral effects in an infinitely long prominence thread. Dimensionless phase speed (left panels) and ratio of the damping time to the period (right panels) as a function of $k_z a$ for Alfvén waves (top panels), kink waves (middle panels), and slow waves (bottom panels). The different linestyles represent different ionization degrees: $\tilde{\mu}_{\rm p} = 0.5$ (dotted), $\tilde{\mu}_{\rm p} = 0.6$ (dashed), $\tilde{\mu}_{\rm p} = 0.8$ (solid), and $\tilde{\mu}_{\rm p} = 0.95$ (dash-dotted). Symbols are the approximate solution given by Equation (36) in Soler *et al.* (2009c) for $\tilde{\mu}_{\rm p} = 0.8$. The shaded zones correspond to the range of typically observed wavelengths of prominence oscillations. The Alfvén speed in the thread, $v_{\rm Af}$, the kink speed, $c_{\rm k}$, and the cusp speed in the thread, $c_{\rm Tp}$, have been used to compute the dimensionless phase speed (adapted from Soler *et al.*, 2009c).

Just like for Alfvén waves, ohmic diffusion dominates for small wavenumbers, while ion-neutral collisions are the dominant damping mechanism for large wavenumbers.

Regarding slow waves (bottom panels of Figure 49), Soler *et al.* (2009c) concentrated their analysis on the radially fundamental mode with $m = 1$, since the behaviour of the slow mode is weakly affected by the value of the azimuthal wavenumber. Slow wave propagation is constrained by only one critical wavenumber, that strongly depends on the ionization fraction, in such a way that for $k_z$ below this critical wavenumber the wave is totally damped. More importantly, for large enough values of the ionization fraction, the corresponding critical wavelength lies in the range of observed wavelengths of filament oscillations. As a consequence, the slow wave might not propagate in filament threads under certain circumstances. As for the damping rate, it is found that ion-neutral collisions are a relevant damping mechanism for slow waves, since very short damping times are obtained, especially close to the critical wavenumber. By comparing the particular effects of ohmic diffusion and ion-neutral collisions, the slow mode damping is seen to be completely dominated by ion-neutral collisions. Ohmic diffusion is found to be irrelevant, since the presence of the critical wavenumber prevents slow wave propagation for small wavenumbers, where ohmic diffusion would start to dominate.

## 5.3 Resonant damping of infinitely long thread oscillations

The phenomenon of resonant wave damping in non-uniform plasmas has been extensively studied in connection to wave-based coronal heating mechanisms (Ionson, 1978) and the damping of transverse coronal loop oscillations (Hollweg and Yang, 1988; Ruderman and Roberts, 2002; Goossens *et al.*, 2002, 2010). The mechanism relies in the energy transfer from the transverse kink mode to small scale Alfvén waves because of the plasma inhomogeneity at the transverse spatial scales of the structures. This idea was put forward by Arregui *et al.* (2008b), whose analysis is restricted to the damping of kink oscillations due to the resonant coupling to Alfvén waves in a pressureless (zero plasma-$\beta$) plasma. It was extended to the case in which both the Alfvén and the slow resonances are present by Soler *et al.* (2009e). Here we discuss the main results from these works, whose aim is to assess the damping properties of resonant absorption. For this reason, the considered configurations are based on the infinitely long thread model of Figure 31.

### 5.3.1 Resonant damping in the Alfvén continuum

Arregui *et al.* (2008b) considered an individual and isolated thread modeled as a cylindrical magnetic flux tube of radius $a$ in a gravity-free environment. The uniform magnetic field points along the axis of the tube (Figure 50). In the zero plasma-$\beta$ approximation, the thread is modeled as a density enhancement with a radial variation of density from its internal constant prominence value $\rho_{\rm p}$ to the coronal constant value $\rho_{\rm c}$ over a non-uniform layer of thickness $l$. A typical value of the density contrast between the filament and coronal plasma is $\zeta = \rho_{\rm p}/\rho_{\rm c} = 200$.

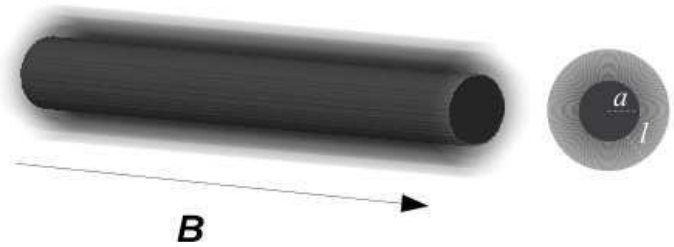


**Figure 50:** Model used by Arregui *et al.* (2008b) to represent a radially non-uniform filament fine structure of mean radius $a$ and transverse inhomogeneity length scale $l$.

MHD waves of axisymmetric one-dimensional cylindrical flux tubes are characterized by two wavenumbers, i.e., the azimuthal wavenumber, $m$, and the axial wavenumber, $k_z$. They can have different nodes in the radial direction. Arregui *et al.* (2008b) concentrated their analysis on the radially and longitudinally fundamental transverse wave with azimuthal number $m = 1$, the kink mode. This eigenmode is consistent with the detected Doppler velocity variations (see Section 3.6.4) and their associated transverse motions, discussed in Section 4.4.1. The frequency of this mode is not influenced by the presence of a layer with small thickness, so the result of Section 4.4.1 is approximately correct; see Equation (22).

When transverse inhomogeneity is considered, the fundamental transverse kink mode resonantly couples to Alfvén waves. The consequence is the transfer of wave energy from the global transverse motion to azimuthal motions of localized nature, and thus the time damping of the kink mode (Goossens *et al.*, 2009). Analytical expressions for the damping time scale can be obtained under the assumption that the transverse inhomogeneity length-scale is small ($l/a \ll 1$). This is the so-called thin boundary approximation. When the long wavelength and the thin boundary approximations are combined, the analytical expression for the damping time over period for the kink mode can be written as (see, e.g., Goossens *et al.*, 1992, 1995; Ruderman and Roberts, 2002; Goossens *et al.*, 2002)

$$\frac{\tau_d}{P} = F \ \frac{a}{l} \ \frac{\zeta + 1}{\zeta - 1}. \tag{30}$$

Here $F$ is a numerical factor that depends on the particular variation of the density in the non-uniform layer. For a linear variation, $F = 4/\pi^2$ (Hollweg and Yang, 1988; Goossens *et al.*, 1992); for a sinusoidal variation, $F = 2/\pi$ (Ruderman and Roberts, 2002). Consider for example $\zeta = 200$ as a typical density contrast and $l/a = 0.1$. Then, Equation (30) predicts a damping time of $\sim 6$ times the oscillatory period, thus producing a time-scale compatible with observations.

Quantitative parametric results for the damping of resonant kink waves in prominence threads as a function of the relevant parameters are provided by Arregui *et al.* (2008b). The accuracy of the analytical approximations is compared to full numerical results, beyond the long wavelength and thin boundary approximations. These results are shown in Figure 51. The damping is affected by the density contrast in the low contrast regime and $\tau_d/P$ rapidly decreases for increasing thread density (Figure 51a). Interestingly, $\tau_d/P$ stops depending on this parameter in the large contrast regime, typical of filament threads. The damping time over period is independent of the wavelength of perturbations (Figure 51b), but rapidly decreases with increasing inhomogeneity length-scale (Figure 51c).

Resonant damping in the Alfvén continuum appears to be a very efficient mechanism for the attenuation of transverse thread oscillations, especially because large density contrasts and transverse plasma inhomogeneities are combined together.

### 5.3.2 Resonant damping in the slow continuum

Although the plasma-$\beta$ in solar prominences is probably small, it is definitely non-zero. Soler *et al.* (2009e) showed that, in prominence plasmas, resonant damping of kink waves can additionally be produced due to the coupling to slow continuum waves. In the context of coronal loops, which are presumably hotter and denser than the surrounding corona, the ordering of sound, Alfvén and kink speeds does not allow for the simultaneous matching of the kink frequency with both Alfvén and slow continuum frequencies. Because of their relatively higher density and lower temperature conditions, this becomes possible in the case of prominence threads. Therefore, the kink mode phase speed is also within the slow (or cusp) continuum, which extends between the internal and external sound speeds, in addition to the Alfvén continuum. By considering gas pressure in the cylindrical thread model of Arregui *et al.* (2008b), Soler *et al.* (2009e) evaluated the contribution of the damping due to the slow continuum to the total resonant damping of the kink mode.

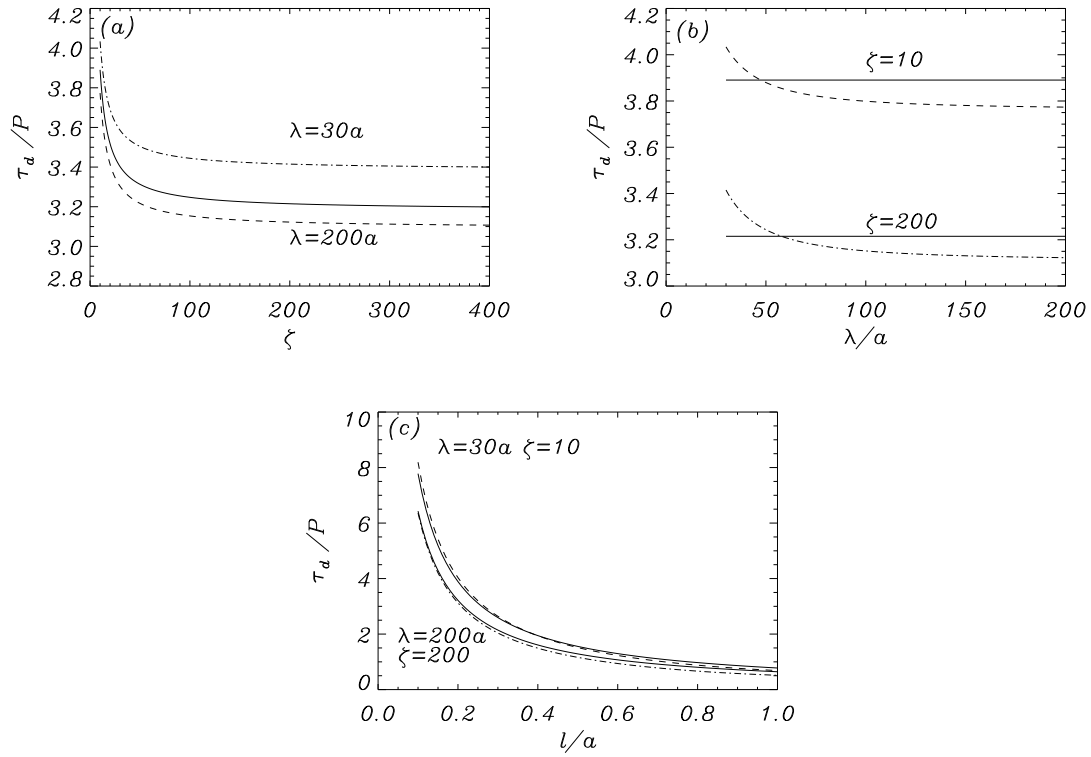


**Figure 51:** Wave damping by Alfvén resonant absorption in an infinitely long prominence thread. Damping time over period for fast kink waves in filament threads with radius $a = 100$ km. (a) As a function of the density contrast, with $l/a = 0.2$ and for two wavelengths. (b) As a function of the wavelength, with $l/a = 0.2$, for two density contrasts. (c) As a function of the transverse inhomogeneity length-scale, for two combinations of wavelength and density contrast. In all plots solid lines correspond to analytical solutions given by Equation (30), with $F = 2/\pi$ (from Arregui *et al.*, 2008b).

Soler *et al.* (2009e) used the density model of Section 5.3.1 and the plasma-$\beta \simeq 0.04$. In order to obtain an analytic expression for the damping rate of the kink mode, first the long wavelength and thin boundary limits were considered. In terms of the physically relevant quantities, the damping time over the period can be cast as

$$\frac{\tau_{\rm d}}{P} = F\,\frac{a}{l}\left(\frac{\zeta+1}{\zeta-1}\right)\left[\frac{m}{\cos\alpha_{\rm A}} + \frac{(k_z a)^2}{m}\left(\frac{c_{\rm s}^2}{c_{\rm s}^2+v_{\rm A}^2}\right)^2\frac{1}{\cos\alpha_{\rm S}}\right]^{-1}. \tag{31}$$

Here $F$ is the same numerical factor as in Equation (30), while $\alpha_{\rm A} = \pi(r_{\rm A}-a)/l$ and $\alpha_{\rm S} = \pi(r_{\rm S}-a)/l$, with $r_{\rm A}$ and $r_{\rm S}$ the Alfvén and slow resonant positions. The term with $k_z$ corresponds to the contribution of the slow resonance. If this term is dropped and $m=1$ and $\cos\alpha_{\rm A}=1$ are taken, Equation (31) becomes Equation (30), that only takes into account the Alfvén resonance.

Equation (31) can now be directly applied to measure the relative contribution of each resonance to the total damping. To do that, Soler *et al.* (2009e) assumed $r_{\rm A} \simeq r_{\rm S} \simeq a$, for simplicity, so $\cos\alpha_{\rm A} \simeq \cos\alpha_{\rm S} \simeq 1$. The ratio of the two terms in Equation (31) is then

$$\frac{\tau_{\rm dA}}{\tau_{\rm dS}} \simeq \frac{(k_z a)^2}{m^2}\left(\frac{c_{\rm s}^2}{c_{\rm s}^2+v_{\rm A}^2}\right)^2, \tag{32}$$

where $\tau_{\rm dA}$ and $\tau_{\rm dS}$ are the respective contributions of the Alfvén and slow resonances in Equation (31). A simple calculation shows that, for typical wavelengths of observed thread oscillations, the contribution of the slow resonance is irrelevant in front of that of the Alfvén resonance. Take for instance, $m=1$ and $k_z a = 10^{-2}$, then Equation (32) gives $\tau_{\rm dA}/\tau_{\rm dS} \simeq 10^{-7}$.

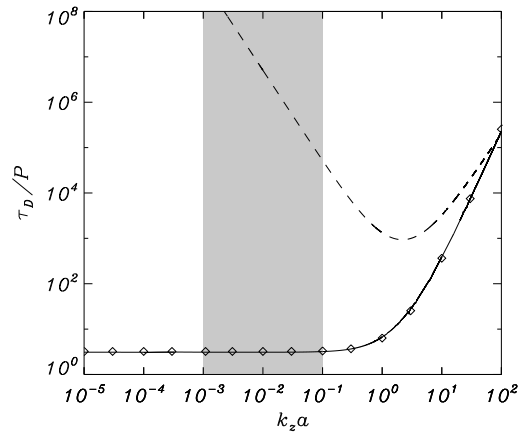


**Figure 52:** Wave damping by Alfvén and slow resonances in an infinitely long prominence thread. Kink mode ratio of the damping time to the period, $\tau_{\rm d}/P$, as a function of the dimensionless wavenumber, $k_z a$, for $l/a = 0.2$. The solid line is the full numerical solution. The symbols and the dashed line are the results of the thin boundary approximation for the Alfvén and slow resonances, i.e., the two terms in Equation (31). The shaded region represents the range of typically observed values for the wavelengths in prominence oscillations (from Soler *et al.*, 2009e).

This analytical predictions were further confirmed by Soler *et al.* (2009e) by performing numerical computations outside the thin tube and thin boundary approximations. Figure 52 shows that the slow resonance is much less efficient than the Alfvén resonance. For the wavenumbers relevant to observed prominence oscillations, the value of $\tau_{\rm d}/P$ due to the slow resonance is between 4 and

8 orders of magnitude larger than the same ratio obtained for the Alfvén resonance. The overall conclusion by Soler *et al.* (2009e) is that the slow resonance is very inefficient when it comes to damping the kink mode for typical prominence conditions and in the observed wavelength range. The damping times obtained with this mechanism are comparable to those due to the thermal effects discussed in Section 5.1. Hence, resonant damping of transverse thread oscillations is governed by the Alfvén resonance.

## 5.4 Resonant damping in partially ionized infinitely long threads

### 5.4.1 Temporal damping

Damping by resonant absorption in a partially ionized prominence plasma was studied by Soler *et al.* (2009d), who integrated both mechanisms in a non-uniform cylindrical prominence thread model in order to assess their combined effects. Partial ionization is relevant for the damping of short wavelength fast waves (Forteza *et al.*, 2007), while resonant damping of kink waves is efficient whenever a transverse density inhomogeneity is present. The question arises on whether partial ionization affects the mechanism of resonant absorption and vice versa.

The model adopted by Soler *et al.* (2009d) has the magnetic and density structuring of the models used in Section 5.3 (see Figure 50), but the plasma properties are also characterized by the ionization fraction, $\tilde{\mu}$. The radial behaviour of the ionization fraction in threads is unknown, so Soler *et al.* (2009d) assumed a one-dimensional transverse profile akin to the one employed to model the equilibrium density. The thread ionization fraction, $\tilde{\mu}_{\rm p}$, is considered a free parameter and the corona is assumed to be fully ionized, so $\tilde{\mu}_{\rm c} = 0.5$. The non-uniform transitional layer of thickness $l$ therefore connects two plasmas with densities $\rho_{\rm p}$ and $\rho_{\rm c}$ and ionization degrees $\tilde{\mu}_{\rm p}$ and $\tilde{\mu}_{\rm c}$. Soler *et al.* (2009d) used the one-fluid approximation and, for simplicity, the $\beta = 0$ limit, which excludes slow waves. The quantities $\eta$, $\eta_{\rm C}$ and $\eta_{\rm H}$ are here functions of the radial direction.

Soler *et al.* (2009d) first considered resonant damping in combination with Cowling's diffusion and excluded Hall's dissipation. They derived the following approximate expression for the damping ratio over the period, under the thin boundary approximation,

$$\frac{\tau_{\rm d}}{P} = \frac{2}{\pi}\left[m\left(\frac{l}{a}\right)\left(\frac{\rho_{\rm p}-\rho_{\rm c}}{\rho_{\rm p}+\rho_{\rm c}}\right) + \frac{2\left(\rho_{\rm p}\tilde{\eta}_{\rm Cp}+\rho_{\rm c}\tilde{\eta}_{\rm Cc}\right)k_z a}{\sqrt{2\rho_{\rm p}\left(\rho_{\rm p}+\rho_{\rm c}\right)}}\right]^{-1}, \tag{33}$$

with $\tilde{\eta}_{\rm Cc,p} = \eta_{\rm C}/v_{\rm Ac,p}a$ the coronal and prominence Cowling's diffusivities in dimensionless form. Notice that Equation (33) reduces to Equation (30) in a fully ionized plasma, and is in agreement with Equation (31), in which the slow resonance is additionally included. In this expression, the term due to resonant damping is independent of the value of Cowling's diffusivity and, therefore, of the ionization degree. The second term, related to the damping by Cowling's diffusion, is proportional to $k_z$, so its influence in the long-wavelength limit is expected to be small. Soler *et al.* (2009d) performed a simple calculation by considering $m = 1$, $k_z a = 10^{-2}$ and $l/a = 0.2$. This results in $\tau_{\rm d}/P \approx 3.18$ for a fully ionized thread ($\tilde{\mu}_{\rm p} = 0.5$) and $\tau_{\rm d}/P \approx 3.16$ for an almost neutral thread ($\tilde{\mu}_{\rm p} = 0.95$). Thus, this approximate expression suggests that the ratio $\tau_{\rm d}/P$ depends very slightly on the ionization degree, suggesting that resonant absorption dominates over Cowling's diffusion.

The analytical estimates described above can be verified and extended by numerically solving the full eigenvalue problem. This approach allowed Soler *et al.* (2009d) to additionally include Hall's diffusion in addition to ohmic and Cowling's dissipation. In their study, these authors first considered a configuration with an abrupt density variation across the thread boundary (that is, $l = 0$), which prevents resonant absorption from working. Next, they included the thin transitional layer between the thread and the corona, so that both resonant absorption and ion-neutral effects are at work.

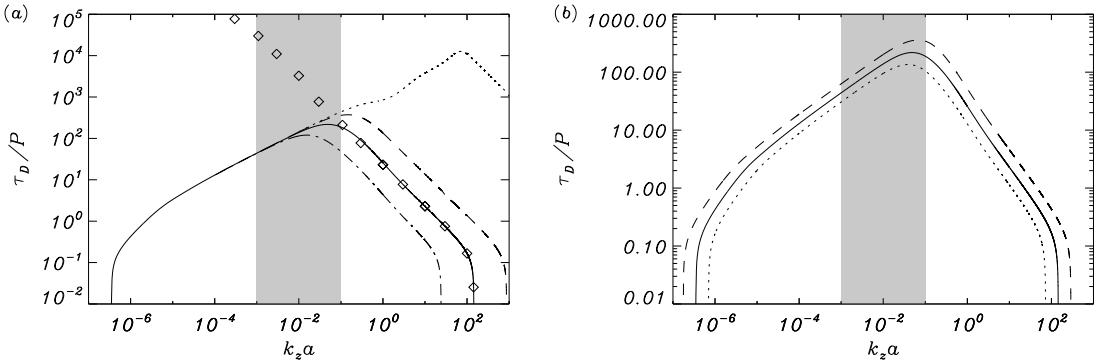


**Figure 53:** Wave damping by ion-neutral effects in an infinitely long cylindrical prominence thread. Ratio of the damping time to the period of the kink mode as a function of $k_z a$ for a thread without transitional layer, i.e., $l/a = 0$. (a) Results for $a = 100$ km and different ionization degrees: $\tilde{\mu}_{\rm p} = 0.5$ (dotted line), $\tilde{\mu}_{\rm p} = 0.6$ (dashed line), $\tilde{\mu}_{\rm p} = 0.8$ (solid line), and $\tilde{\mu}_{\rm p} = 0.95$ (dash-dotted line). Symbols are the approximate solution, given by Equation (33), for $\tilde{\mu}_{\rm p} = 0.8$. (b) Results for $\tilde{\mu}_{\rm p} = 0.8$ and different thread widths: $a = 100$ km (solid line), $a = 50$ km (dotted line) and $a = 200$ km (dashed line). The shaded zone corresponds to the range of typically observed wavelengths of prominence oscillations (from Soler *et al.*, 2009d).

For a homogeneous thread ($l/a = 0$), Soler *et al.* (2009d) computed the damping rate for different ionization degrees (see Figure 53). In agreement with the results displayed for the kink mode in Figure 49, $\tau_{\rm d}/P$ has a maximum at the transition between the ohmic-dominated regime, which is almost independent of the ionization degree, to the region where Cowling's diffusion is more relevant and the ionization degree has a significant influence. The approximate analytical solution for a given value of $\tilde{\mu}_{\rm p}$ agrees very well with the numerical solution in the region where Cowling's diffusion dominates, while it significantly diverges from the numerical solution in the region where ohmic diffusion is relevant. Within the range of typically reported wavelengths, $\tau_{\rm d}/P$ is between 1 and 2 orders of magnitude larger than the measured values, so neither ohmic nor Cowling's diffusion can account for the observed damping time.

For the inhomogeneous thread case ($l/a \neq 0$), Figure 54a displays some relevant differences. First, the damping time is dramatically reduced for intermediate values of $k_z a$, which include the region of typically observed wavelengths. In this region, the ratio $\tau_{\rm d}/P$ becomes smaller as $l/a$ is increased, a behaviour consistent with damping by resonant absorption. The inclusion of the inhomogeneous transitional layer removes the smaller critical wavenumber and consequently the kink mode exists for very small values of $k_z a$. Figure 54a also shows a very good agreement between the numerical and the approximate solutions, this one given by Equation (33), for wavenumbers above $k_z a \sim 10^{-4}$, and a poor agreement in the range for which ohmic diffusion dominates, below $k_z a \sim 10^{-4}$. To understand this behaviour one has to bear in mind that the analytic approximate solution includes the effects of resonant absorption and Cowling's diffusion, but not the influence of ohmic diffusion. Such as shown in Figure 54b, the ionization degree is only relevant for large wavenumbers, where the damping rate significantly depends on the ionization fraction through ohmic diffusion.

Figure 55 displays the ranges of $k_z a$ for which Cowling's and Hall's diffusion dominate. Hall's diffusion is irrelevant in the whole range of $k_z a$ studied by Soler *et al.* (2009d), while Cowling's diffusion dominates the damping for large $k_z a$. In the whole range of relevant wavelengths, resonant absorption is the most efficient damping mechanism and the damping time is independent of the ionization degree, as predicted by the analytical result (Equation [33]). On the contrary,

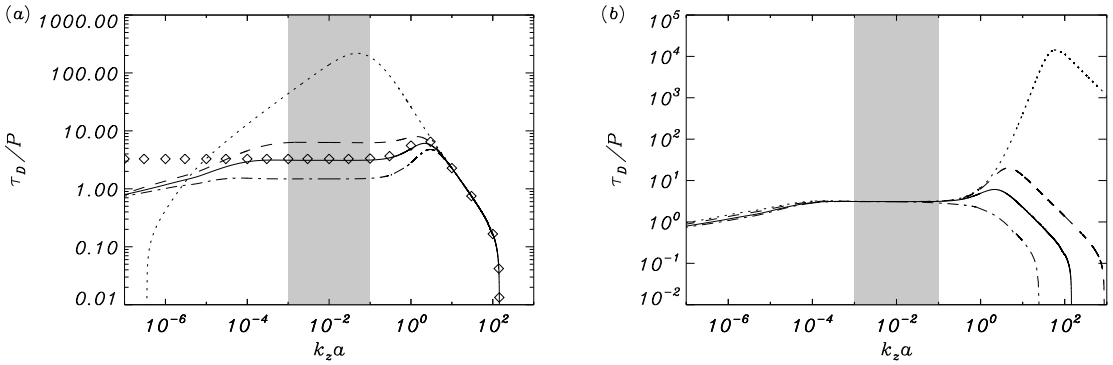


**Figure 54:** Wave damping by resonant absorption and ion-neutral effects in an infinitely long cylindrical prominence thread. Ratio of the damping time to the period of the kink mode as a function of $k_z a$ for a thread with an inhomogeneous transitional layer. (a) Results for $\tilde{\mu}_{\rm p} = 0.8$ and different transitional layer widths: $l/a = 0$ (dotted line), $l/a = 0.1$ (dashed line), $l/a = 0.2$ (solid line), and $l/a = 0.4$ (dash-dotted line). Symbols are the solution in the thin boundary approximation (Equation [33]) for $l/a = 0.2$. (b) Results for $l/a = 0.2$ and different ionization degrees: $\tilde{\mu}_{\rm p} = 0.5$ (dotted line), $\tilde{\mu}_{\rm p} = 0.6$ (dashed line), $\tilde{\mu}_{\rm p} = 0.8$ (solid line), and $\tilde{\mu}_{\rm p} = 0.95$ (dash-dotted line). In both panels $a = 100$ km (from Soler *et al.*, 2009d).

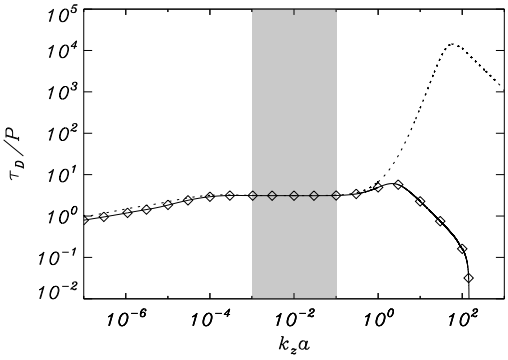


**Figure 55:** Ratio of the damping time to the period of the kink mode as a function of $k_z a$ in an infinitely long thread with $a = 100$ km and $l/a = 0.2$. The different line styles represent the results for a partially ionized thread with $\tilde{\mu}_{\rm p} = 0.8$ and considering all the terms in the induction equation (solid line), for a partially ionized thread with $\tilde{\mu}_{\rm p} = 0.8$ and neglecting Hall's term (symbols) and for a fully ionized thread (dotted line) (from Soler *et al.*, 2009d).

ohmic diffusion dominates for very small $k_z a$. In this region, the damping time related to Ohm's dissipation becomes even shorter than that due to resonant absorption, which means that the kink wave is mainly damped by ohmic diffusion.

### 5.4.2 Spatial damping

Motivated by the spatially damped propagating waves observed by Terradas *et al.* (2002) (see Section 3.6.3), the spatial damping of linear non-adiabatic magnetohydrodynamic waves in a homogenous, unbounded, magnetized, and fully ionized plasma was studied by Carbonell *et al.* (2006). The spatial damping in a flowing partially ionized plasma has been studied by Carbonell *et al.* (2010). Carbonell *et al.* (2006) found that the thermal (fast) wave shows the strongest (weakest) spatial damping. For periods longer than 1 s the spatial damping of magnetoacoustic waves is dominated by radiation, while at shorter periods the spatial damping is dominated by thermal conduction. Therefore, radiative effects on linear magnetoacoustic slow waves can be a viable mechanism for the spatial damping of short period prominence oscillations, while thermal conduction does not play any role. On the other hand, Carbonell *et al.* (2010) found that in the presence of a background flow, new strongly damped fast and Alfvén waves appear whose features depend on the joint action of flow and resistivity. The damping lengths of adiabatic fast and slow waves are strongly affected by partial ionization, which also modifies the ratio between damping lengths and wavelengths. For non-adiabatic slow waves, the unfolding in both wavelength and damping length induced by the flow allows efficient damping for periods compatible with those observed in prominence oscillations. In the case of non-adiabatic slow waves and within the range of periods of interest for prominence oscillations, the joint effect of both flow and partial ionization leads to efficient spatial damping of oscillations. For fast and Alfvén waves, the most efficient damping occurs at very short periods not compatible with those observed in prominence oscillations.

Using the same equilibrium model as in Soler *et al.* (2009d) (see Figure 50), whose results have been presented in Section 5.4.1, Soler *et al.* (2011) investigated the spatial damping of propagating kink MHD waves in transversely non-uniform and partially ionized prominence threads. The damping mechanisms are resonant absorption and ion-neutral collisions (Cowling's diffusion). In the absence of transitional layer, i.e., when the damping is due to Cowling's diffusion exclusively, the non-dimensional wavelength, the damping length, $L_{\rm D}$, and the ratio of the damping length to the wavelength are displayed in Figure 56. Regarding the wavelength, we see that the effect of Cowling's diffusion is only relevant for periods much shorter than those observed (1 – 10 min, corresponding to $40 \leq P/\tau_{\rm Ap} \leq 400$, with $\tau_{\rm Ap} = a/v_{\rm Ap}$ the thread Alfvén travel time). On the other hand, an almost neutral plasma, i.e., $\tilde{\mu}_{\rm p} \to 1$, has to be considered to obtain an efficient damping and to achieve small values of the damping ratio within the relevant range of periods. Such very large values of $\tilde{\mu}_{\rm p}$ are probably unrealistic (Labrosse *et al.*, 2010).

For resonantly damped modes, Figure 57 shows the results for different values of the thickness of the layer and fixed ionization degree. Figure 58 displays the results for different values of the ionization degree and a fixed transverse inhomogeneity length scale. Since the wavelength is not affected by the value of $l/a$ and has the same behaviour as in Figure 56a, both Figures 57 and 58 focus on $L_{\rm D}/a$ and $L_{\rm D}/\lambda$. Depending on the period, two different behaviours of the solutions are obtained. For short periods, the damping length is independent of the layer thickness and is governed by the value of the ionization degree. On the contrary, for large periods, the damping length depends on the value of $l/a$, but is independent of the ionization degree. This result indicates that resonant absorption dominates the damping for large periods, whereas Cowling's diffusion is more relevant for short period oscillations. In addition, we can observe that the approximate transitional period for which the damping length by Cowling's diffusion becomes shorter than that due to resonant absorption is much lower than the typically observed periods. This shows that resonant absorption is the dominant damping mechanism in the relevant range. The analytical ap-

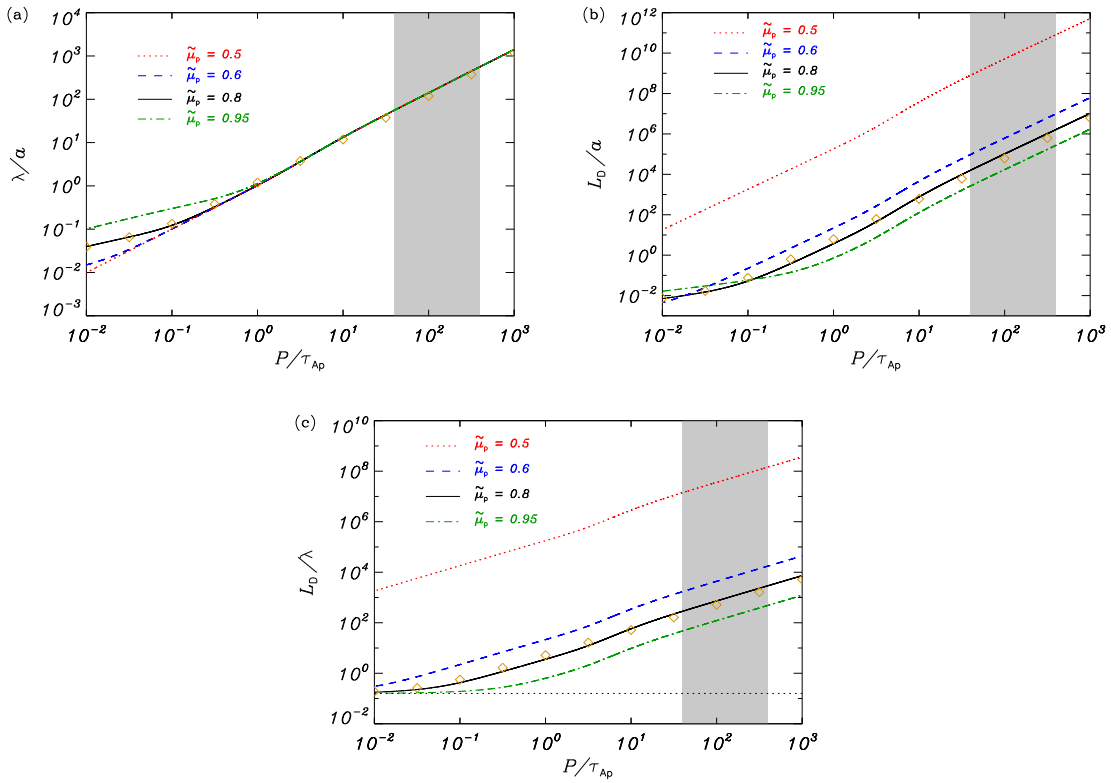


**Figure 56:** Spatial damping of kink waves due to ion-neutral effects in an infinitely long prominence thread. Results for the kink mode spatial damping in the case $l/a = 0$: (a) $\lambda/a$, (b) $L_D/a$, and (c) $L_D/\lambda$ versus $P/\tau_{Ap}$ for $\tilde{\mu}_p = 0.5$, 0.6, 0.8, and 0.95. Symbols in panels (a), (b), and (c) correspond to the analytical solution given by Equations (12), (13), and (14) in Soler *et al.* (2011) in the thin tube approximation, while the horizontal dotted line in panel (c) corresponds to the limit of $L_D/\lambda$ for high frequencies. The shaded area denotes the range of observed periods of thread oscillations.

proximation for the damping ratio obtained by Soler *et al.* (2011) provides an accurate description of the kink mode spatial damping in the relevant range of periods, such as shown by the diamonds in Figures 56 and 57.

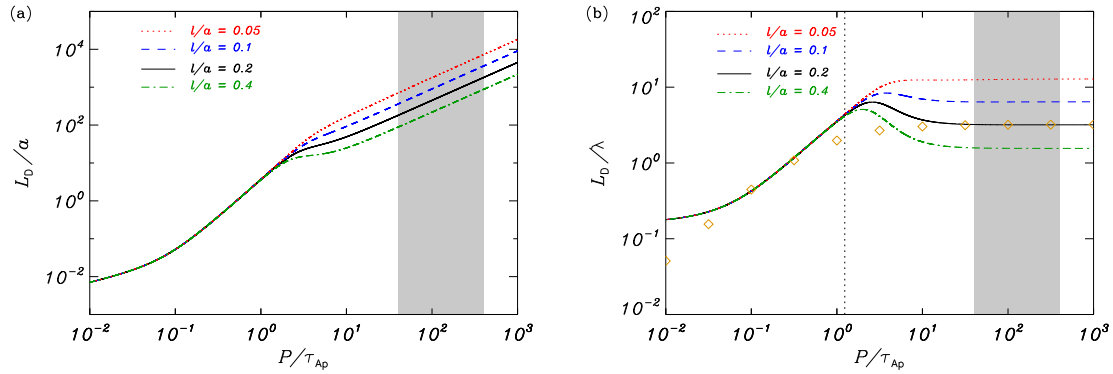


**Figure 57:** Results for the kink mode spatial damping in an infinitely long prominence thread, in the case $l/a \neq 0$: (a) $L_D/a$ and (b) $L_D/\lambda$ versus $P/\tau_{Ap}$ for $l/a = 0.05$, 0.1, 0.2, and 0.4, with $\tilde{\mu}_p = 0.8$. Symbols in panel (b) correspond to the analytical solution in the thin tube approximation, while the vertical dotted line is the approximate transitional period for $l/a = 0.1$. The shaded area denotes the range of observed periods of thread oscillations.

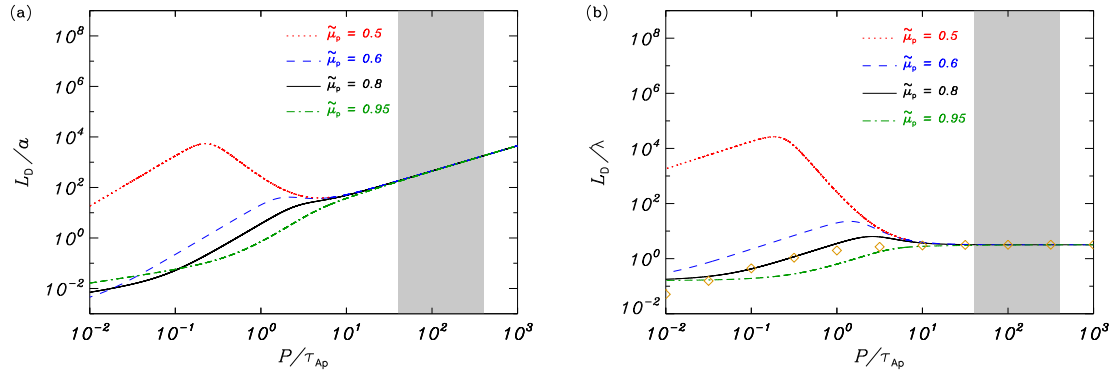


**Figure 58:** Results for the kink mode spatial damping in an infinitely long prominence thread, in the case $l/a \neq 0$: (a) $L_D/a$ and (b) $L_D/\lambda$ versus $P/\tau_{Ap}$ for $\tilde{\mu}_p = 0.5$, 0.6, 0.8, and 0.95, with $l/a = 0.2$. Symbols in panel (b) correspond to the analytical solution in the thin tube approximation. The shaded area denotes the range of observed periods of thread oscillations.

For typically reported periods of thread oscillations, resonant absorption is an efficient mechanism for the kink mode spatial damping, while ion-neutral collisions have a minor role. Cowling's diffusion dominates both the propagation and damping for periods much shorter than those observed, while resonant absorption could explain the observed spatial damping of kink waves in prominence threads.

## 5.5 Resonant damping in partially ionized finite length threads

The results described in Sections 5.3, 5.4.1, and 5.4.2 indicate that, because of the coupling of kink waves to Alfvén waves, resonant absorption constitutes a very plausible mechanism for the explanation of the observed spatial and time decay of transverse oscillations. The main limitation of these studies is that they adopt a one-dimensional density model that might not be appropriate in view of the longitudinal structuring of prominence threads. This led Soler *et al.* (2010a) to investigate the time damping properties of two-dimensional thread models, that is, with density inhomogeneity across the thread and along the magnetic tube in which it is contained. In this study, resonant absorption and damping by partial ionization effects were considered simultaneously.

Soler *et al.* (2010a) (see Figure 59) modeled a prominence fine structure as a straight cylindrical magnetic tube only partially filled with the cold and dense material. The length of the dense part is $L_{\rm p}$. The thread may either occupy the centre of the magnetic tube or be displaced, so that the lengths of both evacuated parts of the tube are different. By denoting the lengths of the right and left hand-side evacuated regions as $L_{\rm e}^{+}$ and $L_{\rm e}^{-}$, one has $L_{\rm e}^{+} = L - L_{\rm e}^{-} - L_{\rm p}$, with $L$ the full length of the tube. Just like in the works discussed in Section 5.4, the prominence plasma is partially ionized and a transverse inhomogeneous transitional layer is included between the prominence thread and the coronal medium. Ion-neutral collisions and resonant absorption are the considered damping mechanisms. The main model improvements in comparison to the thread model by Díaz *et al.* (2002), discussed in Section 4.5 (see Figure 41), are the ability to model non-centered threads, the inclusion of a non-uniform transverse layer and partial ionization of the thread plasma.

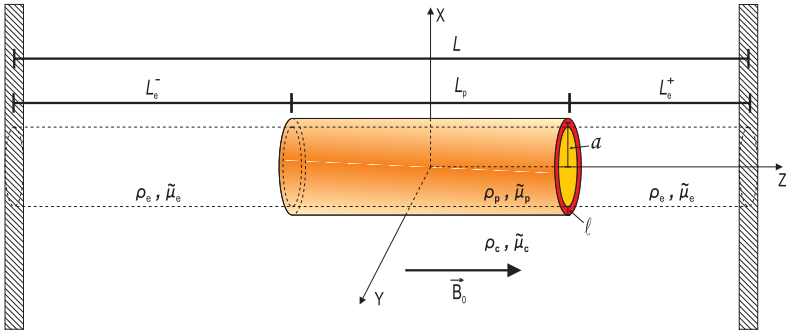


**Figure 59:** Model used by Soler *et al.* (2010a) to represent a finite length thread. A partially filled magnetic flux tube, with length $L$ and radius $a$, is considered. The tube ends are fixed by two rigid walls representing the solar photosphere. The tube is composed of a dense region of length $L_{\rm p}$ surrounded by two much less dense zones corresponding to the evacuated parts of the tube. In the prominence region a transversely inhomogeneous layer of length $l$ is considered. The plasma in the prominence region is assumed to be partially ionized with an arbitrary ionization degree $\tilde{\mu}_{\rm p}$. Both the evacuated part and the corona are taken to be fully ionized.

First, damping by Cowling's diffusion alone is considered by setting $l = 0$. When the thread is located in the center of the tube the ratio of the damping time to the period is given by the approximate expression

$$\frac{\tau_{\rm d}}{P} \approx \frac{1}{2\pi}\left(\frac{\rho_{\rm p}+\rho_{\rm c}}{\rho_{\rm p}}\right)^{1/2} \frac{1}{\tilde{\eta}_{\rm Cp}} \sqrt{2\left(1-\frac{L_{\rm p}}{L}\right)\frac{L_{\rm p}}{L}}, \tag{34}$$

with $\tilde{\eta}_{\rm Cp} = \eta_{\rm C}/v_{\rm Ap}a$ the filament Cowling's diffusivity in dimensionless form. For $\rho_{\rm p}/\rho_{\rm c} = 200$, $L_{\rm p}/L = 0.1$ and $L = 10^5$ km, Equation (34) gives $\tau_{\rm d}/P \approx 5 \times 10^3$ for $\tilde{\mu}_{\rm p} = 0.8$ and $\tau_{\rm d}/P \approx 150$

for $\tilde{\mu}_{\rm p} = 0.99$. Therefore, in a transversally homogeneous thread, an almost neutral prominence plasma is needed, i.e., $\tilde{\mu}_{\rm p} \approx 1$, for the damping due to Cowling's diffusion to be efficient. Although the precise ionization degree is unknown, such large values of $\tilde{\mu}_{\rm p}$ are probably unrealistic in the context of prominences.

Next, Soler *et al.* (2010a) considered $l/a \neq 0$, so that both resonant absorption and Cowling's diffusion can cause wave damping. An approximate expression for the damping ratio for a sinusoidal density variation in the transitional layer is

$$\frac{\tau_{\rm d}}{P} \approx \frac{2}{\pi}\left[m\left(\frac{l}{a}\right)\left(\frac{\rho_{\rm p}-\rho_{\rm c}}{\rho_{\rm p}+\rho_{\rm c}}\right)+\tilde{\eta}_{\rm Cp}\left(\frac{\rho_{\rm p}}{\rho_{\rm p}+\rho_{\rm c}}\right)^{1/2}\frac{4}{\sqrt{2\left(1-\frac{L_{\rm p}}{L}\right)\frac{L_{\rm p}}{L}}}\right]^{-1}. \tag{35}$$

As a numerical example, in the case $m = 1$, $L_{\rm p}/L = 0.1$, $L = 10^7$ m and $l/a = 0.2$, the damping ratio is $\tau_{\rm d}/P \approx 3.18$ for a fully ionized thread ($\tilde{\mu}_{\rm p} = 0.5$) and $\tau_{\rm d}/P \approx 3.16$ for an almost neutral thread ($\tilde{\mu}_{\rm p} = 0.95$). Note that the obtained damping times are consistent with the observations. Moreover, as seen in Section 5.4.1, the contribution of resonant absorption to the damping is much more important than that of Cowling's diffusion, so the ratio $\tau_{\rm d}/P$ depends only very slightly on the ionization degree and the second term on the right-hand side of Equation (35) can in principle be neglected.

When the prominence region is not at the center of the tube, and assuming $l = 0$, an approximate expression for the damping ratio is

$$\frac{\tau_{\rm d}}{P} \approx \frac{1}{2\pi}\left(\frac{\rho_{\rm p}+\rho_{\rm c}}{\rho_{\rm p}}\right)^{1/2}\frac{1}{\tilde{\eta}_{\rm Cp}}\sqrt{2\left[\left(1-\frac{L_{\rm p}}{L}\right)\frac{L_{\rm p}}{L}+4\frac{L_{\rm e}^{-}L_{\rm e}^{+}}{L^2}\right]\frac{L_{\rm p}}{L}}. \tag{36}$$

Taking the limits $L_{\rm e}^{-} \to 0$ or $L_{\rm e}^{+} \to 0$ in this expression, it can be shown that the minimum value of the damping ratio by Cowling's diffusion takes place when the prominence region is located at the magnetic tube center ($L_{\rm e}^{-} = L_{\rm e}^{+}$).

Soler *et al.* (2010a) find that for $l \neq 0$ and under the thin tube and thin boundary approximations, the period and damping time by resonant absorption have the same dependence on $L_{\rm e}^{-}$ and $L_{\rm e}^{+}$. This means that for resonant absorption the damping ratio does not depend on these quantities. Since resonant damping dominates over Cowling's diffusion, this leads to the conclusion that when considering both damping mechanisms, the damping ratio will be almost unaffected by the position of the prominence region within the fine structure.

The accuracy of the above analytical solutions can be assessed by numerically solving the general dispersion relation derived by Soler *et al.* (2010a). Here we only show the results obtained by Soler *et al.* (2010a) for the case in which the prominence thread is centered in the tube.

In the case without transverse transitional layer, $l/a = 0$, damping is only due to Cowling's diffusion. Figure 60a displays the period as a function of $L_{\rm p}/L$ for different values of the ionization degree in the prominence region, whereas Figure 60b shows the corresponding values of the damping time. As can be seen, the period increases when the length of the thread is increased and tends to the value for a homogeneous prominence cylinder when $L_{\rm p}/L \to 1$. In addition, the period is independent of the ionization degree. On the contrary, the damping time strongly depends on the ionization degree, and for a fixed $\tilde{\mu}_{\rm p}$ it slightly increases as $L_{\rm p}/L$ becomes larger. In all solutions, the analytical expressions for the period and the damping time are in agreement with the solution of the full dispersion relation for realistic, small values of $L_{\rm p}/L$, i.e., $L_{\rm p}/L \leq 0.4$, whereas the approximate expressions diverge from the actual solution when the prominence region occupies most of the magnetic tube. Figure 60c displays $\tau_{\rm d}/P$ versus $L_{\rm p}/L$. The numerical solution shows little dependence on $L_{\rm p}/L$, while the analytical approximation (Equation [34]) diverges from the

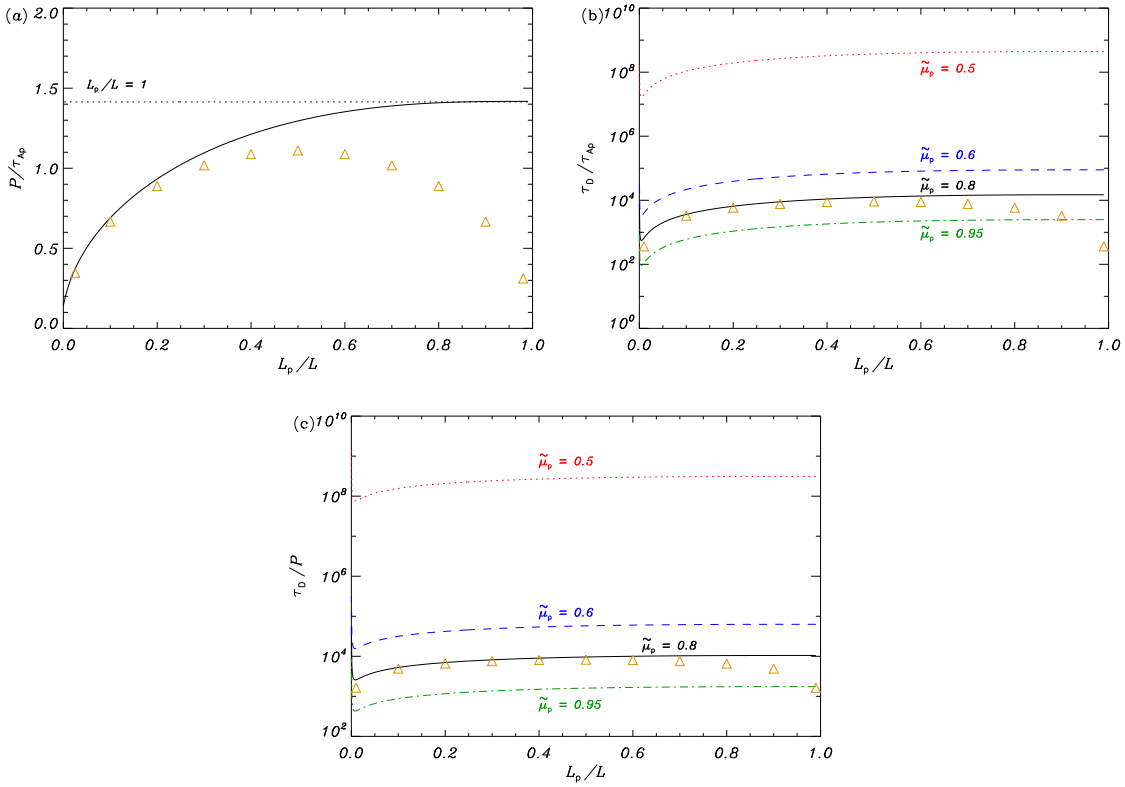


**Figure 60:** Results for the thread model in Figure 59 without transverse transitional layer and for the prominence thread located at the central part of the magnetic tube. (a) Period, $P$, of the fundamental kink mode in units of the internal Alfvén travel time, $\tau_{\rm Ap}$, as a function of $L_{\rm p}/L$. The horizontal dotted line corresponds to the period of the kink mode in a homogeneous prominence cylinder. The symbols are the analytic solution (Equation (24) in Soler *et al.*, 2010a). (b) Damping time, $\tau_{\rm d}$, in units of the internal Alfvén travel time, $\tau_{\rm Ap}$, as a function of $L_{\rm p}/L$. The different lines denote $\tilde{\mu}_{\rm p} = 0.5$ (dotted), 0.6 (dashed), 0.8 (solid), and 0.95 (dash-dotted). The symbols are the analytic approximation for $\tilde{\mu}_{\rm p} = 0.8$ (Equation (27) in Soler *et al.*, 2010a). (c) $\tau_{\rm d}/P$ versus $L_{\rm p}/L$. The line styles have the same meaning as in panel (b) and the symbols are the approximation given by Equation (34) (from Soler *et al.*, 2010a).

numerical value in the limit of large $L_p/L$. Given the obtained large values of $\tau_d/P$, Soler *et al.* (2010a) concluded that the efficiency of the damping due to Cowling's diffusion in a partially filled flux tube does not improve with respect to the longitudinally homogeneous tube case shown in Section 5.4.1.

Next, Soler *et al.* (2010a) included resonant damping. The period and the damping time of the fundamental kink mode were computed as a function of the different parameters, namely $\tilde{\mu}_p$, $l/a$, and $L_p/L$. Regarding the period, Soler *et al.* (2010a) found that both its value and its dependence on $L_p/L$ are the ones plotted in Figure 60a because the period is almost independent $\tilde{\mu}_p$ and $l/a$. For a fixed ionization degree of $\tilde{\mu}_p = 0.8$, the damping time decreases with $l/a$. The approximate analytical estimate of the damping time is in good agreement with the full solution for $L_p/L$ below 0.4. In order to assess the efficiency of resonant damping, Figure 61b displays the corresponding values of $\tau_d/P$. In comparison with the damping ratio by Cowling's diffusion (see Figure 60c), much smaller values of $\tau_d/P$ are now obtained. The damping ratio is almost independent of the length of the thread. This is because, under the assumptions made by Soler *et al.* (2010a), the dependence of the period and damping time on the length of the thread is the same. Overall, a very good agreement is obtained between the numerical result and the analytical approximation, even for large values of the length of the thread.

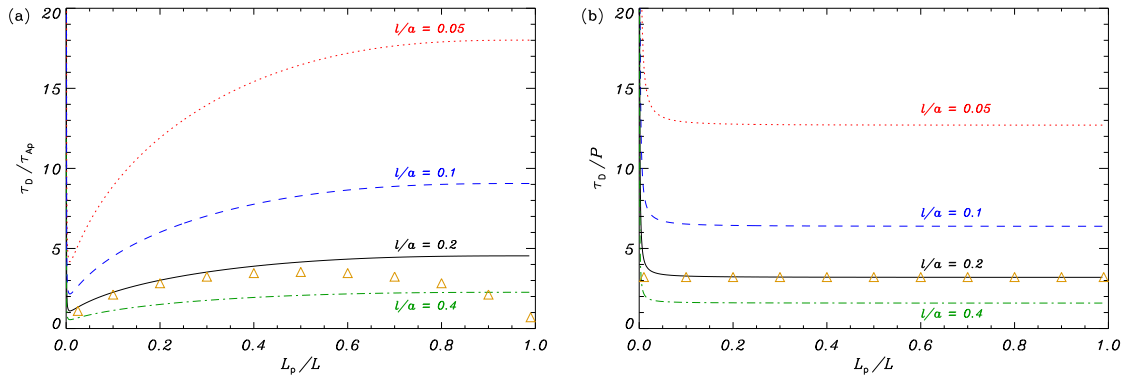


**Figure 61:** Results for a thread configuration with a transverse transitional layer and for the prominence thread located at the central part of the magnetic tube. (a) $\tau_d$ in units of the internal Alfvén travel time, $\tau_{Ap}$, and (b) $\tau_d/P$ as a function of $L_p/L$. The different lines in both panels denote $l/a = 0.05$ (dotted), 0.1 (dashed), 0.2 (solid), and 0.4 (dash-dotted). The symbols in panels (a) and (b) correspond to the analytic approximations with $l/a = 0.2$, Equations (34) and (32) in Soler *et al.* (2010a).

In summary, the dominant damping mechanism is resonant absorption, which provides damping ratios in agreement with the observations, whereas ion-neutral collisions are irrelevant for the damping. The values of the damping ratio are independent of both the prominence thread length and its position within the magnetic tube, and coincide with the values for a tube fully filled with the prominence plasma. A recent study that further analyses resonant damping of thread oscillations in two-dimensional equilibrium models can be found in Arregui *et al.* (2011). These authors additionally analyzed the influence of the density in the evacuated part of the thread. This quantity is seen to influence periods and damping times, but has little influence on the damping rate of transverse thread oscillations. The implications of some of these results for the determination of physical properties in transversely oscillating threads are discussed in Section 6.

## 5.6 Damping by wave leakage

The solutions obtained for the oscillations of prominence line current models (van den Oord and Kuperus, 1992; Schutgens, 1997a,b; van den Oord *et al.*, 1998) mentioned in Section 4.3 suggest the existence of time amplification and damping of the studied oscillations. While the amplification should be linked to a prominence destabilization, the attenuation seems to be very efficient for many of the considered parameter values, and the ratio of the damping time to the period is between 1 and 10 (i.e., in agreement with observations). This indicates that the oscillations are efficiently damped (Figure 62a). On the other hand, in the prominence model used by Schutgens and Tóth (1999) vertical oscillations are very efficiently attenuated for all the parameters considered and the same happens with horizontal oscillations (Figure 62b) for coronal densities above $\simeq 5 \times 10^{-13}$ kg m$^{-3}$. These constraining properties of damped horizontal and vertical oscillations could be used for prominence seismology.

However, the exact nature of the damping mechanism should be pointed out, and Schutgens and Tóth (1999) suggest that the damping of oscillations is due to the emission of waves by the prominence, i.e., wave leakage. The damping of horizontal motions is attributed to the emission of slow waves, whereas fast waves are invoked as the cause of the damping of vertical motions. Taking into account that the main difference between this work and those of van den Oord and Kuperus (1992), Schutgens (1997a,b), and van den Oord *et al.* (1998) lies essentially in the cross section of the filament, it seems that the physics involved should be the same, so wave leakage should be the mechanism responsible for the accounted damping. However, in Schutgens and Tóth (1999), the plasma-$\beta$ in the prominence ranges from $\beta > 1$ in its central part to $\beta < 0.1$ at its boundary. Hence, waves emitted by the prominence into the corona propagate in a $\beta \ll 1$ environment in which magnetic field lines are closed. Under these conditions, slow modes propagate along magnetic field lines and are unable to transfer energy from the prominence into the corona and so wave leakage in the system studied by Schutgens and Tóth (1999) is only possible by fast waves. Then, it is hard to understand how the prominence oscillations can be damped by the emission of slow waves in this particular model, in which the dense, cool plasma is only allowed to emit fast waves. It must be mentioned, however, that the plasma-$\beta$ in the corona increases with the distance from the filament, which implies that the emitted fast waves can transform into slow waves when they traverse the $\beta \simeq 1$ region. This effect has been explored by McLaughlin and Hood (2006) and McDougall and Hood (2007); see also references therein for similar studies.

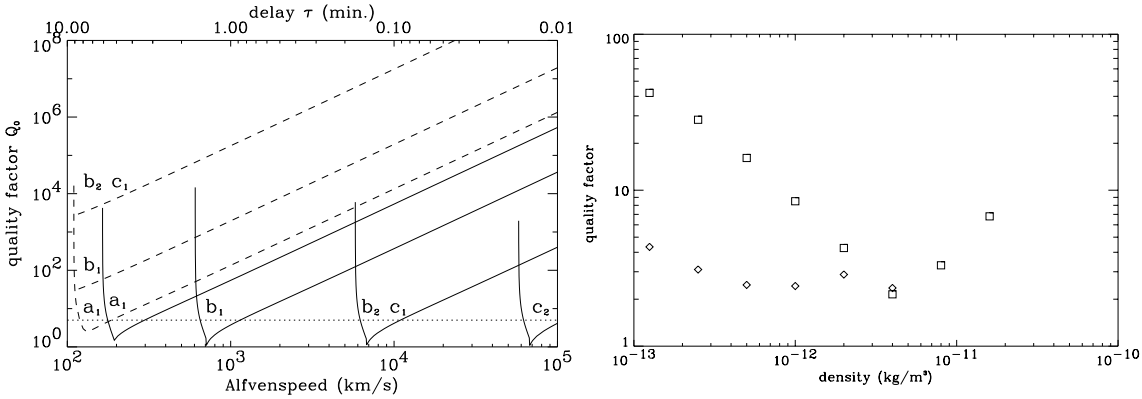


**Figure 62:** Attenuation of prominence oscillations by wave leakage. (a) Quality factor ($Q_0 \equiv \pi\tau_d/P$) of stable IP (solid curves) and NP (dashed curves) prominence oscillations as a function of the coronal Alfvén speed. (b) Quality factor of the horizontally (squares) and vertically (diamonds) polarized stable oscillations versus the coronal density (from Schutgens, 1997b and Schutgens and Tóth, 1999).

# 6 Prominence Seismology

Solar atmospheric seismology aims to determine physical parameters that are difficult to measure by direct means in magnetic and plasma structures. It is a remote diagnostics method that combines observations of oscillations and waves in magnetic structures, together with theoretical results from the analysis of oscillatory properties of given theoretical models. The philosophy behind this discipline is akin to that of Earth seismology, the sounding of the Earth interior using seismic waves, and helio-seismology, the acoustic diagnostic of the solar interior. It was first suggested by Uchida (1970) and Roberts *et al.* (1984), in the coronal context, and by Tandberg-Hanssen (1995) in the prominence context. The increase in the number and quality of high resolution observations in the 1990s has lead to the rapid development of solar atmospheric seismology. In the context of coronal loop oscillations, recent applications of this technique have allowed the estimation and/or restriction of parameters such as the magnetic field strength (Nakariakov and Ofman, 2001), the Alfvén speed in coronal loops (Zaqarashvili, 2003; Arregui *et al.*, 2007a; Goossens *et al.*, 2008), the transversal density structuring (Goossens *et al.*, 2002; Verwichte *et al.*, 2006) or the coronal density scale height (Andries *et al.*, 2005; Verth *et al.*, 2008).

The application of inversion techniques to prominence seismology is less developed. This is due to the complexity of these objects in comparison to, e.g., coronal loops. The recent refinement of theoretical models that incorporate the fine structuring of prominences and the high resolution observations of small amplitude oscillations have produced an increase in prominence seismology studies. Several techniques for the inversion of physical parameters have been developed that make use of observational estimates for quantities such as phase velocities, periods, damping times, and flow speeds. In general, the solution to the inverse problem cannot provide a single value for all the physical parameters of interest. However, important information about unknown physical quantities can be obtained using this method. The most relevant results of the MHD prominence seismology technique are here discussed.

The theoretical models decribed in Section 4 make use of different conceptual views of prominences, such as the string model, the slab model, and the thread model for their fine structure. Seismology efforts in the area have followed the same pattern. We describe them in increasing intricacy order, starting with a mechanical analogue (Section 6.1), followed by slab models (Section 6.2), and ending with the seismology of fine structure oscillations (Sections 6.3 to 6.6).

## 6.1 Seismology of large amplitude prominence oscillations

Several studies have made use of the observed characteristics of large amplitude oscillations in prominences to deduce physical parameters of these objects. The classic example is the interpretation by Hyder (1966) of the winking filament phenomenon in terms of a global mode of the prominence. This author modeled the eleven winking filament events reported by Ramsey and Smith (1965) as damped harmonic oscillators and obtained estimates of the vertical magnetic field strength in the range 2 – 30 G. More recent studies have also used large amplitude oscillations in filaments to deduce the magnetic field strength in these objects.

Vršnak *et al.* (2007) reported on H$\alpha$ observations of periodical plasma motions along the axis of a filament. The motions were both large amplitude and large scale, with an initial displacement of 24 Mm, an initial velocity amplitude of 51 km s$^{-1}$, a period of 50 min, and a damping time of 115 min. Oscillations were interpreted as a global mode of the system and the driver was thought to be the magnetic flux injection by magnetic reconnection at one of the filament legs. Although oscillatory motions along the prominence axis were also reported by Jing *et al.* (2003, 2006), the study by Vršnak *et al.* (2007) proposes an explanation for the triggering process and the restoring force, and performs diagnostics based on these interpretations.

The seismology analysis by Vršnak *et al.* (2007) is based on the fitting of the oscillation proper-

ties to a mechanical analogue model in terms of the classic damped harmonic oscillator equation. This analogue is first used to discard gas pressure as the restoring force, since it leads to sound speed values one order of magnitude larger than those corresponding to the typical temperature of prominence plasmas, and no signature of plasma at those temperatures was observed in TRACE EUV images. In this work a twisted flux rope model with both axial and azimuthal magnetic field components was considered and an excess azimuthal field at one of the prominence legs was assumed. This gives rise to a magnetic pressure gradient and a torque, which in turn drive a combined axial and rotational motion of the plasma. Next, an expression that relates the azimuthal Alfvén speed, $v_{A\varphi}$, and the oscillatory period was obtained. From this relation, the Alfvén speed $v_{A\varphi} \sim 100$ km s$^{-1}$ was inferred. By further assuming that the number density of the prominence plasma is in the range $10^{10} - 10^{11}$ cm$^{-3}$, the azimuthal magnetic field strength results in the range $5 - 15$ G. By measuring the pitch angle, Vršnak *et al.* (2007) additionally determined the internal structure of the flux rope helical magnetic field, from which the axial magnetic field strength was estimated to be in the range $10 - 30$ G.

The twisted flux rope model was also invoked by Pintér *et al.* (2008) in their analysis of SoHO EUV observations of large amplitude transverse oscillations in a polar crown filament previously studied by Isobe and Tripathi (2006). Oscillations were present along a foot belonging to a larger prominence structure and occurred prior to the eruption of the full structure. Wavelet analysis tools were used to shed light into the temporal and spatial behaviour of oscillations. The filament oscillated as a rigid body with a period of 2.5 h, that was constant along the filament, but decreased in time. The line-of-sight velocity was estimated to be about a few tens of km s$^{-1}$. The analysis of the spatial properties of the oscillations shows evidence of a global standing transverse oscillation, although some small scale oscillations within the structure cannot be discarded. Using the twisted flux rope model for the filament and based on the same scenario and analysis as Vršnak *et al.* (2007), the azimuthal Alfvén speed component was estimated to be $v_{A\varphi} = 49$ km s$^{-1}$ and the axial magnetic field strength in the range $2 - 10$ G. In this case, the pitch angle could not be measured. By assuming a mean value of 65°, Pintér *et al.* (2008) estimated that the axial component of the magnetic field must be in the range $1 - 5$ G.

## 6.2 Seismology of prominence slabs

The MHD wave properties for slab models of prominences are described in Section 4.2. Two relevant studies have made use of some of these models to infer physical properties in prominences. Their methodology is based on the identification of observed oscillations with theoretical eigenmodes.

Régnier *et al.* (2001) consider the possible theoretical modes that can explain their observations of oscillations in an active region filament. The slab model with a uniform and inclined magnetic field by Joarder and Roberts (1993b) is used (see Figure 29). The dispersion relations for Alfvén modes and magnetoacoustic modes are considered. They provide the frequency of six fundamental modes: the symmetric Alfvén, slow and fast kink modes and the antisymmetric Alfvén, slow and fast sausage modes, as a function of the prominence parameters. Observations provide with estimates for the width (8000 km) and length (63,000 km) of the filament. Assumptions on other parameters, such as the temperature of the filament (8000 K) and of its environment ($10^6$ K), the density of the slab ($10^{12}$ cm$^{-3}$), the magnetic field strength (20 G) and for the angle between the magnetic field and the long axis of the slab (25°) are made. The dispersion relations are then solved by using these parameters and the corresponding periods are obtained and classified.

Observations and Fourier analysis of Doppler velocity time series enable Régnier *et al.* (2001) to detect intermediate (between 5 and 20 min in this case) and long ($> 40$ min) period oscillations. From the comparison between the observed and calculated frequencies, an identification method of the oscillation modes in the observed filament is presented. The method makes use of the fact that the frequency ratio of the fundamental even Alfvén mode to the fundamental odd Alfvén mode only

depends on the ratio of the half-with of the slab to the half-length of the filament. This quantity is measurable. The same applies to the frequency ratios involving the slow kink/sausage and fast kink/sausage modes. Parametric calculations for the frequencies as a function of the magnetic field strength and the inclination angle, while keeping the slab density constant, are next performed. A diagnostic of the observed filament is obtained by looking for the parameters values that enable the matching of theoretical and observed frequencies. By following this method, the angle between the magnetic field and the long axis of the slab is estimated to be 18°. Using this value, an algebraic relation for the magnetic field strength as a function of the slab density is derived.

A more involved and ambitious diagnostic, using the Joarder and Roberts (1993b) slab model, was performed by Pouget *et al.* (2006). The long duration and high temporal resolution observations with CDS/SoHO enable these authors to detect and measure the entire range of periodicities theoretically expected in a filament. In particular both the short (less that 10 min) and the long ones (more than 40 min) are detected.

The detailed analysis of three filaments is presented. The seismic inversion technique closely follows that by Régnier *et al.* (2001), in the sense that the first step towards the diagnostic is the use of frequency ratios between fundamental even/odd (kink/sausage) modes. These ratios only depend on the ratio of the filament half-width to its half-length. Once this ratio is measured, with a given uncertainty, Pouget *et al.* (2006) assume that their 16-h long observation has allowed them to observe the six modes of interest, since the slowest mode is expected at a period of 5 h, for standard prominence parameters.

The inversion method first assigns a possible triplet of measured frequencies to the 3 odd fundamental frequencies (odd Alfvén, slow sausage, and fast sausage modes). The coherence of each choice is examined against two tests. The first requires to find three corresponding even frequencies, with the condition that the even/odd frequency ratios are consistent with the measured half-width to half-length ratio. The second involves the inferred values for the density, temperature, magnetic field inclination angle, and magnetic field strength to be consistent with typical values reported in the literature. For each test, if the test was negative, the full triplet was changed and the series started again. On the contrary, if the tests succeeded, Pouget *et al.* (2006) considered that the six fundamental modes were identified.

The three filament observations led to coherent diagnostics and a single possible set of frequencies was found for each observation. The importance of this study is its ability to simultaneously determine the values of the inclination angle, temperature, and Alfvén speed for the same prominence. The drawback is that the modeling, as in Régnier *et al.* (2001), does not permit to capture the highly inhomogeneous nature of prominences.

## 6.3 Seismology of propagating transverse thread oscillations

Transverse thread oscillations observed by Lin *et al.* (2009) and discussed in Section 3.6.4 show evidence of waves propagating along individual threads. Ten of the swaying threads were chosen by Lin *et al.* (2009) for further investigation, and for each selected thread two or three perpendicular cuts were made in order to measure the properties of the propagating waves. Periods and amplitudes of the waves, as well as their phase velocity, were derived for each thread. Lin *et al.* (2009) interpreted the observed events as propagating MHD kink waves supported by the thread body. This mode is the only one producing a significant transverse displacement of the cylinder axis. In addition, it also produces short-period oscillations of the order of minutes, compatible with the observed periods (see Section 4.4.1).

If an infinitely long, straight, cylindrical thread model, with the tube fully filled with cool and dense material (Figure 31), is assumed, a comparison between the observed wave properties and the theoretical prediction can be made. This enabled Lin *et al.* (2009) to obtain estimates for some physical parameters of interest, namely the Alfvén speed and the magnetic field strength in the

studied threads. To this end, the observed phase velocity was directly associated to the kink speed

$$c_{\rm k} = \frac{\omega_{\rm k}}{k_z} = v_{\rm Ap}\left[\frac{2\zeta}{1+\zeta}\right]^{1/2}, \tag{37}$$

where Equation (22) for the kink frequency has been used. In this expression $v_{\rm Ap}$ is the Alfvén speed in the prominence thread and $\zeta = \rho_{\rm p}/\rho_{\rm c}$ is the density contrast. Both quantities are unknown, hence no unique solution to Equation (37) can be obtained from the observed period alone. In the limit of high density contrast, typical of prominence plasmas, the ratio $\rho_{\rm p}/\rho_{\rm c}$ is very large and the ratio $c_{\rm k}^2/v_{\rm Ap}^2$ is almost independent from it (see Figure 63a). The kink speed can then be approximated by

$$c_{\rm k} \approx \sqrt{2} v_{\rm Ap}. \tag{38}$$

Lin *et al.* (2009) assumed that thread oscillations observed from the H$\alpha$ sequences were the result of a propagating kink mode, which implies that the measured phase velocity, $c_{\rm p}$, is equal to the kink speed. Then, the thread Alfvén speed can be computed from

$$v_{\rm Ap} \approx \frac{c_{\rm p}}{\sqrt{2}}. \tag{39}$$

The inferred values of $v_{\rm Ap}$ for the ten selected threads are displayed in Table 2 in Lin *et al.* (2009). The results show a strong dispersion, suggesting that the physical conditions in different threads were very different in spite of belonging to the same filament. This result clearly reflects the highly inhomogeneous nature of solar prominences. Once the Alfvén speed in each thread was determined, the magnetic field strength could be computed after a value for the thread density was assumed. For the analyzed events, and considering a typical value $\rho_{\rm p} = 5 \times 10^{-11}$ kg m$^{-3}$, magnetic field strengths in the range 0.9 – 3.5 G were obtained (see Figure 63b).

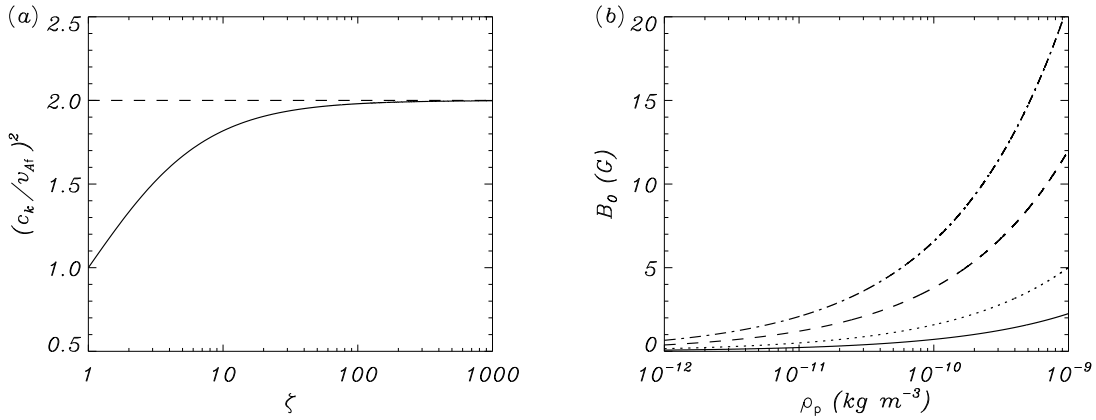


**Figure 63:** (a) Ratio $c_{\rm k}^2/v_{\rm Ap}^2$ (solid line) as a function of the density contrast, $\zeta$. The dotted line corresponds to the value of the ratio $c_{\rm k}^2/v_{\rm Ap}^2$ for $\zeta \to \infty$. (b) Magnetic field strength as a function of the internal density, $\rho_{\rm p}$, corresponding to four selected threads (from Lin *et al.*, 2009).

## 6.4 Seismology of damped transverse thread oscillations

A feature clearly observed by Lin *et al.* (2009) is that the amplitudes of the waves passing through two different cuts along a thread are notably different. Apparent changes can be due to damping of the waves in addition to noise in the data. The damping of prominence oscillations is a

common feature in many observed events and damping time-scales provide an additional source of information that can be used when performing parameter inference using seismology inversion techniques, once a physical model that provides an explanation is available. Among the different damping mechanisms described in Section 5, resonant absorption in the Alfvén continuum seems a very plausible one and has been used to perform prominence thread seismology, using the damping as an additional source of information. In the context of coronal loop seismology, the use of damping rates in combination with oscillatory periods gives information about the transverse density structuring of coronal loops (Goossens *et al.*, 2002; Arregui *et al.*, 2007a; Goossens, 2008; Goossens *et al.*, 2008).

The model considered here is an infinitely long thread of radius $a$ surrounded by a thin transition sheath of thickness $l$ in which a smooth transition from the thread to the coronal density takes place (see Figure 50). For standing kink waves, and without using the thin tube and thin boundary approximation, the normal mode period and damping ratio are functions of the relevant equilibrium parameters,

$$P = P(k_z, \zeta, l/a, v_{\rm Ap}), \qquad \frac{P}{\tau_{\rm d}} = \frac{P}{\tau_{\rm d}}(k_z, \zeta, l/a), \tag{40}$$

with $v_{\rm Ap}$ the prominence thread Alfvén speed. Note that in the thin tube and thin boundary approximations (Equation (23) for $P$ and Equation (30) for the damping ratio), the period does not depend on $l/a$ and the damping ratio is independent of the wavelength. This is not true in the general case (Arregui *et al.*, 2008b). The period is a function of the longitudinal wavenumber, $k_z$, the transverse inhomogeneity length-scale, $l/a$, and the internal Alfvén speed. Similarly for the damping ratio, except for the fact that it cannot depend on any time-scale. The long wavelength approximation further eliminates the $k_z$ dependence of the damping ratio. In the case of coronal loop oscillations, an estimate for $k_z$ can be obtained directly from the length of the loop and the fact that the fundamental kink mode wavelength is twice this quantity. For prominence threads, the wavelength of oscillations needs to be measured. Relations (40) indicate that, if no assumption is made on any of the physical parameters of interest, there are infinite different equilibrium models that can equally well explain the observations (namely the period and damping ratio). The parameter values that define these valid equilibrium models are displayed in Figure 64a, where the analytical algebraic expressions in the thin tube and thin boundary approximations by Goossens *et al.* (2008) have been used to invert the problem. It can be appreciated that, even if an infinite number of solutions is obtained, they define a rather constrained range of values for the thread Alfvén speed. Because of the insensitiveness of the damping rate with the density contrast for the typically large values of this parameter in prominence plasmas, the obtained solution curve displays an asymptotic behaviour for large values of $\zeta$. This makes possible to obtain precise estimates for the thread Alfvén speed, $v_{\rm Ap} \simeq 12$ km s$^{-1}$, and the transverse inhomogeneity length scale, $l/a \simeq 0.16$. Note that these asymptotic values can directly be obtained by inverting Equations (23) and (30) for the period and the damping rate in the limit $\zeta \to \infty$. The computation of the magnetic field strength from the obtained seismological curve requires the assumption of a particular value for either the filament or the coronal density. The resulting curve for a typical coronal density is shown in Figure 64b. Precise values of the magnetic field strength cannot be obtained, unless the density contrast is accurately known.

The transverse inhomogeneity length scale of an oscillating thread could also be estimated by using observations of spatial damping of propagating kink waves and theoretical results described in Section 5.4.2. In the context of coronal loops, Terradas *et al.* (2010) have shown that the ratio of the damping length to the wavelength, due to resonant damping of propagating kink waves, has the same dependence on the density contrast and transverse inhomogeneity length-scale as the ratio of the damping time to the period for standing kink waves. Similar inversion techniques to the ones explained here for the temporal damping of oscillations could be applied to the spatial

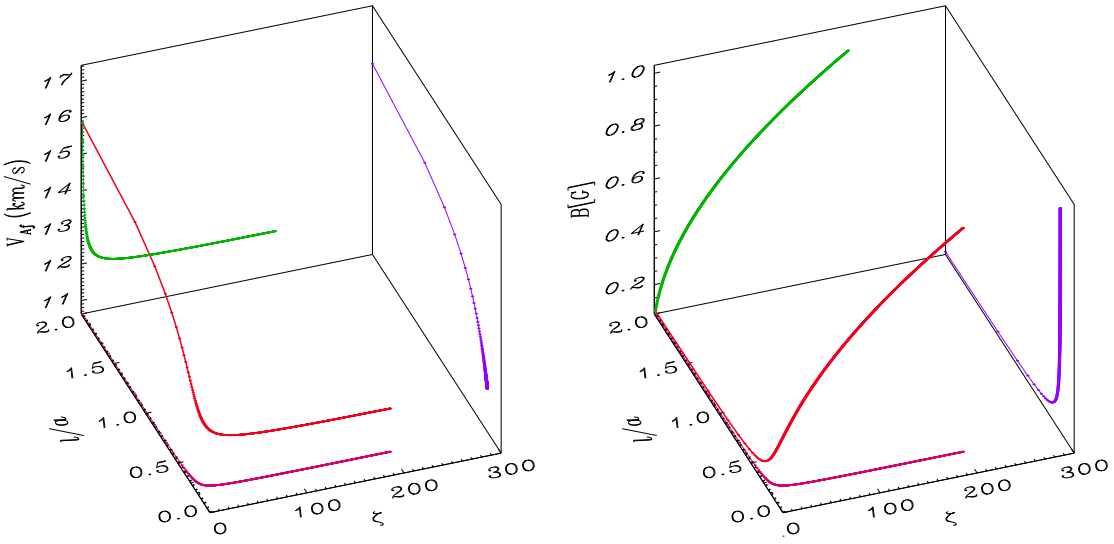


**Figure 64:** *Left:* Analytic inversion of physical parameters in the ($\zeta$, $l/a$, $v_{\rm Ap}$) space for a filament thread oscillation with $P = 3$ min, $\tau_{\rm d} = 9$ min, and a wavelength $\lambda = 3000$ km (see, e.g., Lin *et al.*, 2007). *Right:* Magnetic field strength as a function of the density contrast and transverse inhomogeneity length-scale, derived from the analytic inversion for a coronal density $\rho_{\rm c} = 2.5 \times 10^{-13}$ kg m$^{-3}$.

damping of propagating waves.

The main downside of the technique just described is the use of thread models in which the full magnetic tube is filled with cool and dense plasma. The solution to the forward problem in the case of two-dimensional thread models is discussed in Section 5.5. The analytical and numerical results obtained by Soler *et al.* (2010a) using these models indicate that the length of the thread and its position along the magnetic tube influence the period and damping time of transverse thread oscillations. On the contrary, the damping ratio is rather insensitive to these model properties.

Going back to the inversion curve displayed in Figure 64a, we notice that a change in the period produces a vertical shift of the solution curve, hence the period influences the inferred values for the Alfvén speed. On the other hand, the damping ratio determines the projection of the inversion curve onto the ($\zeta$, $l/a$)-plane. We can conclude that ignorance of the length of the thread or the length of the supporting magnetic flux tube will have a significant impact on the inferred values for the Alfvén speed (hence magnetic field strength) in the thread. On the contrary, because of the smaller sensitivity of the damping ratio to changes in the longitudinal density structuring, seismological estimates of the transverse density structuring will be less affected by our ignorance about the longitudinal density structuring of prominence threads.

An example of the inversion of physical parameters for different values of the thread length was presented by Soler *et al.* (2010a). When partially filled threads, i.e., with the dense part occupying a length $L_{\rm p}$ shorter than the total length of the tube $L$, are considered, one curve is obtained for each value of the length of the thread. The solutions to the inverse problem are shown in Figure 65a for a set of values of $L_{\rm p}$. Even if each curve gives an infinite number of solutions, again each of them defines a rather constrained range of values for the thread Alfvén speed. The figure shows that the ratio $L_{\rm p}/L$ is a fundamental parameter in order to perform an accurate seismology of prominence threads, since different curves produce different estimates for the prominence Alfvén speed, as anticipated above. Because of the insensitiveness of the damping ratio with respect to the length of the thread, all solution curves for different lengths of the threads produce the same projection

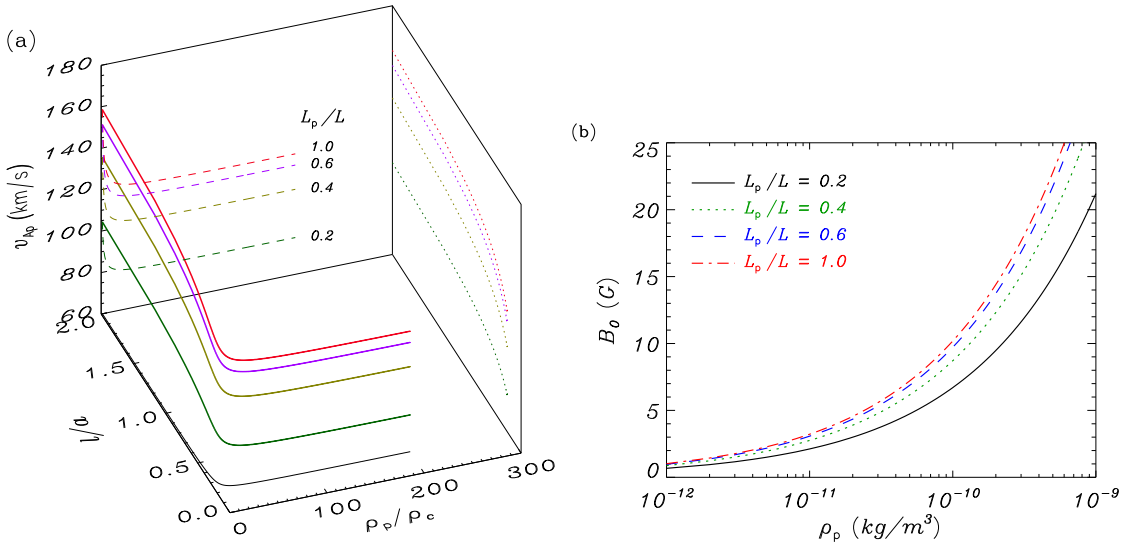


**Figure 65:** Determination of (a) prominence Alfvén speed and (b) magnetic field strength from the computation of periods and damping times for standing kink oscillations in two-dimensional prominence thread models and observations of period and damping times in transverse thread oscillations. The observed period and damping time are 20 and 60 min, respectively, and $L = 10^5$ km (from Soler *et al.*, 2010a).

onto the $(\zeta, l/a)$-plane. Hence, the same precise estimates of the transverse inhomogeneity length scale obtained from infinitely long thread models are valid, irrespective of the length of the thread. The computation of the magnetic field strength from the obtained seismological curve requires the assumption of a particular value for either the filament or the coronal density. The resulting curves for a typical coronal density and several values of $L_p/L$ are shown in Figure 65b. Here again, precise values of the magnetic field strength cannot be obtained, unless the density contrast is accurately known.

## 6.5 Seismology using period ratios of thread oscillations

The widespread use of the concept of period ratios as a seismological tool has been remarkable in the context of coronal loop oscillations (see Andries *et al.*, 2009, for a review). The idea was first put forward by Andries *et al.* (2005) and Goossens *et al.* (2006) as a means to infer the coronal density scale height using multiple mode oscillations in coronal loops embedded in a vertically stratified atmosphere. In coronal loop seismology, the ratio of the fundamental mode period to twice that of its first overtone in the longitudinal direction ($P_1/2P_2$) mainly depends on the density structuring along magnetic field lines. It can therefore be used as a diagnostic tool for the coronal density scale height.

In the context of prominence seismology, a similar approach was proposed by Díaz *et al.* (2010) to obtain information about the density structuring along prominence threads using the piecewise longitudinally structured thread model by Díaz *et al.* (2002) (see Figure 41). These authors showed that the non-dimensional oscillatory frequencies of the fundamental kink mode and the first overtone are almost independent of the ratio of the thread diameter to its length. Thus, the dimensionless oscillatory frequency depends, basically, on the density ratio of the prominence to

the coronal plasma, $\rho_{\rm p}/\rho_{\rm c}$, and the non-dimensional length of the thread, $W/L$,

$$\frac{\omega L}{v_{\rm Ap}} = f(W/L, \rho_{\rm p}/\rho_{\rm c}). \tag{41}$$

Here we follow the notation of Díaz *et al.* (2010), who use $2W$ for the thread length, rather than that of Soler *et al.* (2010a), who denote this length by $L_{\rm p}$. In order to determine the dimensional frequency when comparing to observations, two additional parameters are needed, namely the Alfvén velocity in the corona or in the prominence (involving some knowledge of the magnetic field strength and density) and the length of the magnetic tube, $2L$. Note, however, that the non-dimensional frequencies of the fundamental mode and its first overtone can be cast as

$$\frac{\omega_1 L}{v_{\rm Ap}} = f_1(W/L, \rho_{\rm p}/\rho_{\rm c}), \tag{42}$$

$$\frac{\omega_2 L}{v_{\rm Ap}} = f_2(W/L, \rho_{\rm p}/\rho_{\rm c}), \tag{43}$$

so that the dependence on the length of the tube and the thread Alfvén speed can be removed by considering the period ratio,

$$\frac{P_1}{2P_2} = F(W/L, \rho_{\rm p}/\rho_{\rm c}). \tag{44}$$

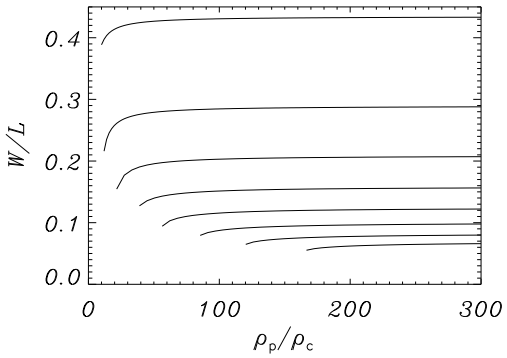


**Figure 66:** Plot of the solution lines satisfying $P_1/2P_2 =$ constant in the parameter space. The upper line corresponds to $P_1/2P_2 = 1.25$ and the lower one to $P_1/2P_2 = 3$, with each line showing an increment in $P_1/2P_2$ of 0.25 from the previous one (from Díaz *et al.*, 2010).

Equation (44) can be used for diagnostic purposes, once reliable measurements of multiple mode periods are obtained. The curves in Figure 66 display the solution to the inverse problem in the ($\rho_{\rm p}/\rho_{\rm c}$, $W/L$) parameter space for several values of the period ratio. Given the period ratio from an observation, it only depends on $W/L$ in first approximation. Once $W/L$ has been obtained, one can estimate the value of the magnetic field length $2L$, since the thread length, $2W$, can be determined quite accurately from the observations.

The use of the period ratio technique needs the unambiguous detection of two periodicities in the same oscillating prominence thread. Díaz *et al.* (2010) pointed out two main difficulties in this respect. From a theoretical point of view, the overtone with period $P_2$ is an antisymmetric mode in the longitudinal direction, with a node in the center of the thread and two maxima located

outside it. Only for sufficiently long threads, with $W/L \sim 0.1$, the anti-nodes of the overtone are located inside the thread and could hence be measured in the part of the tube visible in, e.g., H$\alpha$. From an observational point of view, no conclusive measurement of the first overtone period has been reported so far in the literature, although there seem to be hints of its presence in some observations by, e.g., Lin *et al.* (2007), who reported on the presence of two periods, $P_1 = 16$ min and $P_2 = 3.6$ min in their observations of a prominence region. Díaz *et al.* (2010) used the period ratio from these observations to infer the value for the length of the thread ratio $W/L = 0.12$. Although it is difficult to estimate the length of the particular thread under consideration, assuming a value of 13,000 km, as for other threads analyzed by Lin *et al.* (2007), results in a magnetic tube length $L \sim 130,000$ km.

This new seismological information can be now used to obtain further information about the physical conditions in the oscillating thread. Using analytical approximations for the dimensionless frequency of the first overtone, the following expression for the prominence Alfvén speed as a function of the length of the thread is obtained,

$$v_{\rm Ap} = \frac{\pi L}{P_1}\sqrt{2\frac{W}{L}\left(1-\frac{W}{L}\right)}. \tag{45}$$

Once the length of the tube is known, an estimate for the prominence Alfvén speed can be inferred from Equation (45). In the example shown by Díaz *et al.* (2010), the high density contrast limit was used to infer the value $v_{\rm Ap} \sim 160$ km s$^{-1}$.

## 6.6 Seismology of flowing and oscillating prominence threads

Mass flows in conjunction with phase speeds, oscillatory periods, and damping times might constitute an additional source of information about the physical conditions of oscillating threads. The first application of prominence seismology using Hinode observations of flowing and transversely oscillating threads was presented by Terradas *et al.* (2008), using observations obtained in an active region filament by Okamoto *et al.* (2007) discussed in Section 3.6.4.

The observations show a number of threads that flow following a path parallel to the photosphere while they oscillate in the vertical direction. The relevance of this particular event is that the coexistence of waves and flows can be firmly established, so that there is no ambiguity about the wave or flow character of a given dynamic feature: both seem to be present in this particular event. However, other interpretations for the apparent motion in the plane of the sky could be also possible, for instance, an ionization wave or a thermal front. Okamoto *et al.* (2007) analyzed 6 threads whose relevant measured properties are displayed in Table 1.

**Table 1:** Summary of geometric and wave properties of horizontally flowing and vertically oscillating threads analyzed by Okamoto *et al.* (2007). $L_{\rm thread}$ is the thread length, $v_0$ its horizontal flow velocity, $P$ the oscillatory period, $V$ the oscillatory velocity amplitude, and $H$ the height above the photosphere.

| Thread | $L_{\rm thread}$ (km) | $v_0$ (km s$^{-1}$) | $P$ (s) | $V$ (km s$^{-1}$) | $H$ (km) |
|---|---|---|---|---|---|
| 1 | 3600 | 39 | 174 ± 25 | 16 | 18,300 |
| 2 | 16,000 | 15 | 240 ± 30 | 15 | 12,400 |
| 3 | 6700 | 39 | 230 ± 87 | 12 | 14,700 |
| 4 | 2200 | 46 | 180 ± 137 | 8 | 19,000 |
| 5 | 3500 | 45 | 135 ± 21 | 9 | 14,300 |
| 6 | 1700 | 25 | 250 ± 17 | 22 | 17,200 |

In their seismological analysis of these oscillations Terradas *et al.* (2008) started by neglecting the mass flows. Then, they interpreted these events in terms of the standing kink mode of a

finite-length thread in a magnetic flux tube (see Figure 41 and Section 4.5). By using theoretical results by Díaz *et al.* (2002) and Dymova and Ruderman (2005) (see Section 4.5), Terradas *et al.* (2008) found that, although it is not possible to univocally determine all the physical parameters of interest, a one-to-one relation between the thread Alfvén speed and the coronal Alfvén speed could be established. This relation comes in the form of a number of curves relating the two Alfvén speeds for different values of the length of the magnetic flux tube and the density contrast between the filament and coronal plasma. Figure 68 shows these curves for the selection of six threads made by Okamoto *et al.* (2007). An interesting property of the obtained solution curves is that they display an asymptotic behaviour for large values of the density contrast, which is typical of filament to coronal plasmas and, hence, a lower limit for the thread Alfvén speed can be obtained. Take for instance thread #6. Considering a magnetic flux tube length of 100 Mm, a value of 120 km $s^{-1}$ for the thread Alfvén speed is obtained.

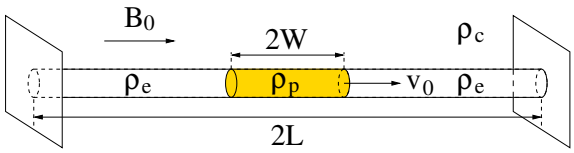


**Figure 67:** Sketch of the magnetic and plasma configuration used to represent a flowing thread (shaded volume) in a thin magnetic tube. The two parallel planes at both ends of the cylinder represent the photosphere (from Terradas *et al.*, 2008).

Terradas *et al.* (2008) next incorporated mass flows into their analysis (see Figure 67). First a simple approximation was made by taking into account that the flow velocity along the cylinder, $v_0$, enters the linear MHD wave equations through the differential operator

$$\frac{\partial}{\partial t} + v_0 \frac{\partial}{\partial z}.$$

The terms coming from the equilibrium flow can, in a first approximation, be ignored because, as noted by Dymova and Ruderman (2005), inside the cylinder the terms with derivatives along the tube are much smaller than those with radial or azimuthal derivatives. By following this approach the problem reduces to solving a time-dependent problem with a varying density profile, $\rho(z,t)$, representing a dense part moving along the tube with the flow speed. By using the flow velocities in Table 1 and after solving the two-dimensional wave equations, Terradas *et al.* (2008) found that the flow velocities measured by Okamoto *et al.* (2007) result in slightly shorter kink mode periods than the ones derived in the absence of flow. Differences are small, however, and produce period shifts between 3 and 5%. As a consequence, the curves in Figure 68 can be considered a good approximation to the solution of the inverse problem.

Finally, a more complete approach to the problem was followed by Terradas *et al.* (2008), who considered the numerical solution of the non-linear, ideal, low-$\beta$ MHD equations with no further approximations, that is, the thin tube approximation was not used and the flow was maintained in the equations. The numerical results confirm the previous approximate results regarding the effect of the flow on the obtained periods and, therefore, on the derived Alfvén speed values. We must note that in this case, and because of the small value of the flow speeds measured by Okamoto *et al.* (2007) in this particular event, there are no significant variations of the wave properties and, hence, of the inferred Alfvén speeds, although larger flow velocities may have more relevant consequences on the determination of physical parameters in prominence threads.

In most of the examples shown here, the number of unknowns is larger that that of observed parameters. This makes difficult to obtain a unique solution that reproduces the observations. Furthermore, the inversions are performed with information that is incomplete and uncertain. The

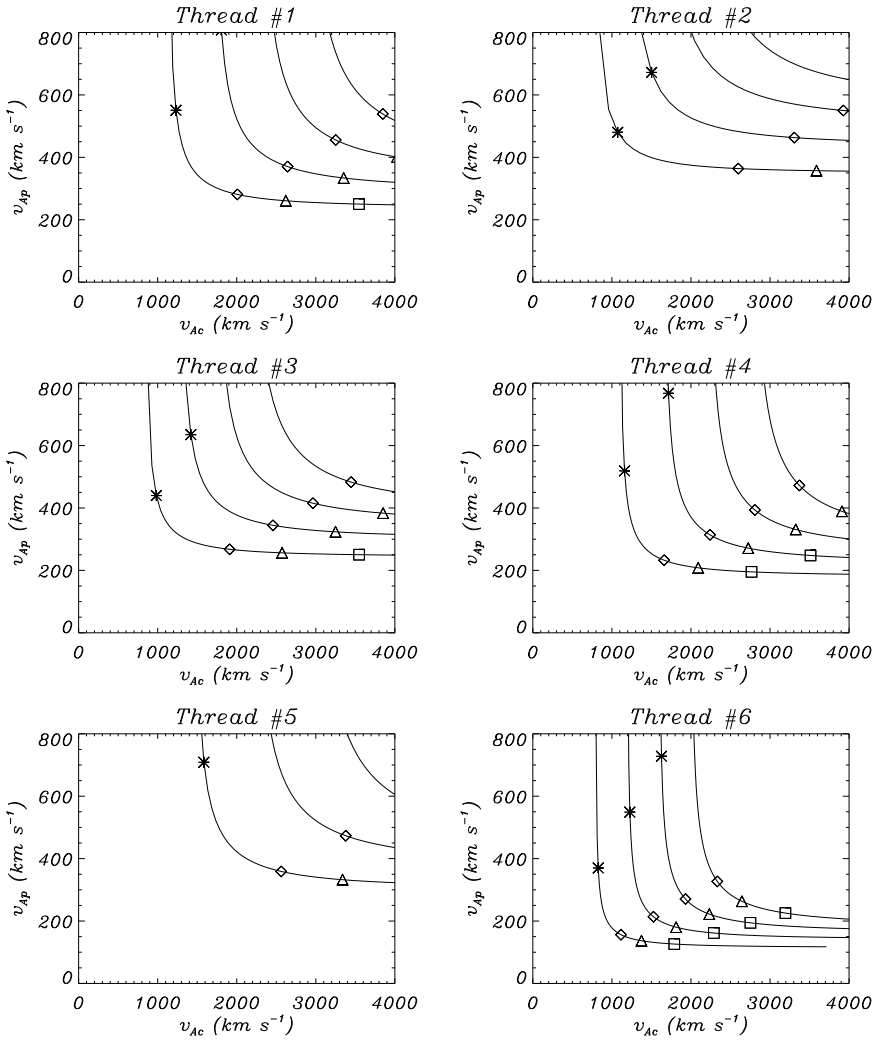


**Figure 68:** Dependence of the Alfvén velocity in the thread as a function of the coronal Alfvén velocity for the six threads observed by Okamoto *et al.* (2007). In each panel, from bottom to top, the curves correspond to a length of magnetic field lines of 100,000 km, 150,000 km, 200,000 km, and 250,000 km, respectively. Asterisks, diamonds, triangles, and squares correspond to density ratios of the thread to the coronal gas $\zeta \simeq 5$, 50, 100, and 200 (from Terradas *et al.*, 2008).

use of statistical techniques, based on bayesian inference, can help to overcome these limitations, as shown by Arregui and Asensio Ramos (2011).

# 7 Open Issues

Solar prominences are among the most complicated structures in the solar corona. A full understanding of their formation, magnetic structure, and disappearance has not been reached yet, and a lot of physical effects remain to be included in prominence models. For this reason, theoretical models set up to interpret small amplitude oscillations are still poor. High-resolution observations of filaments suggest that they are made of threads whose thickness is at the the limit of the available spatial resolution. Then, one may wonder whether future improvements of the spatial resolution will provide with thinner and thinner threads or, on the contrary, there is a lower limit for thickness and we will be able to determine it in the future. The presence of these long and thin threads together with the place where they are anchored and the presence of flows along them suggest that they are thin flux tubes filled with continuous or discontinuous cool material.

This cool material is probably subject to cooling, heating, ionization, recombination, motions, etc., which, altogether, makes very difficult a proper theoretical treatment. For instance, in the case of the considered thermal mechanisms, up to now only optically thin radiation has been taken into account, while the inclusion of optically thick effects would probably be more realistic; the prominence heating mechanisms taken usually into account are tentative and "ad hoc", while true prominence heating processes are still deeply unknown. An important step ahead would be to couple radiative transfer with magnetohydrodynamic waves as a mean to establish a relationship between velocity, density, magnetic field, and temperature perturbations, and the observed signatures of oscillations like spectral line shift, width and intensity. Partial ionization is another topic of interest for prominence oscillations since, apart from influencing the behaviour of magnetohydrodynamic waves, it poses an important problem for prominence equilibrium models since cross-field diffusion of neutral atoms can give place to flows and drain prominence material.

Another issue which still remains a mystery is the triggering mechanism of small amplitude oscillations. In the case of large amplitude oscillations, observations provide with information about the exciting mechanism, but the available observations of small amplitude oscillations show no signature of their exciting mechanism. Are these oscillations of chromospheric or photospheric origin? Are they generated inside prominence magnetic structures by small reconnection events? Are they produced by weak external disturbances coming from far away in the solar atmosphere?

The presence of flows adds another ingredient to be taken into account in the study of prominence oscillations and, up to now, we can only obtain one or two-dimensional information about the flow behaviour. It would be of great interest to collect information about the three-dimensional structure of flows and, probably, in the near future we could acquire this information by means of IRIS (http://iris.lmsal.com/).

The physical changing conditions of prominence plasmas suggest that for an in-depth theoretical study of prominence oscillations more complex models together with numerical simulations are needed. Therefore, and as a step ahead, in the next future numerical studies of the time evolution of magnetohydrodynamic waves in partially ionized flowing inhomogeneous prominence plasmas, subject to different physical processes such as ionization, recombination, etc., should be undertaken. However, a full three-dimensional dynamical prominence model involving magnetic equilibrium, radiative transfer, etc., whose oscillatory behaviour could be studied seems to be still far away in the future.

## 8 Acknowledgements

The authors acknowledge the financial support received from the Spanish MICINN/MINECO and FEDER funds under Grant No. AYA2006-07637 and AYA2011-22486. They also thank R. Soler for providing some of the figures of this review.

All figures from *Astronomy and Astrophysics* reproduced with permission © ESO; from *The Astrophysical Journal* and *The Astrophysical Journal Letters* reproduced by permission of the AAS; from *Geophysical & Astrophysical Fluid Dynamics* reprinted by permission of Taylor & Francis Ltd.; from *Science* reprinted with permission from AAAS; and from *Solar Physics* reproduced with kind permission from Springer Science+Business Media B.V.

## References


Anderson, G.F., 1967, *Transient Flare-Associated Phenomena in the Solar Atmosphere*, Ph.D. thesis, University of Colorado at Boulder, Boulder, CO. [ADS] (Cited on page 8.)

Andries, J., Arregui, I. and Goossens, M., 2005, "Determination of the Coronal Density Stratification from the Observation of Harmonic Coronal Loop Oscillations", *Astrophys. J. Lett.*, **624**, L57–L60. [DOI], [ADS] (Cited on pages 84 and 90.)

Andries, J., Arregui, I. and Goossens, M., 2009, "The influence of longitudinal density variation in coronal loops on the eigenfunctions of kink-oscillation overtones", *Astron. Astrophys.*, **497**, 265–272. [DOI], [ADS] (Cited on page 90.)

Anzer, U., 2009, "Global prominence oscillations", *Astron. Astrophys.*, **497**, 521–524. [DOI], [ADS] (Cited on pages 39, 40, and 41.)

Anzer, U. and Heinzel, P., 2005, "On the Nature of Dark Extreme Ultraviolet Structures Seen by SOHO/EIT and TRACE", *Astrophys. J.*, **622**, 714–721. [DOI], [ADS] (Cited on page 13.)

Arregui, I. and Asensio Ramos, A., 2011, "Bayesian Magnetohydrodynamic Seismology of Coronal Loops", *Astrophys. J.*, **740**, 44. [DOI], [ADS], [arXiv:1107.3943 [astro-ph.SR]] (Cited on page 95.)

Arregui, I. and Ballester, J.L., 2011, "Damping Mechanisms for Oscillations in Solar Prominences", *Space Sci. Rev.*, **158**, 169–204. [DOI], [ADS], [arXiv:1002.3489 [astro-ph.SR]] (Cited on page 61.)

Arregui, I., Andries, J., Van Doorsselaere, T., Goossens, M. and Poedts, S., 2007a, "MHD coronal seismology using the period and damping of resonantly damped quasi-mode kink oscillations", *Astron. Astrophys.*, **463**, 333–338. [DOI] (Cited on pages 84 and 88.)

Arregui, I., Terradas, J., Oliver, R. and Ballester, J.L., 2007b, "Resonantly Damped Surface and Body MHD Waves in a Solar Coronal Slab with Oblique Propagation", *Solar Phys.*, **246**, 213–230. [DOI], [ADS], [arXiv:0708.3783] (Cited on page 60.)

Arregui, I., Ballester, J.L. and Goossens, M., 2008a, "On the Scaling of the Damping Time for Resonantly Damped Oscillations in Coronal Loops", *Astrophys. J. Lett.*, **676**, L77–L80. [DOI], [ADS], [arXiv:0802.1143] (Cited on page 8.)

Arregui, I., Terradas, J., Oliver, R. and Ballester, J.L., 2008b, "Damping of Fast Magnetohydrodynamic Oscillations in Quiescent Filament Threads", *Astrophys. J. Lett.*, **682**, L141–L144. [DOI], [ADS] (Cited on pages 8, 69, 70, 71, and 88.)

Arregui, I., Soler, R., Ballester, J.L. and Wright, A.N., 2011, "Magnetohydrodynamic kink waves in two-dimensional non-uniform prominence threads", *Astron. Astrophys.*, **533**, A60. [DOI], [ADS], [arXiv:1011.5175 [astro-ph.SR]] (Cited on page 82.)

Aschwanden, M.J., Fletcher, L., Schrijver, C.J. and Alexander, D., 1999, "Coronal Loop Oscillations Observed with the Transition Region and Coronal Explorer", *Astrophys. J.*, **520**, 880–894. [DOI], [ADS] (Cited on page 61.)

Bakhareva, N.M., Zaitsev, V.V. and Khodachenko, M.L., 1992, "Dynamic regimes of prominence evolution", *Solar Phys.*, **139**, 299–314. [DOI], [ADS] (Cited on page 9.)

Ballai, I., 2003, "On dissipative effects in solar prominences", *Astron. Astrophys.*, **410**, L17–L19. [DOI], [ADS] (Cited on page 61.)

Ballester, J.L., 2010, "The damping of small-amplitude oscillations in quiescent prominences", *Adv. Space Res.*, **46**, 364–376. [DOI], [ADS] (Cited on page 61.)

Ballester, J.L. and Priest, E.R., 1989, "Model for the fibril structure of solar prominences", *Astron. Astrophys.*, **225**, 213–221. [ADS] (Cited on pages 54 and 55.)

Balthasar, H. and Wiehr, E., 1994, "Temporal and spatial variation of physical parameters in a quiescent prominence", *Astron. Astrophys.*, **286**, 639–644. [ADS] (Cited on pages 11, 13, and 16.)

Balthasar, H., Knoelker, M., Wiehr, E. and Stellmacher, G., 1986, "Evidence for quasi-periodic Doppler motions in solar prominences", *Astron. Astrophys.*, **163**, 343–346. [ADS] (Cited on pages 13 and 14.)

Balthasar, H., Wiehr, E. and Stellmacher, G., 1988, "Periodic and quasiperiodic Doppler velocity variations in solar prominences along one spatial direction", *Astron. Astrophys.*, **204**, 286–300. [ADS] (Cited on page 16.)

Balthasar, H., Wiehr, E., Schleicher, H. and Wohl, H., 1993, "Doppler oscillations in solar prominences simultaneously observed with two telescopes. Discovery of a 30 s oscillation", *Astron. Astrophys.*, **277**, 635–638. [ADS] (Cited on pages 11, 14, and 16.)

Bashkirtsev, V.S. and Mashnich, G.P., 1984, "Oscillatory processes in prominences", *Solar Phys.*, **91**, 93–101. [DOI], [ADS] (Cited on pages 10, 11, and 14.)

Bashkirtsev, V.S. and Mashnich, G.P., 1993, "Some regularities of velocity oscillations in prominences", *Astron. Astrophys.*, **279**, 610–614. [ADS] (Cited on page 14.)

Bashkirtsev, V.S., Kobanov, N.I. and Mashnich, G.P., 1983, "The observations of 80-min oscillations in the quiescent prominences", *Solar Phys.*, **82**, 443–445. [DOI], [ADS] (Cited on page 14.)

Berger, T.E., Shine, R.A., Slater, G.L., Tarbell, T.D., Title, A.M., Okamoto, T.J., Ichimoto, K., Katsukawa, Y., Suematsu, Y., Tsuneta, S., Lites, B.W. and Shimizu, T., 2008, "Hinode SOT Observations of Solar Quiescent Prominence Dynamics", *Astrophys. J. Lett.*, **676**, L89–L92. [DOI], [ADS] (Cited on pages 5, 11, 12, 16, 18, and 22.)

Bernstein, I.B., Frieman, E.A., Kruskal, M.D. and Kulsrud, R.M., 1958, "An Energy Principle for Hydromagnetic Stability Problems", *Proc. R. Soc. London, Ser. A*, **244**, 17–40. [DOI], [ADS] (Cited on page 45.)

Blanco, S., Bocchialini, K., Costa, A., Domenech, G., Rovira, M. and Vial, J.-C., 1999, "Multiresolution wavelet analysis of SUMER/SOHO observations in a solar prominence", *Solar Phys.*, **186**, 281–290. [DOI], [ADS] (Cited on pages 11, 13, 14, and 22.)

Bommier, V. and Leroy, J.-L., 1998, "Global Pattern of the Magnetic Field Vector Above Neutral Lines from 1974 to 1982: Pic-du-Midi Observations of Prominences", in *New Perspectives on Solar Prominences*, IAU Colloq. 167, Aussois, France, April 28 – May 4, 1997, (Eds.) Webb, D.F., Schmieder, B., Rust, D.M., vol. 150 of ASP Conference Series, pp. 434–438, Astronomical Society of the Pacific, San Francisco. [ADS] (Cited on page 5.)

Bommier, V., Landi Degl'Innocenti, E., Leroy, J.-L. and Sahal-Bréchot, S., 1994, "Complete determination of the magnetic field vector and of the electron density in 14 prominences from linear polarization measurements in the HeI $D_3$ and H$\alpha$ lines", *Solar Phys.*, **154**, 231–260. [DOI], [ADS] (Cited on page 5.)

Cally, P.S., 1986, "Leaky and non-leaky oscillations in magnetic flux tubes", *Solar Phys.*, **103**, 277–298. [DOI], [ADS] (Cited on page 48.)

Carbonell, M., Oliver, R. and Ballester, J.L., 2004, "Time damping of linear non-adiabatic magnetohydrodynamic waves in an unbounded plasma with solar coronal properties", *Astron. Astrophys.*, **415**, 739–750. [DOI], [ADS] (Cited on page 61.)

Carbonell, M., Terradas, J., Oliver, R. and Ballester, J.L., 2006, "Spatial damping of linear non-adiabatic magnetoacoustic waves in a prominence medium", *Astron. Astrophys.*, **460**, 573–581. [DOI], [ADS] (Cited on pages 61 and 76.)

Carbonell, M., Oliver, R. and Ballester, J.L., 2009, "Time damping of non-adiabatic MHD slow and thermal waves in a prominence medium: Effect of a background flow", *New Astronomy*, **14**, 277–284. [DOI], [ADS] (Cited on pages 61 and 62.)

Carbonell, M., Forteza, P., Oliver, R. and Ballester, J.L., 2010, "The spatial damping of magnetohydrodynamic waves in a flowing partially ionised prominence plasma", *Astron. Astrophys.*, **515**, A80. [DOI], [ADS], [arXiv:1001.4962 [astro-ph.SR]] (Cited on page 76.)

Chen, P.F., Wu, S.T., Shibata, K. and Fang, C., 2002, "Evidence of EIT and Moreton Waves in Numerical Simulations", *Astrophys. J. Lett.*, **572**, L99–L102. [DOI], [ADS] (Cited on page 9.)

Chen, P.F., Innes, D.E. and Solanki, S.K., 2008, "SOHO/SUMER observations of prominence oscillation before eruption", *Astron. Astrophys.*, **484**, 487–493. [DOI], [ADS], [arXiv:0802.1961] (Cited on page 7.)

Chin, R., Verwichte, E., Rowlands, G. and Nakariakov, V.M., 2010, "Self-organization of magnetoacoustic waves in a thermally unstable environment", *Phys. Plasmas*, **17**(3), 032107. [DOI], [ADS] (Cited on page 9.)

de Jager, C., 1959, "Structure and Dynamics of the Solar Atmosphere", in *Astrophysik 3: Das Sonnensystem*, (Ed.) Flügge, S., vol. 52 of Handbuch der Physik, p. 80, Springer, Berlin. [ADS] (Cited on page 5.)

De Pontieu, B., Martens, P.C.H. and Hudson, H.S., 2001, "Chromospheric Damping of Alfvén Waves", *Astrophys. J.*, **558**, 859–871. [DOI], [ADS] (Cited on page 65.)

Díaz, A.J. and Roberts, B., 2006, "Fast Magnetohydrodynamic Oscillations in a Fibril Prominence Model", *Solar Phys.*, **236**, 111–126. [DOI], [ADS] (Cited on pages 58 and 60.)

Díaz, A.J., Oliver, R., Erdélyi, R. and Ballester, J.L., 2001, "Fast MHD oscillations in prominence fine structures", *Astron. Astrophys.*, **379**, 1083–1097. [DOI], [ADS] (Cited on pages 55, 56, 57, and 58.)

Díaz, A.J., Oliver, R. and Ballester, J.L., 2002, "Fast Magnetohydrodynamic Oscillations in Cylindrical Prominence Fibrils", *Astrophys. J.*, **580**, 550–565. [DOI], [ADS] (Cited on pages 55, 57, 58, 79, 90, and 93.)

Díaz, A.J., Oliver, R. and Ballester, J.L., 2003, "Fast MHD oscillations of a 3-dimensional prominence fibril", *Astron. Astrophys.*, **402**, 781–789. [DOI], [ADS] (Cited on pages 55 and 56.)

Díaz, A.J., Oliver, R. and Ballester, J.L., 2005, "Fast magnetohydrodynamic oscillations in a multifibril Cartesian prominence model", *Astron. Astrophys.*, **440**, 1167–1175. [DOI], [ADS] (Cited on pages 58, 59, and 60.)

Díaz, A.J., Oliver, R. and Ballester, J.L., 2010, "Prominence Thread Seismology Using the $P_1/2P_2$ Ratio", *Astrophys. J.*, **725**, 1742–1748. [DOI], [ADS] (Cited on pages 90, 91, and 92.)

Dungey, J.W., 1953, "A family of solutions of the magneto-hydrostatic problem in a conducting atmosphere in a gravitational field", *Mon. Not. R. Astron. Soc.*, **113**, 180–187. [ADS] (Cited on page 45.)

Dymova, M.V. and Ruderman, M.S., 2005, "Non-Axisymmetric Oscillations of Thin Prominence Fibrils", *Solar Phys.*, **229**, 79–94. [DOI], [ADS] (Cited on pages 57, 58, 60, and 93.)

Edwin, P.M. and Roberts, B., 1983, "Wave propagation in a magnetic cylinder", *Solar Phys.*, **88**, 179–191. [DOI], [ADS] (Cited on page 48.)

Engvold, O., 1981, "The small scale velocity field of a quiescent prominence", *Solar Phys.*, **70**, 315–324. [DOI], [ADS] (Cited on page 11.)

Engvold, O., 1998, "Observations of Filament Structure and Dynamics", in *New Perspectives on Solar Prominences*, IAU Colloq. 167, Aussois, France, April 28 – May 4, 1997, (Eds.) Webb, D.F., Schmieder, B., Rust, D.M., vol. 150 of ASP Conference Series, pp. 23–31, Astronomical Society of the Pacific, San Francisco. [ADS] (Cited on page 5.)

Engvold, O., 2008, "Observational aspects of prominence oscillations", in *Waves & Oscillations in the Solar Atmosphere: Heating and Magneto-Seismology*, Porlamar, Isla De Margarita, Venezuela, 17 – 22 September 2007, (Eds.) Erdélyi, R., Mendoza-Briceño, C.A., vol. 247 of IAU Symposia, pp. 152–157, Cambridge University Press, Cambridge; New York. [DOI], [ADS] (Cited on page 5.)

Eto, S., Isobe, H., Narukage, N., Asai, A., Morimoto, T., Thompson, B., Yashiro, S., Wang, T., Kitai, R., Kurokawa, H. and Shibata, K., 2002, "Relation between a Moreton Wave and an EIT Wave Observed on 1997 November 4", *Publ. Astron. Soc. Japan*, **54**, 481–491. [ADS] (Cited on page 7.)

Field, G.B., 1965, "Thermal Instability", *Astrophys. J.*, **142**, 531–567. [DOI], [ADS] (Cited on page 61.)

Forteza, P., Oliver, R., Ballester, J.L. and Khodachenko, M.L., 2007, "Damping of oscillations by ion-neutral collisions in a prominence plasma", *Astron. Astrophys.*, **461**, 731–739. [DOI], [ADS] (Cited on pages 61, 65, 67, and 73.)

Forteza, P., Oliver, R. and Ballester, J.L., 2008, "Time damping of non-adiabatic MHD waves in an unbounded partially ionised prominence plasma", *Astron. Astrophys.*, **492**, 223–231. [DOI], [ADS] (Cited on pages 61, 65, and 67.)

Foullon, C., Verwichte, E. and Nakariakov, V.M., 2004, "Detection of ultra-long-period oscillations in an EUV filament", *Astron. Astrophys.*, **427**, L5–L8. [DOI], [ADS] (Cited on pages 11, 13, 14, 22, 23, and 41.)

Foullon, C., Verwichte, E. and Nakariakov, V.M., 2009, "Ultra-long-period Oscillations in EUV Filaments Near to Eruption: Two-wavelength Correlation and Seismology", *Astrophys. J.*, **700**, 1658–1665. [DOI], [ADS] (Cited on page 14.)

Galindo Trejo, J., 1987, "Stability analysis of two-dimensional models of quiescent prominences", *Solar Phys.*, **108**, 265–313. [ADS] (Cited on pages 45 and 47.)

Galindo Trejo, J., 1989a, "MHD stability of a filament immersed in a solar bipolar magnetic region", *Geophys. Astrophys. Fluid Dyn.*, **47**, 69–91. [DOI], [ADS] (Cited on pages 45 and 47.)

Galindo Trejo, J., 1989b, "Influence of a Non-Uniform Axial Magnetic Field on the Instability of a Quiescent Prominence Overlying a Solar Bipolar Region", *Rev. Mex. Astron. Astrof.*, **17**, 47–58. [ADS] (Cited on pages 45 and 47.)

Galindo Trejo, J., 1998, "Hydromagnetic stability analysis of a solar prominence suspended in an external horizontal magnetic field", *Astron. Nachr.*, **319**, 391–408. [ADS] (Cited on pages 45 and 47.)

Galindo Trejo, J., 2006, "MHD Stabiblity of a Solar Prominence Embedded in an External Vertical Magnetic Field", *Rev. Mex. Astron. Astrof.*, **42**, 89–98. [ADS] (Cited on pages 45 and 47.)

Gilbert, H.R., Daou, A.G., Young, D., Tripathi, D. and Alexander, D., 2008, "The Filament-Moreton Wave Interaction of 2006 December 6", *Astrophys. J.*, **685**, 629–645. [DOI], [ADS] (Cited on page 7.)

Goossens, M., 2003, *An Introduction to Plasma Astrophysics and Magnetohydrodynamics*, vol. 294 of Astrophysics and Space Science Library, Kluwer, Dordrecht; Norwell, MA. [ADS], [Google Books] (Cited on page 65.)

Goossens, M., 2008, "Seismology of kink oscillations in coronal loops: Two decades of resonant damping", in *Waves & Oscillations in the Solar Atmosphere: Heating and Magneto-Seismology*, Porlamar, Isla De Margarita, Venezuela, 17 – 22 September 2007, (Eds.) Erdélyi, R., Mendoza-Briceño, C.A., vol. 247 of IAU Symposia, pp. 228–242, Cambridge University Press, Cambridge; New York. [DOI], [ADS] (Cited on pages 61 and 88.)

Goossens, M., Hollweg, J.V. and Sakurai, T., 1992, "Resonant behaviour of MHD waves on magnetic flux tubes. III. Effect of equilibrium flow", *Solar Phys.*, **138**, 233–255. [DOI], [ADS] (Cited on page 70.)

Goossens, M., Ruderman, M.S. and Hollweg, J.V., 1995, "Dissipative MHD solutions for resonant Alfvén waves in 1-dimensional magnetic flux tubes", *Solar Phys.*, **157**, 75–102. [DOI], [ADS] (Cited on page 70.)

Goossens, M., Andries, J. and Aschwanden, M.J., 2002, "Coronal loop oscillations. An interpretation in terms of resonant absorption of quasi-mode kink oscillations", *Astron. Astrophys.*, **394**, L39–L42. [DOI] (Cited on pages 69, 70, 84, and 88.)

Goossens, M., Andries, J. and Arregui, I., 2006, "Damping of magnetohydrodynamic waves by resonant absorption in the solar atmosphere", *Philos. Trans. R. Soc. London, Ser. A*, **364**, 433–446. [ADS] (Cited on pages 61 and 90.)

Goossens, M., Arregui, I., Ballester, J.L. and Wang, T.J., 2008, "Analytic approximate seismology of transversely oscillating coronal loops", *Astron. Astrophys.*, **484**, 851–857. [DOI], [ADS] (Cited on pages 84 and 88.)

Goossens, M., Terradas, J., Andries, J., Arregui, I. and Ballester, J.L., 2009, "On the nature of kink MHD waves in magnetic flux tubes", *Astron. Astrophys.*, **503**, 213–223. [DOI], [ADS], [arXiv:0905.0425 [astro-ph.SR]] (Cited on page 70.)

Goossens, M., Erdélyi, R. and Ruderman, M.S., 2010, "Resonant MHD Waves in the Solar Atmosphere", *Space Sci. Rev.*, **158**, 289–338. [DOI], [ADS] (Cited on pages 61 and 69.)

Gouttebroze, P. and Labrosse, N., 2009, "Radiative transfer in cylindrical threads with incident radiation. VI. A hydrogen plus helium system", *Astron. Astrophys.*, **503**, 663–671. [DOI], [ADS], [arXiv:0905.3466] (Cited on page 65.)

Harvey, J.W., 1969, *Magnetic Fields Associated with Solar Active-Region Prominences*, Ph.D. thesis, University of Colorado at Boulder, Boulder, CO. [ADS] (Cited on pages 5, 10, 11, 13, 14, and 15.)

Heinzel, P. and Anzer, U., 2006, "On the Fine Structure of Solar Filaments", *Astrophys. J. Lett.*, **643**, L65–L68. [DOI], [ADS] (Cited on page 5.)

Hershaw, J., Foullon, C., Nakariakov, V.M. and Verwichte, E., 2011, "Damped large amplitude transverse oscillations in an EUV solar filament, triggered by large-scale transient coronal waves", *Astron. Astrophys.*, **531**, A53. [DOI], [ADS] (Cited on pages 7 and 8.)

Hollweg, J.V. and Yang, G., 1988, "Resonance Absorption of Compressible Magnetohydrodynamic Waves at Thin 'Surfaces"', *J. Geophys. Res.*, **93**, 5423–5436. [DOI], [ADS] (Cited on pages 60, 69, and 70.)

Hyder, C.L., 1966, "Winking Filaments and Prominence and Coronal Magnetic Fields", *Z. Astrophys.*, **63**, 78–84. [ADS] (Cited on pages 7, 8, and 84.)

Ionson, J.A., 1978, "Resonant absorption of Alfvénic surface waves and the heating of solar coronal loops", *Astrophys. J.*, **226**, 650–673. [DOI], [ADS] (Cited on page 69.)

Isobe, H. and Tripathi, D., 2006, "Large amplitude oscillation of a polar crown filament in the pre-eruption phase", *Astron. Astrophys.*, **449**, L17–L20. [DOI], [ADS], [arXiv:astro-ph/0602432] (Cited on pages 7 and 85.)

Isobe, H., Tripathi, D., Asai, A. and Jain, R., 2007, "Large-Amplitude Oscillation of an Erupting Filament as Seen in EUV, H$\alpha$, and Microwave Observations", *Solar Phys.*, **246**, 89–99. [DOI], [ADS], [arXiv:0711.3952] (Cited on page 7.)

James, S.P., Erdélyi, R. and De Pontieu, B., 2003, "Can ion-neutral damping help to form spicules?", *Astron. Astrophys.*, **406**, 715–724. [DOI], [ADS] (Cited on page 65.)

Jing, J., Lee, J., Spirock, T.J., Xu, Y., Wang, H. and Choe, G.S., 2003, "Periodic Motion along a Solar Filament Initiated by a Subflare", *Astrophys. J. Lett.*, **584**, L103–L106. [DOI], [ADS] (Cited on pages 7 and 84.)

Jing, J., Lee, J., Spirock, T.J. and Wang, H., 2006, "Periodic Motion Along Solar Filaments", *Solar Phys.*, **236**, 97–109. [DOI], [ADS] (Cited on pages 7 and 84.)

Joarder, P.S. and Roberts, B., 1992a, "The modes of oscillation of a prominence. I. The slab with longitudinal magnetic field", *Astron. Astrophys.*, **256**, 264–272. [ADS] (Cited on pages 35, 41, 42, and 62.)

Joarder, P.S. and Roberts, B., 1992b, "The modes of oscillation of a prominence. II. The slab with transverse magnetic field", *Astron. Astrophys.*, **261**, 625–632. [ADS] (Cited on pages 35, 36, 38, 39, 41, 42, 43, 44, and 58.)

Joarder, P.S. and Roberts, B., 1993a, "The modes of oscillation of a Menzel prominence", *Astron. Astrophys.*, **273**, 642–646. [ADS] (Cited on pages 44 and 61.)

Joarder, P.S. and Roberts, B., 1993b, "The modes of oscillation of a prominence. III. The slab in a skewed magnetic field", *Astron. Astrophys.*, **277**, 225–234. [ADS] (Cited on pages 43, 44, 45, 46, 85, and 86.)

Joarder, P.S., Nakariakov, V.M. and Roberts, B., 1997, "Oscillations in Prominence Fine-Structures", *Solar Phys.*, **173**, 81–101. [DOI], [ADS] (Cited on page 55.)

Khodachenko, M.L., Arber, T.D., Rucker, H.O. and Hanslmeier, A., 2004, "Collisional and viscous damping of MHD waves in partially ionized plasmas of the solar atmosphere", *Astron. Astrophys.*, **422**, 1073–1084. [DOI], [ADS] (Cited on page 65.)

Kippenhahn, R. and Schlüter, A., 1957, "Eine Theorie der solaren Filamente", *Z. Astrophys.*, **43**, 36–62. [ADS] (Cited on pages 39, 40, 44, and 45.)

Kleczek, J. and Kuperus, M., 1969, "Oscillatory Phenomena in Quiescent Prominences", *Solar Phys.*, **6**, 72–79. [DOI], [ADS] (Cited on pages 7 and 8.)

Kobanov, N.I., 1983, "The study of velocity oscillations in the solar photosphere using the velocity substraction technique", *Solar Phys.*, **82**, 237–243. [DOI], [ADS] (Cited on page 11.)

Kuperus, M. and Raadu, M.A., 1974, "The Support of Prominences Formed in Neutral Sheets", *Astron. Astrophys.*, **31**, 189–193. [ADS] (Cited on page 47.)

Kuperus, M. and Tandberg-Hanssen, E., 1967, "The Nature of Quiescent Solar Prominences", *Solar Phys.*, **2**, 39–48. [DOI], [ADS] (Cited on page 5.)

Labrosse, N., Heinzel, P., Vial, J.-C., Kucera, T., Parenti, S., Gunár, S., Schmieder, B. and Kilper, G., 2010, "Physics of Solar Prominences: I Spectral Diagnostics and Non-LTE Modelling", *Space Sci. Rev.*, **151**, 243–332. [DOI], [ADS], [arXiv:1001.1620 [astro-ph.SR]] (Cited on pages 5 and 76.)

Landman, D.A., Edberg, S.J. and Laney, C.D., 1977, "Measurements of H$\beta$, He $D_3$, and $Ca^+$ $\Lambda$8542 line emission in quiescent prominences", *Astrophys. J.*, **218**, 888–897. [DOI], [ADS] (Cited on pages 13, 14, and 18.)

Leake, J.E., Arber, T.D. and Khodachenko, M.L., 2005, "Collisional dissipation of Alfvén waves in a partially ionised solar chromosphere", *Astron. Astrophys.*, **442**, 1091–1098. [DOI], [ADS], [arXiv:astro-ph/0510265] (Cited on pages 65 and 67.)

Lerche, I. and Low, B.C., 1980, "On the equilibrium of a cylindrical plasma supported horizontally by magnetic fields in uniform gravity", *Solar Phys.*, **67**, 229–243. [DOI], [ADS] (Cited on page 45.)

Leroy, J.-L., 1980, "Mass Balance and Magnetic Structure in Quiescent Prominences", in *Proceedings of the Japan-France Seminar on Solar Physics*, Japan Society for the Promotion of Sciences and CNRS, Tokyo 15 – 18 October 1980, (Eds.) Moriyama, F., Henoux, J.C., p. 155, Nihon Gakujutsu Shinkokai and CNRS, Tokyo. [ADS] (Cited on page 5.)

Leroy, J.-L., 1988, "Observations of Prominence Magnetic Field", in *Dynamics and Structure of Solar Prominences*, Proceedings of a workshop held at Palma de Mallorca, November 18 – 20, 1987, (Eds.) Ballester, J.L., Priest, E.R., vol. 5 of Conferències i comunicacions, pp. 33–40, Universitat de les Illes Balears, Palma de Mallorca. [ADS] (Cited on page 44.)

Leroy, J.-L., 1989, "Observation of Prominence Magnetic Fields", in *Dynamics and Structure of Quiescent Solar Prominences*, Based on a workshop held at Palma de Mallorca, November 18 – 20, 1987, (Ed.) Priest, E.R., vol. 150 of Astrophysics and Space Science Library, pp. 77–113, Kluwer, Dordrecht; Boston. [ADS], [Google Books] (Cited on page 44.)

Lin, Y., 2005, *Magnetic Field Topology Inferred from Studies of Fine Threads in Solar Filaments*, Ph.D. thesis, University of Oslo, Oslo (Cited on pages 5, 11, 13, 16, 18, 19, 20, 30, and 58.)

Lin, Y., 2010, "Filament Thread-like Structures and Their Small-amplitude Oscillations", *Space Sci. Rev.*, **158**, 237–266. [DOI], [ADS] (Cited on page 5.)

Lin, Y., Engvold, O. and Wiik, J.E., 2003, "Counterstreaming in a Large Polar Crown Filament", *Solar Phys.*, **216**, 109–120. [DOI], [ADS] (Cited on pages 5, 13, 16, and 30.)

Lin, Y., Engvold, O., Rouppe van der Voort, L.H.M., Wiik, J.E. and Berger, T.E., 2005, "Thin Threads of Solar Filaments", *Solar Phys.*, **226**, 239–254. [DOI], [ADS] (Cited on pages 5, 13, and 16.)

Lin, Y., Engvold, O., Rouppe van der Voort, L.H.M. and van Noort, M.J., 2007, "Evidence of Traveling Waves in Filament Threads", *Solar Phys.*, **246**, 65–72. [DOI], [ADS] (Cited on pages 13, 16, 20, 31, 34, 49, 89, and 92.)

Lin, Y., Martin, S.F. and Engvold, O., 2008, "Filament Substructures and their Interrelation", in *Subsurface and Atmospheric Influences on Solar Activity*, Proceedings of a workshop held at NSO, Sacramento Peak, Sunspot, NM, 16 – 20 April 2007, (Eds.) Howe, R., Komm, R.W., Balasubramaniam, K.S., Petrie, G.J.D., vol. 383 of ASP Conference Series, pp. 235–242, Astronomical Society of the Pacific, San Francisco. [ADS] (Cited on page 5.)

Lin, Y., Soler, R., Engvold, O., Ballester, J.L., Langangen, Ø., Oliver, R. and Rouppe van der Voort, L.H.M., 2009, "Swaying Threads of a Solar Filament", *Astrophys. J.*, **704**, 870–876. [DOI], [ADS] (Cited on pages 13, 16, 32, 48, 86, and 87.)

Low, B.C., 1981, "The field and plasma configuration of a filament overlying a solar bipolar magnetic region", *Astrophys. J.*, **246**, 538–548. [DOI], [ADS] (Cited on page 47.)

Luna, M., Terradas, J., Oliver, R. and Ballester, J.L., 2008, "Transverse Oscillations of Two Coronal Loops", *Astrophys. J.*, **676**, 717–727. [DOI], [ADS], [arXiv:0707.0758] (Cited on pages 17 and 51.)

Mackay, D.H., Karpen, J.T., Ballester, J.L., Schmieder, B. and Aulanier, G., 2010, "Physics of Solar Prominences: II Magnetic Structure and Dynamics", *Space Sci. Rev.*, **151**, 333–399. [DOI], [ADS], [arXiv:1001.1635 [astro-ph.SR]] (Cited on page 5.)

Malherbe, J.M., Schmieder, B. and Mein, P., 1981, "Dynamics in the filaments. I. Oscillations in a quiescent filament", *Astron. Astrophys.*, **102**, 124–128. [ADS] (Cited on page 11.)

Malherbe, J.M., Schmieder, B., Mein, P. and Tandberg-Hanssen, E., 1987, "Dynamics of solar filaments. V. Oscillations in the H$\alpha$ and 1548 Å C IV lines", *Astron. Astrophys.*, **172**, 316–322. [ADS] (Cited on page 11.)

Malville, J.M. and Schindler, M., 1981, "Oscillations of a loop prominence preceding a limb flare", *Solar Phys.*, **70**, 115–128. [DOI], [ADS] (Cited on page 22.)

Martin, S.F., Lin, Y. and Engvold, O., 2008, "A Method of Resolving the 180-Degree Ambiguity by Employing the Chirality of Solar Features", *Solar Phys.*, **250**, 31–51. [DOI], [ADS] (Cited on page 5.)

Mashnich, G.P. and Bashkirtsev, V.S., 1990, "Observations of Doppler velocity oscillations of mass motion in a quiescent prominence during three consecutive days", *Astron. Astrophys.*, **235**, 428–430. [ADS] (Cited on page 14.)

Mashnich, G.P. and Bashkirtsev, V.S., 1999, "Latitudinal Variations of Line-of-Sight Velocity Oscillations in the Photosphere, Chromosphere and Prominences", *Solar Phys.*, **185**, 35–40. [DOI], [ADS] (Cited on page 14.)

Mashnich, G.P., Bashkirtsev, V.S. and Khlystova, A.I., 2009a, "Velocity structure and variations in the region of quiet solar filaments", *Astron. Lett.*, **35**, 253–260. [DOI], [ADS] (Cited on pages 10 and 16.)

Mashnich, G.P., Bashkirtsev, V.S. and Khlystova, A.I., 2009b, "Spatial distribution of oscillations in filaments", *Geomagn. Aeron.*, **49**, 891–897. [DOI], [ADS] (Cited on pages 10 and 16.)

McDougall, A.M.D. and Hood, A.W., 2007, "A New Look at Mode Conversion in a Stratified Isothermal Atmosphere", *Solar Phys.*, **246**, 259–271. [DOI], [ADS], [arXiv:0707.0830] (Cited on page 83.)

McLaughlin, J.A. and Hood, A.W., 2006, "MHD mode coupling in the neighbourhood of a 2D null point", *Astron. Astrophys.*, **459**, 641–649. [DOI], [ADS], [arXiv:0712.2402] (Cited on page 83.)

Menzel, D.H., 1951, "Solar Electromagnetism", in *The Dynamics of Ionised Media*, Massey Conference, University College, London, March 19 – 21, 1951, UCL, London. Online version (accessed 3 August 2011):
http://discovery.ucl.ac.uk/14698/ (Cited on page 45.)

Molowny-Horas, R., Oliver, R., Ballester, J.L. and Baudin, F., 1997, "Observations of Doppler oscillations in a solar prominence", *Solar Phys.*, **172**, 181–188. [DOI], [ADS] (Cited on pages 16, 19, 20, 21, 23, and 24.)

Molowny-Horas, R., Baudin, F., Oliver, R. and Ballester, J.L., 1998, "He I 10830 Å Doppler Oscillations in a Solar Filament", in *Cool Stars, Stellar Systems, and the Sun*, The Tenth Cambridge Workshop on Cool Stars, Stellar Systems and the Sun, Cambridge, MA, 15 – 19 July 1997, (Eds.) Donahue, R.A., Bookbinder, J.A., vol. 154 of ASP Conference Series, pp. 650–657, Astronomical Society of the Pacific, San Francisco. [ADS] (Cited on page 19.)

Molowny-Horas, R., Wiehr, E., Balthasar, H., Oliver, R. and Ballester, J.L., 1999, "Prominence Doppler oscillations", in *JOSO Annual Report 1998*, (Eds.) Antalová, A., Balthasar, H., Kučera, A., pp. 126–127, Astronomical Institute of Slovak Academy of Sciences, Tatranská Lomnica, Slovakia. [ADS]. Online version (accessed 3 August 2011):
http://www.joso-info.org/JOSO_PROJEKT/annual/annual90.htm (Cited on pages 10, 13, 18, 19, and 25.)

Moreton, G.E. and Ramsey, H.E., 1960, "Recent Observations of Dynamical Phenomena Associated with Solar Flares", *Publ. Astron. Soc. Pac.*, **72**, 357–358. [DOI], [ADS] (Cited on page 7.)

Murawski, K., 1993, "Cross-talk in solar coronal loops", *Acta Astron.*, **43**, 161–176. [ADS] (Cited on page 51.)

Nakariakov, V.M. and Ofman, L., 2001, "Determination of the coronal magnetic field by coronal loop oscillations", *Astron. Astrophys.*, **372**, L53–L56. [DOI], [ADS] (Cited on page 84.)

Nakariakov, V.M. and Roberts, B., 1995, "Magnetosonic Waves in Structured Atmospheres with Steady Flows. I. Magnetic Slabs", *Solar Phys.*, **159**, 213–228. [DOI], [ADS] (Cited on page 49.)

Nakariakov, V.M., Ofman, L., DeLuca, E.E., Roberts, B. and Davila, J.M., 1999, "TRACE observations of damped coronal loop oscillations: implications for coronal heating", *Science*, **285**, 862–864. [DOI], [ADS] (Cited on page 61.)

Nakariakov, V.M., Aschwanden, M.J. and Van Doorsselaere, T., 2009, "The possible role of vortex shedding in the excitation of kink-mode oscillations in the solar corona", *Astron. Astrophys.*, **502**, 661–664. [DOI], [ADS] (Cited on page 7.)

Ning, Z., Cao, W. and Goode, P.R., 2009a, "Behavior of the Spines in a Quiescent Prominence Observed by Hinode/SOT", *Astrophys. J.*, **707**, 1124–1130. [DOI], [ADS] (Cited on pages 10, 11, 16, 17, and 18.)

Ning, Z., Cao, W., Okamoto, T.J., Ichimoto, K. and Qu, Z.Q., 2009b, "Small-scale oscillations in a quiescent prominence observed by HINODE/SOT. Prominence oscillations", *Astron. Astrophys.*, **499**, 595–600. [DOI], [ADS] (Cited on pages 10, 11, 16, 17, 18, and 33.)

Ofman, L. and Aschwanden, M.J., 2002, "Damping Time Scaling of Coronal Loop Oscillations Deduced from Transition Region and Coronal Explorer Observations", *Astrophys. J. Lett.*, **576**, L153–L156. [DOI], [ADS] (Cited on page 8.)

Okamoto, T.J., Nakai, H., Keiyama, A., Narukage, N., UeNo, S., Kitai, R., Kurokawa, H. and Shibata, K., 2004, "Filament Oscillations and Moreton Waves Associated with EIT Waves", *Astrophys. J.*, **608**, 1124–1132. [DOI], [ADS] (Cited on page 7.)

Okamoto, T.J., Tsuneta, S., Berger, T.E., Ichimoto, K., Katsukawa, Y., Lites, B.W., Nagata, S., Shibata, K., Shimizu, T., Shine, R.A., Suematsu, Y., Tarbell, T.D. and Title, A.M., 2007, "Coronal Transverse Magnetohydrodynamic Waves in a Solar Prominence", *Science*, **318**, 1577–1580. [DOI], [ADS] (Cited on pages 5, 13, 16, 30, 31, 32, 33, 60, 92, 93, and 94.)

Oliver, R., 2009, "Prominence Seismology Using Small Amplitude Oscillations", *Space Sci. Rev.*, **149**, 175–197. [DOI], [ADS] (Cited on page 61.)

Oliver, R. and Ballester, J.L., 1995, "Magnetohydrodynamic Waves in a Bounded Inhomogeneous Medium with Prominence-Corona Properties", *Astrophys. J.*, **448**, 444–458. [DOI], [ADS] (Cited on page 44.)

Oliver, R. and Ballester, J.L., 1996, "The Influence of the Temperature Profile on the Magnetohydrodynamic Modes of a Prominence-Corona System", *Astrophys. J.*, **456**, 393–398. [DOI], [ADS] (Cited on pages 44 and 45.)

Oliver, R. and Ballester, J.L., 2002, "Oscillations in Quiescent Solar Prominences Observations and Theory (Invited Review)", *Solar Phys.*, **206**, 45–67. [DOI], [ADS] (Cited on page 22.)

Oliver, R., Ballester, J.L., Hood, A.W. and Priest, E.R., 1992, "Magnetohydrodynamic waves in a solar prominence", *Astrophys. J.*, **400**, 369–379. [DOI], [ADS] (Cited on pages 44 and 61.)

Oliver, R., Ballester, J.L., Hood, A.W. and Priest, E.R., 1993, "Oscillations of a quiescent solar prominence embedded in a hot corona", *Astrophys. J.*, **409**, 809–821. [DOI], [ADS] (Cited on pages 36, 37, 38, 39, 43, and 44.)

Osherovich, V.A., 1985, "Solar prominence model based on eigenvalue solutions. I. Isolated filaments and their properties under the influence of external horizontal magnetic field", *Astrophys. J.*, **297**, 314–323. [DOI], [ADS] (Cited on page 47.)

Osherovich, V.A., 1989, "Solar prominence model based on eigenvalue solutions. II. Filaments in the vertical magnetic fields", *Astrophys. J.*, **336**, 1041–1049. [DOI], [ADS] (Cited on page 47.)

Pandey, B.P. and Wardle, M., 2008, "Hall magnetohydrodynamics of partially ionized plasmas", *Mon. Not. R. Astron. Soc.*, **385**, 2269–2278. [DOI], [ADS], [arXiv:0707.2688] (Cited on pages 65 and 67.)

Patsourakos, S. and Vial, J.-C., 2002, "SOHO Contribution to Prominence Science", *Solar Phys.*, **208**, 253–281. [DOI], [ADS] (Cited on page 65.)

Pintér, B., Jain, R., Tripathi, D. and Isobe, H., 2008, "Prominence Seismology: Wavelet Analysis of Filament Oscillations", *Astrophys. J.*, **680**, 1560–1568. [DOI], [ADS] (Cited on page 85.)

Poland, A. and Anzer, U., 1971, "Energy Balance in Cool Quiescent Prominences", *Solar Phys.*, **19**, 401–413. [DOI], [ADS] (Cited on page 39.)

Pouget, G., 2007, *Analyse des protubérances solaires observées à partir de la sonde solaire SOHO et du télescope Sacramento Peak: Oscillations, diagnostic, instabilités*, Ph.D. thesis, Univdersité de Paris-Sud, Paris (Cited on page 7.)

Pouget, G., Bocchialini, K. and Solomon, J., 2006, "Oscillations in a solar filament: first observation of long periods in the He I 584.33 Å line, modelling and diagnostic", *Astron. Astrophys.*, **450**, 1189–1198. [DOI], [ADS] (Cited on pages 11, 13, 14, 41, and 86.)

Ramsey, H.E. and Smith, S.F., 1965, "Flare-Initiated Filament Oscillations", *Astron. J.*, **70**, 688. [DOI], [ADS] (Cited on pages 7 and 84.)

Ramsey, H.E. and Smith, S.F., 1966, "Flare-Initiated Filament Oscillations", *Astron. J.*, **71**, 197–199. [DOI], [ADS] (Cited on page 7.)

Régnier, S., Solomon, J. and Vial, J.-C., 2001, "Oscillations in an active region filament: Observations and comparison with MHD waves", *Astron. Astrophys.*, **376**, 292–301. [DOI], [ADS] (Cited on pages 11, 13, 14, 85, and 86.)

Rempel, M., Schmitt, D. and Glatzel, W., 1999, "Stability of a flux tube model for prominences", *Astron. Astrophys.*, **343**, 615–623. [ADS] (Cited on pages 54 and 55.)

Roberts, B., 1991, "Waves in the solar atmosphere", *Geophys. Astrophys. Fluid Dyn.*, **62**, 83–100. [DOI], [ADS] (Cited on pages 35 and 36.)

Roberts, B. and Joarder, P.S., 1994, "Oscillations in quiescent prominences", in *Advances in Solar Physics*, Proceedings of the Seventh European Meeting on Solar Physics Held in Catania, Italy, 11 – 15 May 1993, (Eds.) Belvedere, G., Rodono, M., Simnett, G.M., vol. 432 of Lecture Notes in Physics, pp. 173–178, Springer, Berlin; New York. [DOI], [ADS] (Cited on pages 37, 38, 39, and 41.)

Roberts, B., Edwin, P.M. and Benz, A.O., 1984, "On coronal oscillations", *Astrophys. J.*, **279**, 857–865. [DOI], [ADS] (Cited on page 84.)

Robertson, D. and Ruderman, M.S., 2011, "Resonantly damped oscillations of two coronal loops", *Astron. Astrophys.*, **525**, A4. [DOI], [ADS] (Cited on page 51.)

Ruderman, M.S. and Roberts, B., 2002, "The Damping of Coronal Loop Oscillations", *Astrophys. J.*, **577**, 475–486. [DOI], [ADS] (Cited on pages 8, 69, and 70.)

Sakai, J., Colin, A. and Priest, E., 1987, "Dynamical model of prominence formation and oscillation", *Solar Phys.*, **114**, 253–271. [DOI], [ADS] (Cited on page 9.)

Schutgens, N.A.J., 1997a, "Prominence oscillations and stability. Communicating the distant photospheric boundary", *Astron. Astrophys.*, **323**, 969–985. [ADS] (Cited on pages 47 and 83.)

Schutgens, N.A.J., 1997b, "Vertical prominence oscillations and stability. A comparison of the influence of the distant photosphere in Inverse Polarity and Normal Polarity prominence models", *Astron. Astrophys.*, **325**, 352–359. [ADS] (Cited on pages 47 and 83.)

Schutgens, N.A.J. and Tóth, G., 1999, "Numerical simulation of prominence oscillations", *Astron. Astrophys.*, **345**, 1038–1048. [ADS], [arXiv:astro-ph/9903128] (Cited on pages 48 and 83.)

Soler, R. and Goossens, M., 2011, "Kink oscillations of flowing threads in solar prominences", *Astron. Astrophys.*, **531**, A167. [DOI], [ADS], [arXiv:1106.3937 [astro-ph.SR]] (Cited on page 60.)

Soler, R., Oliver, R. and Ballester, J.L., 2007, "The effect of the solar corona on the attenuation of small-amplitude prominence oscillations. I. Longitudinal magnetic field", *Astron. Astrophys.*, **471**, 1023–1033. [DOI], [ADS], [arXiv:0704.1566] (Cited on pages 61, 62, and 64.)

Soler, R., Oliver, R. and Ballester, J.L., 2008, "Nonadiabatic Magnetohydrodynamic Waves in a Cylindrical Prominence Thread with Mass Flow", *Astrophys. J.*, **684**, 725–735. [DOI], [ADS], [arXiv:0803.2600] (Cited on pages 49, 50, 61, 62, 63, and 64.)

Soler, R., Oliver, R. and Ballester, J.L., 2009a, "Propagation of Nonadiabatic Magnetoacoustic Waves in a Threaded Prominence With Mass Flows", *Astrophys. J.*, **693**, 1601–1609. [DOI], [ADS], [arXiv:0809.4765] (Cited on pages 51, 52, 53, 54, and 64.)

Soler, R., Oliver, R. and Ballester, J.L., 2009b, "Attenuation of small-amplitude oscillations in a prominence corona model with a transverse magnetic field", *New Astronomy*, **14**, 238–248. [DOI], [ADS], [arXiv:0801.3744] (Cited on pages 61 and 62.)

Soler, R., Oliver, R. and Ballester, J.L., 2009c, "Magnetohydrodynamic Waves in a Partially Ionized Filament Thread", *Astrophys. J.*, **699**, 1553–1562. [DOI], [ADS], [arXiv:0904.3013] (Cited on pages 67, 68, and 69.)

Soler, R., Oliver, R. and Ballester, J.L., 2009d, "Resonantly Damped Kink Magnetohydrodynamic Waves in a Partially Ionized Filament Thread", *Astrophys. J.*, **707**, 662–670. [DOI], [ADS], [arXiv:0909.3599] (Cited on pages 65, 73, 74, 75, and 76.)

Soler, R., Oliver, R., Ballester, J.L. and Goossens, M., 2009e, "Damping of Filament Thread Oscillations: Effect of the Slow Continuum", *Astrophys. J. Lett.*, **695**, L166–L170. [DOI], [ADS], [arXiv:0902.0572] (Cited on pages 69, 70, 72, and 73.)

Soler, R., Arregui, I., Oliver, R. and Ballester, J.L., 2010a, "Seismology of Standing Kink Oscillations of Solar Prominence Fine Structures", *Astrophys. J.*, **722**, 1778–1792. [DOI], [ADS], [arXiv:1007.1959 [astro-ph.SR]] (Cited on pages 79, 80, 81, 82, 89, 90, and 91.)

Soler, R., Oliver, R. and Ballester, J.L., 2010b, "Time damping of non-adiabatic magnetohydrodynamic waves in a partially ionized prominence plasma: effect of helium", *Astron. Astrophys.*, **512**, A28. [DOI], [ADS], [arXiv:0910.2883 [astro-ph.SR]] (Cited on pages 65 and 66.)

Soler, R., Oliver, R. and Ballester, J.L., 2011, "Spatial Damping of Propagating Kink Waves in Prominence Threads", *Astrophys. J.*, **726**, 102. [DOI], [ADS], [arXiv:1009.4871 [astro-ph.SR]] (Cited on pages 76, 77, and 78.)

Spruit, H.C., 1982, "Propagation speeds and acoustic damping of waves in magnetic flux tubes", *Solar Phys.*, **75**, 3–17. [DOI], [ADS] (Cited on page 48.)

Suematsu, Y., Yoshinaga, R., Terao, N. and Tsubaki, T., 1990, "Oscillatory and transient features detected simultaneously in the Ca II K and H$\beta$ line spectra of a quiescent prominence", *Publ. Astron. Soc. Japan*, **42**, 187–203. [ADS] (Cited on pages 11, 13, 16, and 22.)

Suetterlin, P., Wiehr, E., Bianda, M. and Kueveler, G., 1997, "Problems in measuring prominence oscillations", *Astron. Astrophys.*, **321**, 921–926. [ADS] (Cited on pages 11, 13, 14, and 16.)

Sych, R., Nakariakov, V.M., Karlicky, M. and Anfinogentov, S., 2009, "Relationship between wave processes in sunspots and quasi-periodic pulsations in active region flares", *Astron. Astrophys.*, **505**, 791–799. [DOI], [ADS], [arXiv:1005.3594 [astro-ph.SR]] (Cited on page 10.)

Tandberg-Hanssen, E., 1995, *The Nature of Solar Prominences*, vol. 199 of Astrophysics and Space Science Library, Kluwer, Dordrecht; Boston. [ADS] (Cited on page 84.)

Terradas, J., Oliver, R. and Ballester, J.L., 2001, "Radiative damping of quiescent prominence oscillations", *Astron. Astrophys.*, **378**, 635–652. [DOI], [ADS] (Cited on page 61.)

Terradas, J., Molowny-Horas, R., Wiehr, E., Balthasar, H., Oliver, R. and Ballester, J.L., 2002, "Two-dimensional distribution of oscillations in a quiescent solar prominence", *Astron. Astrophys.*, **393**, 637–647. [DOI], [ADS] (Cited on pages 13, 16, 18, 20, 23, 25, 26, 27, 28, 29, 32, 49, and 76.)

Terradas, J., Carbonell, M., Oliver, R. and Ballester, J.L., 2005, "Time damping of linear non-adiabatic magnetoacoustic waves in a slab-like quiescent prominence", *Astron. Astrophys.*, **434**, 741–749. [DOI], [ADS] (Cited on page 61.)

Terradas, J., Arregui, I., Oliver, R. and Ballester, J.L., 2008, "Transverse Oscillations of Flowing Prominence Threads Observed with Hinode", *Astrophys. J. Lett.*, **678**, L153–L156. [DOI], [ADS] (Cited on pages 60, 92, 93, and 94.)

Terradas, J., Goossens, M. and Verth, G., 2010, "Selective spatial damping of propagating kink waves due to resonant absorption", *Astron. Astrophys.*, **524**, A23. [DOI], [ADS], [arXiv:1004.4468 [astro-ph.SR]] (Cited on page 88.)

Thompson, W.T. and Schmieder, B., 1991, "Oscillations in H$\alpha$ filaments: center-to-limb study", *Astron. Astrophys.*, **243**, 501–511. [ADS] (Cited on pages 11, 16, 20, and 22.)

Tripathi, D., Isobe, H. and Jain, R., 2009, "Large Amplitude Oscillations in Prominences", *Space Sci. Rev.*, **149**, 283–298. [DOI], [ADS], [arXiv:0910.4059 [astro-ph.SR]] (Cited on page 9.)

Tsubaki, T. and Takeuchi, A., 1986, "Periodic oscillations found in the velocity field of a quiescent prominence", *Solar Phys.*, **104**, 313–320. [DOI], [ADS] (Cited on pages 11, 13, 14, 16, 18, and 22.)

Tsubaki, T., Ohnishi, Y. and Suematsu, Y., 1987, "Short-period oscillations found in a quiescent prominence", *Publ. Astron. Soc. Japan*, **39**, 179–188. [ADS] (Cited on pages 13 and 22.)

Tsubaki, T., Toyoda, M., Suematsu, Y. and Gamboa, G.A.R., 1988, "New evidence for oscillatory motions in a quiescent prominence", *Publ. Astron. Soc. Japan*, **40**, 121–126. [ADS] (Cited on pages 13, 16, and 22.)

Uchida, Y., 1970, "Diagnosis of Coronal Magnetic Structure by Flare-Associated Hydromagnetic Disturbances", *Publ. Astron. Soc. Japan*, **22**, 341–364. [ADS] (Cited on page 84.)

van den Oord, G.H.J. and Kuperus, M., 1992, "The effect of retardation on the stability of current filaments", *Solar Phys.*, **142**, 113–129. [DOI], [ADS] (Cited on pages 47 and 83.)

van den Oord, G.H.J., Schutgens, N.A.J. and Kuperus, M., 1998, "The effect of delays on filament oscillations and stability", *Astron. Astrophys.*, **339**, 225–238. [ADS] (Cited on pages 47 and 83.)

Van Doorsselaere, T., Nakariakov, V.M. and Verwichte, E., 2008a, "Detection of Waves in the Solar Corona: Kink or Alfvén?", *Astrophys. J. Lett.*, **676**, L73–L75. [DOI], [ADS] (Cited on page 31.)

Van Doorsselaere, T., Ruderman, M.S. and Robertson, D., 2008b, "Transverse oscillations of two parallel coronal loops", *Astron. Astrophys.*, **485**, 849–857. [DOI], [ADS] (Cited on page 51.)

Verth, G., Erdélyi, R. and Jess, D.B., 2008, "Refined Magnetoseismological Technique for the Solar Corona", *Astrophys. J. Lett.*, **687**, L45–L48. [DOI], [ADS] (Cited on page 84.)

Verwichte, E., Nakariakov, V.M., Ofman, L. and DeLuca, E.E., 2004, "Characteristics of transverse oscillations in a coronal loop arcade", *Solar Phys.*, **223**, 77–94. [DOI], [ADS] (Cited on page 49.)

Verwichte, E., Foullon, C. and Nakariakov, V.M., 2006, "Seismology of curved coronal loops with vertically polarised transverse oscillations", *Astron. Astrophys.*, **452**, 615–622. [DOI] (Cited on page 84.)

Vršnak, B., Veronig, A.M., Thalmann, J.K. and Žic, T., 2007, "Large amplitude oscillatory motion along a solar filament", *Astron. Astrophys.*, **471**, 295–299. [DOI], [ADS], [arXiv:0707.1752] (Cited on pages 7, 84, and 85.)

Wiehr, E., Balthasar, H. and Stellmacher, G., 1984, "Oscillations of the H$\alpha$ emission in solar prominences", *Solar Phys.*, **94**, 285–288. [DOI], [ADS] (Cited on pages 11, 13, 14, and 19.)

Wiehr, E., Balthasar, H. and Stellmacher, G., 1989, "Doppler Velocity Oscillations in Quiescent Prominences", *Hvar Obs. Bull.*, **13**, 131–135. [ADS] (Cited on page 18.)

Yi, Z. and Engvold, O., 1991, "Vertical velocities and oscillations in quiescent filaments", *Solar Phys.*, **134**, 275–286. [DOI], [ADS] (Cited on pages 11, 13, 28, and 33.)

Yi, Z., Engvold, O. and Keil, S.L., 1991, "Structure and oscillations in quiescent filaments from observations in He I $\lambda$ 10830 Å", *Solar Phys.*, **132**, 63–80. [ADS] (Cited on pages 10, 11, 13, 14, 16, 17, 28, and 49.)

Zaqarashvili, T.V., 2003, "Observation of coronal loop torsional oscillation", *Astron. Astrophys.*, **399**, L15–L18. [DOI], [ADS], [arXiv:astro-ph/0301316] (Cited on page 84.)

Zirker, J.B., Engvold, O. and Martin, S.F., 1998, "Counter-streaming gas flows in solar prominences as evidence for vertical magnetic fields", *Nature*, **396**, 440–441. [DOI], [ADS] (Cited on page 5.)